

INVESTIGATION INTO THE EFFECT OF TEMPERATURE  
ON NITROGEN FOAM BEHAVIOR

by  
Hamed Al-Riyami

**Copyright by Hamed Al-Riyami 2022**

All Rights Reserved

A thesis submitted to the Faculty and the Board of Trustees of the Colorado School of Mines in partial fulfillment of the requirements for the degree of Doctor of Philosophy (Petroleum Engineering).

Golden, Colorado

Date \_\_\_\_\_

Signed: \_\_\_\_\_

Hamed Al-Riyami

Signed: \_\_\_\_\_

Dr. Luis Zerpa  
Thesis Advisor

Golden, Colorado

Date \_\_\_\_\_

Signed: \_\_\_\_\_

Dr. Jennifer Miskimins  
Professor and Department Head  
Department of Petroleum Engineering

## ABSTRACT

Thermal enhanced oil recovery is touted as the most effective recovery method for heavy oil with steam being the most common injectant, but unfortunately, conformance issues such as gravity override and channeling are rife in steam injection processes. Foam has been used to mitigate conformance issues in gas injection processes, however, at high temperatures these issues return due to the rapid decay of foams and degradation of surfactants.

Literature reports many investigations of the formulation of surfactants and additives to improve the stability of foams. However, the study of foam behavior at higher temperatures is lacking as most studies aim to understand foam decay at ambient temperatures for dry foams. This work aims to shine some light on the issues of studying foam behavior at lower temperature for high temperature applications and to generate better insight into the decay behavior of foams at higher temperatures in closed environments.

Established foam decay analysis methods such as test tubes and dynamic foam column tests were employed to highlight the dependence of foamability and stability of surfactant foams on temperature and the inadequacy of low temperature analysis to predict high temperature foam performance. It was found that some surfactants perform comparatively better than others when stabilizing foams at high temperatures, even when their low-temperature performance was worse. It was also shown that foamability was differently sensitive to temperature for the different surfactants.

This work introduces a methodology to visually analyze foams in a sealed high-pressure high-temperature cell. Using three different surfactants, foam was visually analyzed at different temperatures, and it was found that the decay behavior of foams tends to split around the 40 °C mark. Below that temperature, a dry polyhedral foam is observed for most of the decay that is

primarily driven by drainage and evaporation, while at temperatures above 40 °C, a wet spherical foam is observed for most of the decay and the mechanisms governing the decay depend on the surfactant being used.

For anionic surfactants, it was found that wet foams decay through the Marangoni flow induced by temperature fluctuations across the bubbles' surfaces, which are exacerbated at higher temperatures. When a lamella ruptures, if the adjacent bubbles are sufficiently different in size, the gas influx from the smaller bubble to the larger one combined with the liquid in the lamella and the bubbles themselves causes new bubbles to be formed due to the shearing of the liquid.

The results also showed that at temperatures above 120 °C the decay of the foams was primarily occurring at a middle layer within the foam structure rather than the top layer that is exposed to the gas phase. The decay occurred in the form of splitting, where large bubbles burst and form smaller ones, that shifts the foam downwards making it appear as if the top layer is exhibiting the bulk of the decay.

For nonionic surfactants, the decay is more complex and depends on the phase behavior of the surfactant molecule with temperature. As the temperature increases, the aggregation of the monomers into larger structures such as micellar, lamellar, and isotropic structures, changes the way foam decays. It was found that at 90 °C, the decay of the foam occurred primarily at the liquid-foam interface which is attributed to the preferential aggregation of the monomers into larger structures in the liquid phase, as opposed to adsorption to the gas-liquid interface.

Overall, this work showed that foam behavior can either be independent of the surfactant behavior with temperatures, as is the case with anionic surfactants, or coupled to the thermodynamic behavior of the surfactant molecule, as in the nonionic surfactant, and is significantly different between low and high temperatures.

## TABLE OF CONTENTS

ABSTRACT .....	iii
LIST OF FIGURES .....	ix
LIST OF TABLES .....	xiii
LIST OF SYMBOLS.....	xiv
ACKNOWLEDGEMENT.....	xv
CHAPTER 1 INTRODUCTION.....	1
1.1 Research Motivation.....	2
1.2 Scope of Study.....	2
1.3 Organization of Dissertation .....	4
CHAPTER 2 LITERATURE REVIEW ON STEAM FOAM FLOODING AND FOAMS .....	5
2.1 Thermal EOR .....	5
2.2 Steam Injection.....	5
2.3 Steam-foam flooding.....	6
2.4 Foam Properties.....	7
2.4.1 Interfacial Tension.....	8
2.4.2 Foamability.....	9
2.4.3 Stability .....	10
2.4.4 Morphology.....	10
2.5 Bulk Foam Behavior .....	11
2.6 Foams in Porous Media.....	12
2.7 Recent Advances in Surfactant Foam Stability Enhancement .....	14

CHAPTER 3 PRELIMINARY EXPERIMENTS ON FOAMS USING TEST TUBES .....	18
3.1 Introduction.....	18
3.2 Materials.....	18
3.3 Setup and Procedures .....	19
3.3.1 Preparation of Surfactant Solutions.....	19
3.3.2 Preparation of Test Tubes.....	20
3.3.3 Fresh Solution Foamability and Stability Tests .....	21
3.3.4 Precipitation Test.....	21
3.3.5 Aged Solution Foamability and Stability Tests.....	22
3.4 Experimental Results.....	23
3.4.1 Fresh Solution Foamability and Stability Tests .....	23
3.4.2 Precipitation Test.....	24
3.4.3 Aged Solution Foamability and Stability Tests.....	24
3.5 Discussion .....	26
CHAPTER 4 FOAMABILITY EVALUATION USING DYNAMIC FOAM EXPERIMENTS .....	29
4.1 Introduction.....	29
4.2 Materials.....	31
4.3 Setup and Procedure.....	32
4.3.1 Preparation of the Mixing Chamber.....	32
4.3.2 Preparation of Nitrogen for the Experiment.....	32
4.3.3 Running the Experiment.....	33
4.4 Experimental Results.....	34
4.5 Discussion .....	35
CHAPTER 5 STATIC FOAM EXPERIMENTS IN CLOSED ENVIRONMENTS .....	38
5.1 Introduction.....	38

5.2 Materials.....	38
5.2.1 Foamability and Stability Apparatus.....	39
5.2.2 IFT Measurement Apparatus.....	40
5.3 Setup and Procedure.....	42
5.3.1 Foamability and Stability Procedure.....	42
5.3.2 High Pressure Stability and Foamability Procedure.....	45
5.3.3 IFT Measurement Procedure.....	45
5.4 Experimental Results.....	47
5.4.1 Effect of Temperature on Interfacial Tension.....	50
5.4.2 Effect of Temperature on Cell Humidity.....	51
5.4.3 Effect of Temperature on Foamability.....	55
5.4.4 Effect of Temperature on Stability.....	57
5.4.5 Effect of Temperature on Morphology.....	58
5.4.6 Effect of Temperature on Decay Pattern.....	61
5.4.6.1 Anionic Surfactants.....	62
5.4.6.2 Nonionic Surfactants.....	67
5.4.7 Thermal Degradation of Surfactants.....	69
5.4.7.1 Thermal Degradation Effect on Foamability.....	70
5.4.7.2 Thermal Degradation Effect on Stability.....	71
5.4.8 High Pressure Foamability and Stability Results.....	73
5.4.8.1 Temperature Effect on Foamability at High Pressures.....	73
5.4.8.2 Temperature Effect on Stability at High Pressures.....	74
5.4.8.3 Temperature Effect on Morphology at High Pressures.....	76
5.4.8.4 Temperature Effect on Decay Pattern at High Pressures.....	79
5.5 Discussion.....	81

CHAPTER 6 SUMMARY AND CONCLUSIONS .....83

    6.1 Summary .....83

    6.2 Conclusions .....86

    6.3 Future Work .....87

REFERENCES .....90

APPENDIX A SUPPLEMENTAL COPYRIGHT PERMISSIONS .....96

## LIST OF FIGURES

Figure 2.1	Gravity override and channeling in a steamflood process.....	6
Figure 2.2	Steam-foam flooding process with minimal gravity drainage and channeling.....	7
Figure 2.3	Typical foam system (Adapted with permission from Schramm 1994. Copyright 1994 American Chemical Society).....	8
Figure 2.4	Foam morphology changes from small spherical bubbles before aging (right) to large polyhedral bubbles after aging (left) .....	11
Figure 2.5	Schematic of foams in a porous medium. Flowing gas is unshaded while trapped gas is shaded in black (Reproduced with permission from Radke and Gillis 1990)..	14
Figure 3.1	Surfactant structures for (a) AOS, (b) Surfonic, and (c) Elevate .....	19
Figure 3.2	Test tube experimental setup showing the cardboard housing used.....	21
Figure 3.3	Types of precipitation that can be observed in test tubes. (a) separation, (b) sedimentation, (c) suspension (Modified with permission from Boeije et al. 2017) ..	22
Figure 3.4	Foam height for fresh surfactants with time using test tubes.....	23
Figure 3.5	Foam texture from run 4 of the fresh experiment for (a) AOS, (b) Surfonic, (c) Elevate. Contrast is enhanced to highlight foam texture.....	24
Figure 3.6	Foam height for aged surfactants with time using test tubes (error bars may be too small to be seen in AOS data).....	25
Figure 3.7	Foam texture for AOS, Surfonic, and Elevate (left to right) after 130 minutes from run 1 of the aged experiments.....	26
Figure 4.1	Experimental setup used for dynamic foam experiments.....	32
Figure 4.2	Foamability comparison between AOS, Surfonic, and Elevate using dynamic test ..	35
Figure 4.3	AOS precipitate at 110 °C due to evaporation of water (highlighted in the red box)	37
Figure 5.1	Apparatus used for foamability and stability during the static foam tests .....	40

Figure 5.2	A view of the HPHT cell and its components.....	40
Figure 5.3	Apparatus used for IFT measurements. The bottom large part is the Eurotechnica HPHT system and the top small part is the DSA100 .....	41
Figure 5.4	Example foam boundary using ImageJ software. ....	44
Figure 5.5	A N <sub>2</sub> bubble protruding from the injection needle in AOS surfactant solution .....	46
Figure 5.6	Kinematics of the decay for AOS while increasing the temperature .....	47
Figure 5.7	Kinematics of the decay for AOS while decreasing the temperature.....	48
Figure 5.8	Kinematics of the decay for Surfonic while increasing the temperature.....	48
Figure 5.9	Kinematics of the decay for Surfonic while decreasing the temperature.....	49
Figure 5.10	Kinematics of the decay for Elevate while increasing the temperature .....	49
Figure 5.11	Kinematics of the decay for Elevate while decreasing the temperature.....	50
Figure 5.12	IFT measurements for AOS, Surfonic, Elevate, and DI water.....	51
Figure 5.13	Condensation comparison at different temperatures for an AOS run .....	52
Figure 5.14	Equilibrium relative humidity vs. temperature.....	54
Figure 5.15	Moisture content and absolute humidity vs. temperature.....	55
Figure 5.16	Averaged initial foam area from the ascending and descending runs vs. temperature (error bars may be too small to be seen for some data points).....	57
Figure 5.17	Averaged half-life from the ascending and descending runs vs. temperature (⌘ symbol indicates the value is higher than reported, error bars may be too small to be seen for some data points) .....	58
Figure 5.18	AOS foam morphology at the half-life at different temperatures (21 °C is not at the half-life as explained above) .....	60
Figure 5.19	Surfonic foam morphology at the half-life at different temperatures.....	61
Figure 5.20	Elevate foam morphology at the half-life at different temperatures .....	61

Figure 5.21	Marangoni flow induced by nonuniform evaporation.....	63
Figure 5.22	Maxwell-Boltzmann energy distribution.....	64
Figure 5.23	Probability of a molecule being in an energy state for a given temperature compared to a molecule at 20 °C.....	64
Figure 5.24	Splitting of an AOS bubble (left to right) into smaller ones reducing the overall foam height at 70 °C (the reference line at the top of the left peak is to illustrate height decay) .....	67
Figure 5.25	Complex phase diagram for a typical nonionic surfactant (W: water, H: hexagonal, L: lamellar, I <sub>1</sub> and I <sub>2</sub> : isotropic phases, S: solid). I <sub>1</sub> is normally a micellar solution. Blue dots represent the temperatures and concentration tested in this work (Adapted with permission from Myers 2020).....	69
Figure 5.26	Thermal degradation effect on AOS foamability.....	70
Figure 5.27	Thermal degradation effect on Surfonic foamability .....	71
Figure 5.28	Thermal degradation effect on Elevate foamability.....	71
Figure 5.29	Thermal degradation effect on AOS stability.....	72
Figure 5.30	Thermal degradation effect on Surfonic stability.....	72
Figure 5.31	Thermal degradation effect on Elevate stability.....	73
Figure 5.32	AOS foamability results for 30, 100, and 200 psia runs .....	74
Figure 5.33	AOS stability results for 30, 100, and 200 psia runs.....	75
Figure 5.34	AOS half-life isotherms in log-log scale.....	76
Figure 5.35	AOS morphology at the half-life for the 30 psia run .....	77
Figure 5.36	AOS morphology at the half-life for the 100 psia run .....	78
Figure 5.37	AOS morphology at the half-life for the 200 psia run .....	79

Figure 5.38 AOS foam regions at 150 °C and 200 psia: (a) top layer, fine foam that decays through liquid inventory loss; (b) middle layer, coarse foam that decays through Marangoni flow; (c) bottom layer, coarse foam that does not exhibit decay .....80

Figure 5.39 AOS bubbles in the middle layer exhibiting splitting decay behavior (left to right) while bubbles in the top layer remain unaffected (taken from 100 psia run at 150 °C) .....81

## LIST OF TABLES

Table 4.1	N <sub>2</sub> density at different temperatures and the corresponding flowrate multiplier used to convert from injected flowrate to column flowrate .....35
Table 5.1	Experimental matrix for the high pressure foamability and stability experiments for AOS .....45
Table 5.2	Physical properties of the aqueous phase for a pure water-N <sub>2</sub> system.....57

## LIST OF SYMBOLS

$A$	Area, m <sup>2</sup>
$AH$	Absolute humidity, kg/m <sup>3</sup>
$E$	Energy, J
$G$	Shear stress, N/m <sup>2</sup>
$g$	Gravity constant, m/s <sup>2</sup>
$m$	Mass, kg
$MW$	Molecular weight, kg/mol
$P$	Pressure, psi
$R$	Radius of bubble, m
$R_g$	Gas constant, J/K·mol
$RH$	Relative humidity
$r$	Radius of curvature, m
$T$	Temperature, K
$V$	Volume, m <sup>3</sup>
$v$	Velocity, m/s
$W$	Work, J
$W_e$	Weber number
$\zeta$	Moisture content, g/kg
$\mu$	Viscosity, N·s/m <sup>2</sup>
$\rho$	Density, kg/m <sup>3</sup>
$\sigma$	Interfacial tension, mN/m

## ACKNOWLEDGEMENT

I would like to first thank my parents, Fahar and Rahma, and my uncle Tariq for setting me on this path and encouraging me to enroll at Colorado School of Mines. Without your encouragement and assistance, I would not have achieved what I have today. Your words marked the start of my journey at Mines, a journey I hope you are proud of.

Mines has been the heart of my career, and for that I would like to extend my deepest gratitude to all my professors here at Mines, both those who taught me in my undergraduate years and those who did so during my graduate studies. Your knowledge imparted, your legacy continued, you will not be forgotten.

A special thank you to Dr. Luis Zerpa for his continued help and guidance over the years with my thesis. Without his assistance and understanding, this work would not have been possible.

Thank you, Joe Chen, for your support throughout the years. Your help with procuring items and designing experimental apparatuses for this work was irreplaceable.

I am grateful to my thesis committee, Dr. Xiaolong Yin, Dr. Carolyn Koh, Dr. James Ranville, and Dr. Hossein Kazemi for their help and advice.

Finally, throughout my journey, I have been surrounded by many friends and my family whose support allowed me to persevere through the trying times. I have fond memories with many of you, those of you who are still with us, and those of you who have left us for a better place.

# CHAPTER 1

## INTRODUCTION

As global energy demand increases and as conventional reservoir oil reserves decline, the drive to maximize oil recovery is greater than ever (IEA 2021; EIA 2022). While carbon dioxide (CO<sub>2</sub>) has gained favorable traction in the recent years as a competitive Enhanced Oil Recovery (EOR) method (Majeed et al. 2021), when it comes to heavy oil, thermal EOR is the mainstay technique. Among those thermal EOR methods, steamflooding and cyclical steam stimulation (CSS) are the most prolific and have been utilized extensively since the early 1960s (Speight 2013; Delamaide et al. 2016). Steam injection is a process in which heat is injected into a reservoir in order to impart some of that injected heat into the oil to reduce its viscosity thereby promoting its mobility. Steam injection processes in heavy oil reservoirs tend to suffer from conformance issues that arise from the low density and viscosity of steam, such as, gravity override and channeling (Dilgren et al. 1982; Hirasaki 1989; Farajzadeh et al. 2012).

Steam foam has been studied in lab scales and implemented on reservoir scales since the early 1970s as a way to combat the issues with typical steam injection processes (Lau and O'Brien 1988a, b; Patzek and Koinis 1990; Patzek and Myhill 1989). However, steam foam comes with its own host of issues that have prevented it from being widely adopted. This is because steam foam requires surfactants to propagate significantly far into the reservoir, and this process is both slow and expensive due to the rapid degradation of surfactants and foams from being exposed to high temperatures.

The study conducted in this work aims to provide a better understanding of foam behavior with temperature in order to facilitate the formulation of improved surfactants that can produce heat

resistant foams. Multiple surfactants were employed and the foam decay was visually observed with changes in temperature to identify mechanisms that dictate the decay of foams.

## **1.1 Research Motivation**

The success of thermal EOR does not only hinge on the viscosity reduction effect of temperature but also on the multitude of factors related to oil chemistry and oil-rock interactions that heat injection promotes (Speight 2013). In 2007, it was estimated that worldwide there were 3,396 billion barrels of heavy oil in original oil in place, half of which exists in the Middle East (Meyer et al. 2007). For these resources, steamflooding and CSS are the most reliable recovery methods and mitigating the conformance issues is paramount to their success.

Surfactants have been studied and successfully designed for a wide range of temperatures (Al-Khafaji et al. 1985; Muijs et al. 1988; Stoll et al. 1993), however, there is yet to be surfactants designed for temperatures higher than 325 °C and even those that can withstand such high temperature suffer from poor foamability and stability (Delamaide et al. 2016). Given the desire to inject more heat into heavy oil reservoirs to increase recovery, the need for foaming surfactant formulations that can withstand elevated temperatures become more vital. However, to design such surfactants, a more robust understanding of foam behavior with temperature is needed, which is the primary motivator for this work.

## **1.2 Scope of Study**

The objective of this study is to generate a better understanding of foam behavior with temperature. Specifically, to visually analyze foam decay and identify mechanisms governing the collapse of foam bubbles and their significance at different temperatures. This is supplemented by experiments conducted in different protocols to compare their applicability for foam decay analysis at higher temperatures.

The first step we took was to generate preliminary data on foams by referring to a commonly adopted method to qualify foams for high temperature analysis. These were the test tube methods and were used to generate data for foamability and stability for three surfactants for fresh samples and aged samples, along with checking for precipitation.

In the second step, we used a glass column to dynamically generate foams and measure their foamability and stability for a small range of temperatures. This method was adopted from literature as a means to visually inspect foam decay with time, however, we noticed that foam decay in the center of the cylindrical column made difficult to analyze the decay of the foam clearly. The data generated using this method was used to compare with the proposed method in this study.

To properly visualize foam decay, we utilized a High-Pressure High-Temperature (HPHT) system with a viewing window that afforded us a wide view of the foam. We started by recording the decay of the foam at near ambient conditions and analyzing the recording. Once we confirmed that the decay of the foam was interpretable (i.e., foam bubbles can be individually observed and studied from the recording), we generated data points at low pressures for a wide range of temperatures. The foamability, stability, morphology, and the decay pattern of the foams at different temperatures were analyzed to identify the changes in the system's behavior as temperature increased. After confirming that different mechanisms dictate the decay of foams at different temperatures, we expanded our data at different pressures in order to check if the behavior changes with pressure. Lastly, we repeated these experiments for all three surfactants in an effort to generalize the behavior of foams.

We would like to note that the surfactants used in this work were anionic and nonionic surfactants and nitrogen was the main gas used in the experiments, so our observations and conclusions pertain specifically to anionic and nonionic surfactant foams in nitrogen only.

### **1.3 Organization of Dissertation**

This dissertation describes laboratory experimental work presented in six chapters. Chapter 1 presents a short introduction, research motivation, and the scope of this work. Chapter 2 includes a literature review on thermal EOR, steam-foam flooding, and foam properties. Chapter 3 presents the experimental setup, methodology, and results obtained from the preliminary test tube experiments. Chapter 4 summarizes the experimental work conducted with dynamic foams including the experimental setup, apparatus, and results. Chapter 5 describes the work performed to visually analyze foam decay and it includes the experimental setup, methodology, and results. Chapter 6 summarizes the experimental work done and the main results obtained, presents our conclusions, and suggests investigative path for future work.

## CHAPTER 2

### LITERATURE REVIEW ON STEAM-FOAM FLOODING AND FOAMS

In this chapter, a short introduction to thermal EOR, steamflooding, and steam-foam flooding is presented. This is followed with a literature review on foam properties such as interfacial tension, foam behavior in both bulk and porous media, and advancements in foam stabilization.

#### **2.1 Thermal EOR**

Heavy oil, which is characterized as oil with high viscosities (over 100 cp) and an API gravity between 10 °API and 20 °API inclusive, often requires the use of heat to recover (Meyer et al. 2007; Speight 2013). Thermal EOR operates on the premise of heating the reservoir to lower the viscosity of heavy oil and increase its mobility which promotes oil flow. Typically, in a thermal EOR, heat is either delivered to the reservoir by injecting a hot fluid (often steam) into the reservoir or is generated in-situ through a process like combustion. Injection of hot water, hot gas, and steam, have been reliably used in field scales to extract heavy oil or even residual conventional oil in depleted reservoirs as these processes also provide the drive energy. Of these fluids, steam is the most common and is used in processes such as steamflooding, CSS, and steam-assisted gravity drainage (SAGD) (Meyer et al. 2007; Speight 2013; Hama et al. 2014).

#### **2.2 Steam Injection**

As steam injection is the most successful of the thermal EOR methods, it has undergone the most development. It is well known that steam processes suffer from heat losses to adjacent rock formations and conformance issues in the form of gravity override and channeling as shown in Figure 2.1 (Dilgren et al. 1982; Hirasaki 1989; Delamaide et al. 2016). Heat losses are inevitable as part of the injected heat is transferred to the rock formation rather than the oil. Gravity override is a

phenomenon pertaining to the difference in density between steam and oil phases and occurs in reservoirs with relatively low horizontal to vertical permeability ratios. Since steam is lighter than oil, the steam will override the oil and sweep mainly the top portion of the reservoir. Channeling, which occurs in layered reservoirs that have high permeability zones, is a direct result of steam having a low viscosity which results in the steam getting diverted from the intended targeted areas to the high permeability zones.

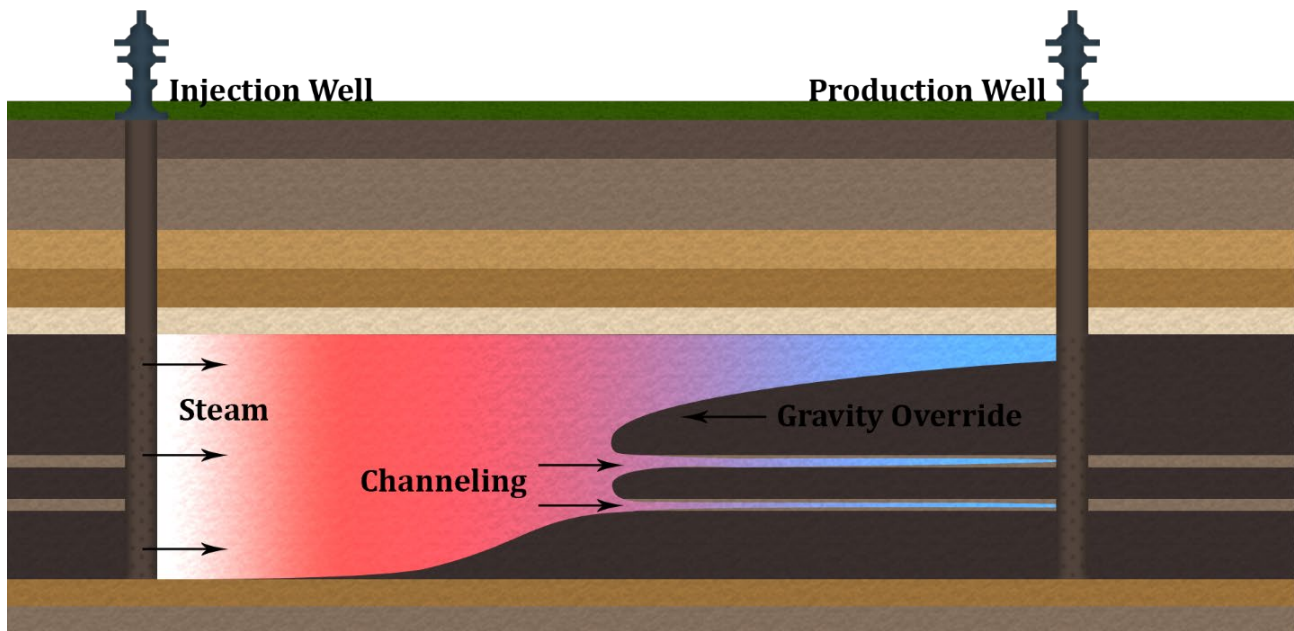


Figure 2.1 Gravity override and channeling in a steamflood process

### 2.3 Steam-foam flooding

Due to the conformance issues plaguing steam injection processes, foam was introduced as a method to control the viscosity of the steam and, to a certain extent, its density (Hirasaki 1989). In this process, a non-condensable gas (NCG) such as nitrogen ( $N_2$ ) or  $CO_2$  is co-injected with steam to generate the foam which is both promoted and stabilized using surfactants, polymers, or nanoparticles, ideally resulting in a flow behavior as shown in Figure 2.2 (Lau and O'Brien 1988a, b; Patzek and Koinis 1990; Patzek and Myhill 1989). As steam is injected, the foam generated blocks the more favorable paths which forces the steam to divert to less favorable paths such as the

lower portions of the reservoir and the less permeable zones. Steam foam, however, is not without problems. Foam breakage and surfactant degradation impede the success of this process.

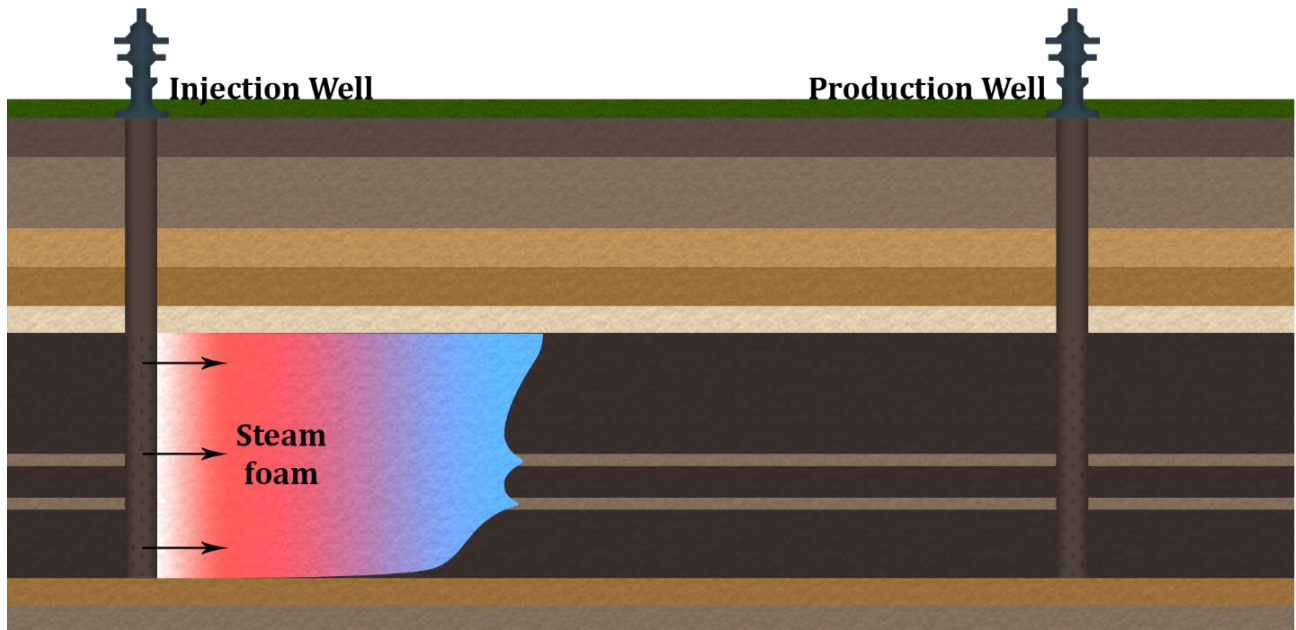


Figure 2.2 Steam-foam flooding process with minimal gravity drainage and channeling

## 2.4 Foam Properties

Foams are a type of colloidal dispersion in which a discontinuous gas phase exists within a continuous liquid phase in the form of dispersed bubbles as shown in Figure 2.3 and they exist in a thermodynamically unstable state as the total interfacial area is naturally driven to be reduced (Schramm 1994; Myers 2020). The work required to create an interface is given by Equation 2.1:

$$W = \sigma \Delta A \quad (2.1)$$

where  $W$  is the work,  $\sigma$  is the surface tension, and  $\Delta A$  is the change in area. Often this equation is represented in terms of force instead and surface tension or interfacial tension (IFT) is represented in units of force/length. Even though foams are thermodynamically unstable, they can be made to last for long periods of time given the right conditions, and in some cases lasting years (Liu et al. 2005; Myers 2020).

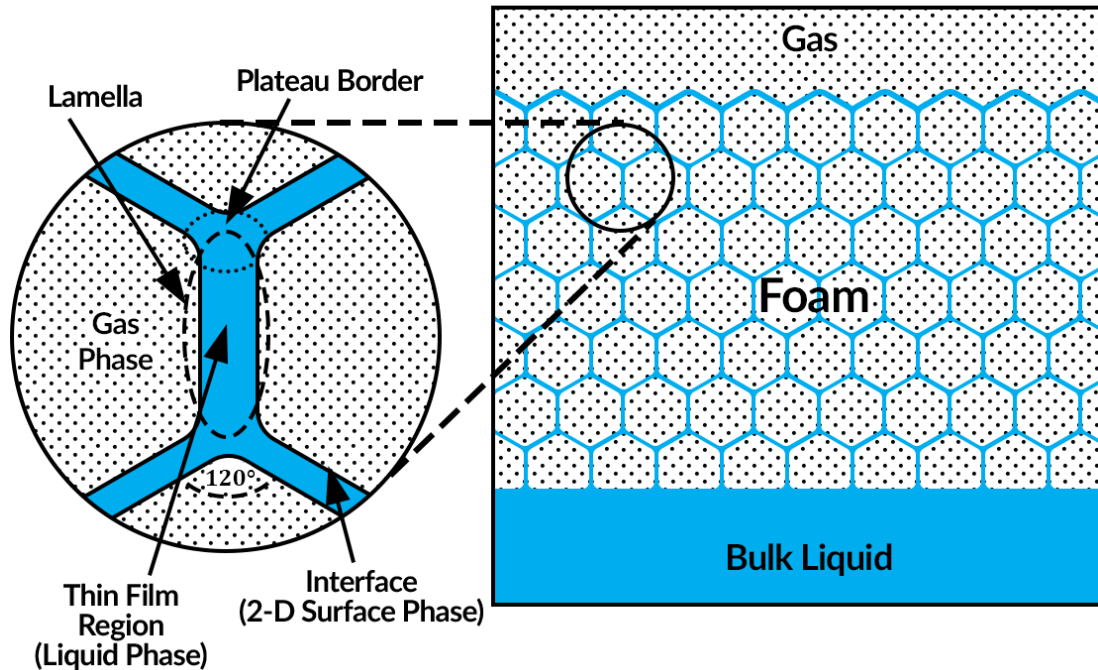


Figure 2.3 Typical foam system (Adapted with permission from Schramm 1994. Copyright 1994 American Chemical Society)

Foam behavior is quite complicated and conflicting explanations can be found in literature for evaluating foam performance owing to the temporary nature of foams, however, in general, foam performance is often evaluated using two criteria: the amount of foam generated (foamability) and the duration of the foam’s lifetime (stability). Foamability is closely related to IFT, while the stability is related to the properties of the liquid film (Tyrode et al. 2003; Wang et al. 2017; Sun et al. 2019).

### 2.4.1 Interfacial Tension

Molecules in bulk fluid are equally affected by molecular forces in all directions, however, at interfaces or surfaces, the molecules are missing a single dimension which creates a net force in the direction of the bulk fluid since they will be attracted to their “like” phase. Surfactants, which are molecules with a lyophobic part and a lyophilic part, adsorb to the interfaces between two phases. This occurs since the lyophobic part is driven away from the solvent and towards the interface in

order to reduce the energy of the system. This results in a lower IFT since less work is now required to bring a surfactant molecule to the interface, effectively increasing the interfacial area (Schramm 1994; Myers 2020).

For surfactants, as they are the primary foam generators, the IFT will depend on the critical micellar concentration (CMC), among other factors. CMC is the point at which the surfactant concentration at the interfaces reaches its maximum and any additional surfactant molecule will tend to aggregate to form micelles. At the CMC, the IFT will reach its minimum. Aside from increasing foamability, lowering IFT can significantly increase oil recovery by both contacting oil and reducing the capillary forces which trap residual oil in pores (Negin et al. 2017).

#### **2.4.2 Foamability**

Foamability is a primary criterion in determining the effectiveness of a foam booster, as higher foamability will correspond to a better vertical sweep efficiency and a higher apparent viscosity during a steam-foam flood. Wang et al. (2016) reported that foam bubbles are produced when the Weber number ( $W_e$ ), which is the ratio of inertial forces, which distort the surface, to surface tension, which restores the surface, exceeds the critical value of one, as shown in Equation 2.2:

$$W_e = \frac{G\mu_s R}{\sigma} \quad (2.2)$$

where  $G$  is the shear stress,  $\mu_s$  is the viscosity of the continuous phase,  $R$  is bubble radius, and  $\sigma$  is the interfacial tension. It can be seen that lower IFT values result in higher foamability, emphasizing the role surfactants play in increasing the foamability. Sun et al. (2019) noted that low IFT values take longer to reach equilibrium thus dynamic IFT plays a role in determining the foamability, however, they also note that no consistent connection in literature has been found between the dynamic IFT and foamability.

### **2.4.3 Stability**

Foam stability is another primary criterion in which to evaluate the success of foam boosters since higher stability will result in longer lasting foams that allow for better reservoir penetration of the steam. While foamability primarily depends on IFT, stability depends on the physical and chemical properties of the surfactant and fluids such as IFT, CMC, viscosity, density, and attractive and repulsive forces, all of which are affected by temperature (Raney et al. 1998; Liu et al. 2005). Foam stability in bulk foams is usually measured in terms of half-life (the time it takes the foam to reach half the original foam volume) as it presents a convenient method of comparing foams at different conditions (Iglesias et al. 1995; Turner et al. 1999; Tyrode et al. 2003; Delamaide et al. 2016). However, in a porous medium, foams are constantly generated and destroyed so the stability values in bulk foams do not directly translate to foams in porous media (Delamaide et al. 2016).

### **2.4.4 Morphology**

Foam morphology or texture refers to the rheology of the foam; the shape and size of the bubbles in the foam. Morphology can help generate insight into foam behavior so it is often in literature that experiments are conducted following the Bikerman method or the Ross-Miles method (Tyrode et al. 2003) in a transparent container. Both methods involve a vertical cylindrical column that is used to contain the foam generated. Foam is typically generated from the bottom of the column. In these experiments, the foam is visually analyzed to measure the height with time, however, when pressures and temperatures above standard conditions are applied, the apparatuses used often require modifications that render visualization of the foam near-impossible. For example, Tyrode et al. (2003) used sensors to measure the foam height in their high pressure foam column; Sanders et al. (2017) used a HPHT column with two viewing windows that did not afford a complete view of the foam; Etminan et al. (2016) used a HPHT cell with a glass slit as a viewing window which restricted their visibility to a small section of the foam; Cuenca et al. (2014) used a

pressure cell that allowed for a complete visualization of the foam, however, the cell was too small and limited the amount of foam they can observe.

Foam morphology is not constant and changes as the foam ages. Initially, foam will be entirely composed of small spherical bubbles since spheres represent the geometry with the smallest surface area for the bubble, but as aging takes place, the liquid between the bubbles will drain downwards due to gravity and gas will diffuse from smaller bubbles to larger ones due to the difference in Laplace pressure in those bubbles. This results in the bubbles meeting at a point known as the plateau border (intersection between three bubbles) and due to the curvature difference between the lamellae (intersection between two bubbles) and the plateau border, liquid will move from the lamellae towards the plateau border resulting in the polyhedral shape of the bubbles as in Figure 2.4 below. The anatomy of a bubble is shown in Figure 2.3.

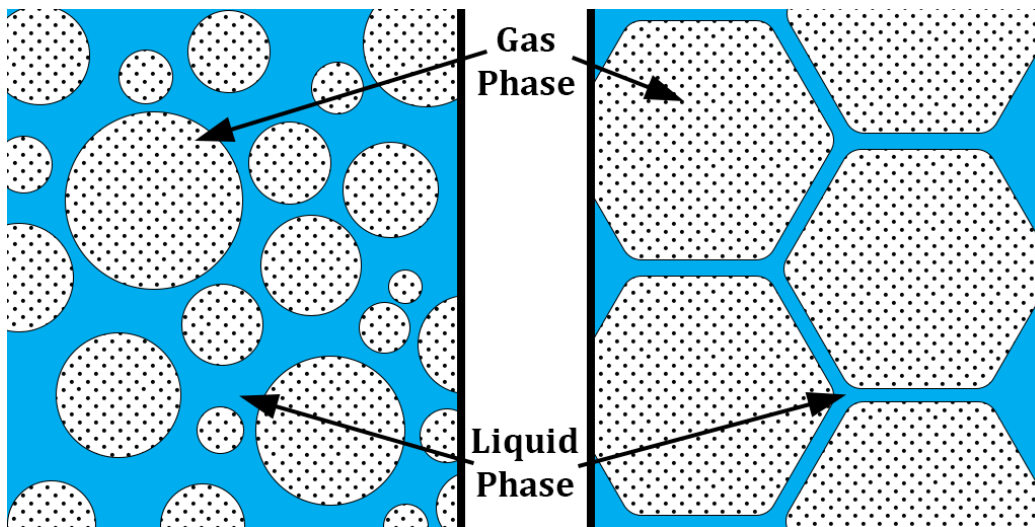


Figure 2.4 Foam morphology changes from small spherical bubbles before aging (right) to large polyhedral bubbles after aging (left)

## 2.5 Bulk Foam Behavior

Bulk foam properties are measured in static conditions where no new gas bubbles are generated. The decay can be quantified by measuring the change in foam volume with time (Turner et al. 1999). Bulk foams are commonly generated through bubbling, where gas is introduced to a liquid

and as it travels upwards the shearing effect causes bubbles to form, and mechanical agitation, where gas and liquid are stirred promoting the generation of bubbles. The destabilization of bulk foams is governed by four main mechanisms: gravity drainage, Ostwald ripening, coalescence, and evaporation (Tyrode et al. 2003; Delamaide et al. 2016; Sun et al. 2019). Gravity drainage refers to the liquid within the foam structure traveling downwards due to gravity which causes the liquid fraction within the film to lower. This process is counterbalanced by capillary forces that drive liquid upwards through small capillaries such as lamellae and is slowed down by the viscosity of the liquid. This balance between drainage and capillary forces results in a foam's characteristic profile (wet at the bottom and dry at the top). Ostwald ripening or disproportionation occurs when gas diffuses from smaller bubbles to larger ones due to the difference in Laplace pressure. Since smaller bubbles have higher curvature, they are at a higher pressure, and the gas inside them will diffuse to neighboring larger bubbles effectively reducing the number of bubbles in the foam. Saint-Jalmes and Langevin (2002) have shown that Ostwald ripening enhances gravity drainage as larger bubbles will drain faster. Coalescence occurs when the film between two or more bubbles become thin and rupture, fusing the bubbles together, which reduces the total surface area in the foam. Evaporation typically refers to the water in the films diffusing into the gas phase which causes thinning and rupturing of the bubble films. Evaporation is usually seen in the foam parts that are in contact with the free gas phase so in a foam column, this is typically the top portion of the foam. Li et al. (2010, 2012) have shown that humidity can considerably affect foamability and stability such that an increase in humidity will often increase both foamability and stability as it reduces evaporation in the top portion of the foam column.

## **2.6 Foams in Porous Media**

Unlike bulk foams, foams in porous media are continuously generated, and so the decay of bulk foams does not directly translate to the durability of foams in field applications (Delamaide et al.

2016). However, this is not to say there is no correlation between the two as Jones et al. (2016) found that in the absence of oil, there is a good correlation between the half-life of a bulk foam and the apparent viscosity of that foam in a coreflood, but in the presence of oil this correlation is reduced.

Foams in porous media can be described as a dispersion of gas separated by liquid lamellae as shown in Figure 2.5. The shape and size of the gas bubbles are limited to the geometry of the pores (Hirasaki 1989; Delamaide et al. 2016; Jones et al. 2016). Foam is generated by snap-off, leave-behind, and lamellae division and destroyed by evaporation and condensation, coalescence by capillary pressure, and gas diffusion (Lau and O'Brien 1988b; Hirasaki 1989; Schramm 1994). Snap-off occurs when a gas finger enters a pore-throat filled with liquid, as the gas exits the pore-throat, the capillary pressure difference between the pore-throat and the larger exit pore-body induces a pressure difference on the liquid surrounding the gas driving the liquid towards the pore-throat. This accumulation of liquid in the pore-throat causes the gas bubble to split forming a new gas bubble. Leave-behind refers to a process whereby gas enters two adjacent pores and as the gas drives the liquid away from the grain, a liquid film is left behind connecting the original grain and the one following it downstream. Lamellae division happens when a gas bubble encounters a branching path and enters both paths which forces the original bubble to split into two to continue flowing downstream. Coalescence of foam by capillary pressure occurs when lamellae exit a pore constriction and as a result stretch. If the stretching is too rapid for the surfactant to flow into the interface, the film ruptures. Gas diffusion occurs due to differences in capillary pressure from the pore geometry. Gas will diffuse from the concave side to the convex side driving the lamellae towards pore-throats and when two lamellae meet, coalescence occurs. Evaporation and condensation as a process refers to the evaporation of water from one side of a lamella and condensation on the other side of the lamella effectively exacerbating the effect of gas diffusion.

The success of steam-foam projects depends on the propagation of surfactants in porous media and the stability of the foams generated. Surfactant propagation is retarded by adsorption onto clay surfaces, precipitation by divalent ions, and partitioning into the oil phase (Al-Khafaji et al. 1985). At higher temperatures, surfactant propagation improves since partitioning and adsorption decrease as the temperature increases (Lau and O'Brien 1988b). However, higher temperatures degrade surfactants more rapidly and destabilize the foam through evaporation and condensation.

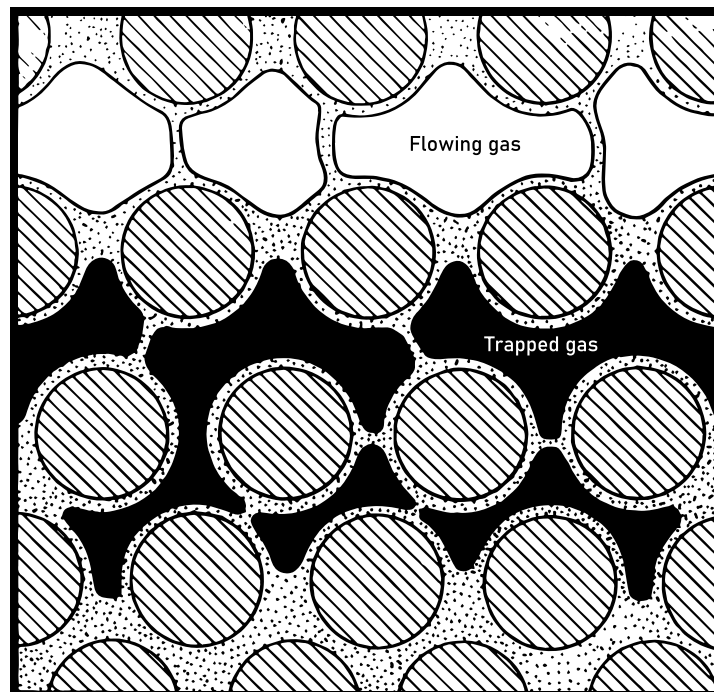


Figure 2.5 Schematic of foams in a porous medium. Flowing gas is unshaded while trapped gas is shaded in black (Reproduced with permission from Radke and Gillis 1990)

## 2.7 Recent Advances in Surfactant Foam Stability Enhancement

Several avenues have been explored to enhance foam performance by stabilizing the liquid films. Surfactants are the most commonly used foam boosters for steam-foam flooding and among those Alpha Olefin Sulfonate (AOS) has been the most common due to its high temperature and salinity resistance (Farajzadeh et al. 2008). Alvares-Jurgenson et al. (2012) studied surfactants for high temperatures and found that adding at least one linear alkylalkoxysulfonate to a surfactant composition with a chain length between 22 and 28 and 1 to 10 alkoxy units made it foamable up to

250 °C and had improved stability in the presence of salts, specifically potassium chloride. Etminan et al. (2016) looked at the foamability and stability of an arylalkyl sulfonate at a temperature of 260 °C and a pressure of 47 bar. Wu et al. (2016) compared the performance of sodium dodecyl sulfate (SDS), AOS, and Dodecyl Dimethyl Betaine (DDB) at temperatures up to 90 °C and found that SDS performed the best in terms of both foamability and stability. Cuenca et al. (2014) explored over 100 formulations using a test tube method at a temperature of 90 °C and at ambient pressure. They followed that with a high temperature visual cell experiments for AOS, Linear Dodecyl Benzene Sulfonate (LDBS), and an AOS/LDBS with a foam booster mix at temperatures up to 200 °C and a pressure of 30 bar and found that the stability of the mix was significantly higher than only AOS or LDBS but at temperatures above 170 °C the stability decreased significantly. They hinted at the Marangoni effect as a possible reason for the stability loss at high temperature due to thermal inhomogeneity, however, they could not confirm it. Wang et al. (2017) studied 10 cationic, anionic, nonionic, and amphiprotic surfactants at temperatures up to 65 °C and found that anionic surfactants were the best in terms of both foamability and stability. They believed that at elevated temperatures the stability of foams was primarily influenced by surface viscosity which caused increased liquid drainage.

Lau (1986, 1988, 2011) and Lau and Borchardt (1991) investigated alkaline steam foam which combines the benefits of both thermal and chemical EOR processes. The concept of alkaline steam foam is that the injected alkali reacts with the petroleum acid in the crude oil to form a primary surfactant (petroleum soap), which is aided by the injected surfactant to allow the alkaline to achieve satisfactory reservoir penetration. They found that petroleum soap was not very stable at high temperatures.

CO<sub>2</sub> has garnered recent favor in steam-foam processes due to some favorable interactions with the oil and reservoir rock both physically and chemically (Bayat et al. 2016). CO<sub>2</sub> can dissolve into

the oil phase which causes swelling, reduces oil viscosity, and can reduce capillary forces through a reduction in IFT between the oil and itself. Chen et al. (2016) investigated the stability of cationic alkyltrimethylammonium surfactants in CO<sub>2</sub> foams at temperatures up to 120 °C and salinities of 22% to find an optimal chain length for these conditions which was less than 15. Zhang et al. (2020) reported that a switchable diamine surfactant exhibited good solubility in ultrahigh salinity brine at 135 °C and less than 20% residual oil saturation. Kamal (2019) conducted a study to compare hydrocarbon and fluorinated surfactants for temperatures up to 80 °C and showed that regardless of temperature, salinity, and gas type, the foamability of hydrocarbon surfactants was higher than that of fluorinated surfactants but the foam stability of fluorinated surfactants was higher.

Nanoparticles were also shown to improve the stability of foams at elevated temperatures (Sun et al. 2019; Al Yousef et al. 2020; Pandey et al. 2021). Bashir et al. (2019) experimented with nanoparticle stabilized surfactant foams using silica and rice husk ash nanoparticles supplemented with polymers and found that the nanoparticles increased foam stability at 85 °C and 2.0% NaCl and that the optimum concentration was 0.2 wt% for both nanoparticles. They also found that polymers such as xanthan gum and acacia gum improved stability even more without affecting the IFT. Emrani and Nasr-El-Din (2017) experimented with AOS surfactants using silica and iron oxide nanoparticles and found that adding iron oxide particles made the foam more stable than silica. They also found that increasing the pressure decreased stability at 25 °C regardless of the use of nanoparticles. Xu et al. (2018) Investigated the behavior of surfactant foams stabilized by positively charged nanoparticles and found that a monolayer and a bilayer adsorption of surfactant on the nanoparticles helped stabilize the foam by enhancing the interfacial elasticity of the films and that monolayer adsorption was more stable.

Polymers are another additive that was studied to improve performance of surfactant foams as polymers retard desorption of surfactant molecules from interfaces thus slowing down drainage

(Romero-Zeron and Kantzas 2005; Majeed et al. 2021). Ahmed et al. (2017) investigated the effect of polymer addition at 80 °C and found that associative polymers improve foam stability by increasing viscosity and lowering drainage. Zhou et al. (2020) conducted experiments with polymer-enhanced foams using partially hydrolyzed polyacrylamide polymer and found that the new foam was more stable than surfactant foams and had high resistance to oil. Raghav Chaturvedi et al. (2018) experimented with polymers and nanoparticles at a temperature of 80 °C and reported that polymer adsorption onto the nanoparticles created complex structures that enhanced foam stability.

## CHAPTER 3

### PRELIMINARY EXPERIMENTS ON FOAMS USING TEST TUBES

This chapter presents laboratory experiments conducted to investigate the feasibility of test tube foam evaluation of surfactants and compare it to other evaluation methods such as dynamic foam testing and PVT cell experiments. It will go over the purpose of these experiments, the procedures, and experimental results.

#### **3.1 Introduction**

Part of this work aims to compare different methodologies of evaluating foam behavior in an effort to point out whether testing foams at lower temperatures can reliably predict their performance at higher temperatures. Test tube experiments are common when evaluating a wide range of surfactants where speed is of the essence and conducting Bikerman experiments or long-term experiments such as coreflows is not feasible. This also provides us with preliminary evaluation of foamability and stability for surfactants.

#### **3.2 Materials**

For these experiments, three surfactants were used. The first surfactant is an Alfa Chemistry, Protheragen Inc. AOS which is an anionic surfactant with chain lengths between 14 and 16 and a reported purity of 92%. Specifically, this surfactant is a Sodium Olefin Sulfonate but for the purposes of this work, AOS will be the abbreviation used for this surfactant for the remainder of this paper. AOS has the appearance of a white powder. The second surfactant is a Huntsman International LLC. SURFONIC® L24-22, hereafter referred to as Surfonic, which is a nonionic ethoxylated alcohol with a chain length between 12 and 16. The reported purity of this surfactant is  $\geq 95\%$ . Surfonic has the appearance of a white soap-like solid. The third surfactant is a The Dow

Chemical Company ELEVATE™ SF 160 LT, hereafter referred to as Elevate, which is a mixture containing the following compounds: ethylene glycol at 10% to 50%, water at 30% to 70%, disodium hexadecyldiphenyloxide disulfonate at 5% to 40%, disodium dihexadecyldiphenyloxide disulfonate at  $\leq 20\%$ , undisclosed sodium salt at  $\leq 5\%$ , and undisclosed chloride compound at  $\leq 5\%$ . Its appearance is that of a colorless or yellowish liquid. The two disodium molecules in Elevate are anionic surfactants. The structure of the three surfactants is shown in Figure 3.1 below.

The test tubes used are made of glass and are approximately 120 mm long and 20 mm in diameter with black plastic caps. The neck of each test tube was wrapped in Teflon tape to minimize evaporation.

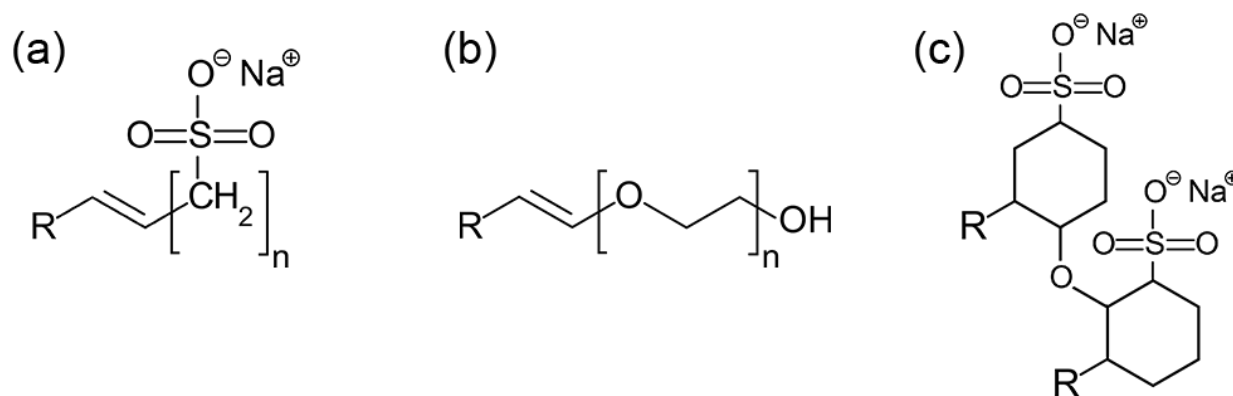


Figure 3.1 Surfactant structures for (a) AOS, (b) Surfonic, and (c) Elevate

### 3.3 Setup and Procedures

Below we will be discussing the methodology used to prepare the surfactant solutions and the test tubes, and the conduction of the foamability and stability experiments for both the fresh and aged surfactants and the aging test.

#### 3.3.1 Preparation of Surfactant Solutions

The surfactant solutions were prepared using different methods given the nature of each surfactant. For all surfactants, a 250 ml plastic bottle was used to contain the solution. To prepare AOS surfactant solution, a wax paper was used to scoop the powder from its original container and

2 g were deposited into the bottle. 198 g of deionized (DI) water was added for a total of 200 g solution at 1 wt%. For the Surfonic, small pieces were scraped from the original container using a plastic pipette tip and placed into the bottle until 2 g are collected then 198 g of DI water was poured into the bottle. As for Elevate, a 3 ml plastic syringe was used to withdraw 2 g of the surfactant and deposit it into the bottle which was then filled with 198 g of DI water. Once all three bottles are filled, the contents are gently stirred so that no foam is formed for approximately 10 minutes then left overnight for the surfactants to fully dissolve into the water. This is especially important for the Surfonic as the solid substance takes approximately 12 hours to dissolve into solution. This process was repeated whenever a new batch of surfactant was needed.

### **3.3.2 Preparation of Test Tubes**

Three test tubes were rinsed with DI water and dried with paper towels. A masking tape with markings was attached to each tube and labeled for each surfactant. The masking tape was marked every 10 mm to facilitate the reading of foam height with the first marking starting at 8 mm from the bottom of the tube. A 170 × 80 × 85 mm (L × W × H) cardboard housing was prepared by cutting three circular holes matching the diameter of the test tube and was used as a convenient way to compare the three solutions side by side as shown in Figure 3.2. The housing was placed on a scale and a test tube was inserted into the middle slot. Using a 3 ml plastic syringe, 5 g of a surfactant solution was withdrawn from its bottle and deposited into the test tube which was then capped and placed in a safe location. This was done for each surfactant solution using the same syringe with multiple flushes of DI water between each surfactant to ensure that no cross contamination was present. The height of liquid in the test tube comes to 18 mm. When all three test tubes were prepared, they were placed into the cardboard housing.

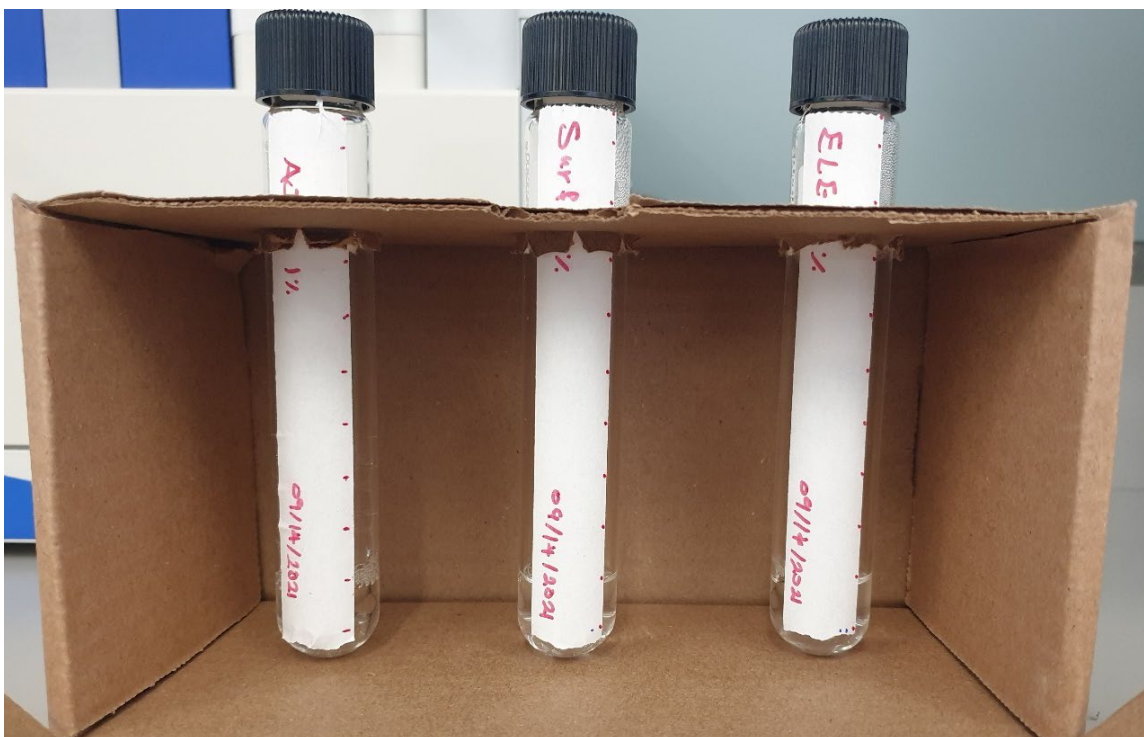


Figure 3.2 Test tube experimental setup showing the cardboard housing used

### 3.3.3 Fresh Solution Foamability and Stability Tests

The experiment was conducted by taking all three test tubes out of the cardboard housing and shaking them all simultaneously by hand for approximately 30 seconds to ensure that foam was adequately generated then placed back into the housing. Immediately a photo was taken of the foam before any decay occurs. Another photo was taken after 5, 10, and 30 minutes from the initial decay. The height of the foam was measured using ImageJ software by drawing a line between the markings on the test tube and the foam surface. This was repeated 10 times.

### 3.3.4 Precipitation Test

The surfactant solutions were left in the housing and remained untouched for four months from the initial stability test. To check for precipitation, each test tube was visually inspected, specifically at the bottom of the tube and at the surface of the liquid, using a flashlight shined from the side of the tube. Two checks were done one after two weeks from the initial stability test and another after four months. Precipitation can occur in different forms as shown in Figure 3.3 and these are:

separation, in which a thin layer of surfactant aggregates at the water-air interface forming a separate layer from the solution; sedimentation, where the surfactant aggregates and settles at the bottom of the test tube; and suspension; where the surfactant forms into large aggregates that are visible throughout the solutions and may end up either settling or separating.

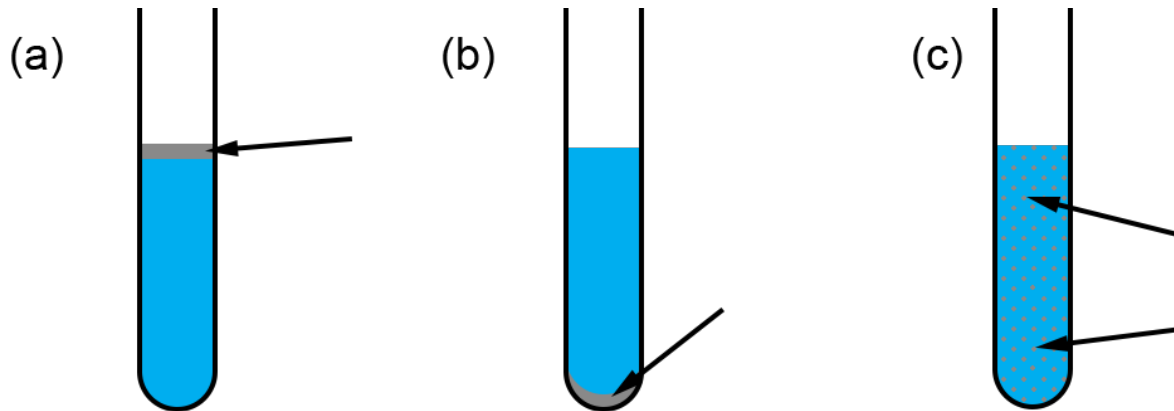


Figure 3.3 Types of precipitation that can be observed in test tubes. (a) separation, (b) sedimentation, (c) suspension (Modified with permission from Boeije et al. 2017)

### 3.3.5 Aged Solution Foamability and Stability Tests

The surfactant solutions were left in the test tubes for four months mostly undisturbed. After the visual inspection for precipitation was done, they were prepared for another set of foamability and stability test. To prepare for the aged tests, each test tube was taken out of the cardboard housing and the height of the liquid remaining was measured then the caps were loosened and DI water was injected using a syringe to restore the original surfactant solution height of 18 mm. Just like the in the fresh tests, 10 tests were performed where the three tubes were taken out of the housing and shaken for approximately 30 seconds then replaced back into the housing. A photo was immediately taken, then another one after 5, 10, and 30 minutes and measurements of the heights were recorded for each time period.

### 3.4 Experimental Results

The results show that AOS was the most foamable and most stable of the three surfactants. Surfonic was better at foaming than Elevate but Elevate proved more stable. Aging did not seem to change this ranking, however, it was observed that both Surfonic and Elevate improved after aging.

#### 3.4.1 Fresh Solution Foamability and Stability Tests

The results show that AOS was by far the most foamable and stable surfactant and was uncontested among the three surfactants, as shown in Figure 3.4. In fact, AOS usually filled the entire test tube with foam meaning it probably would have created more foam than measured. Even after 30 minutes, the foam height of AOS remained that of the entire test tube which is another indication that the foamability could be too high to be measured by the test tube. As for the other two, the experiment shows that Surfonic is more foamable than Elevate but in terms of stability, Elevate which retained 66% of its original foam height after 30 minutes was more stable than Surfonic with its 20% foam height retention.

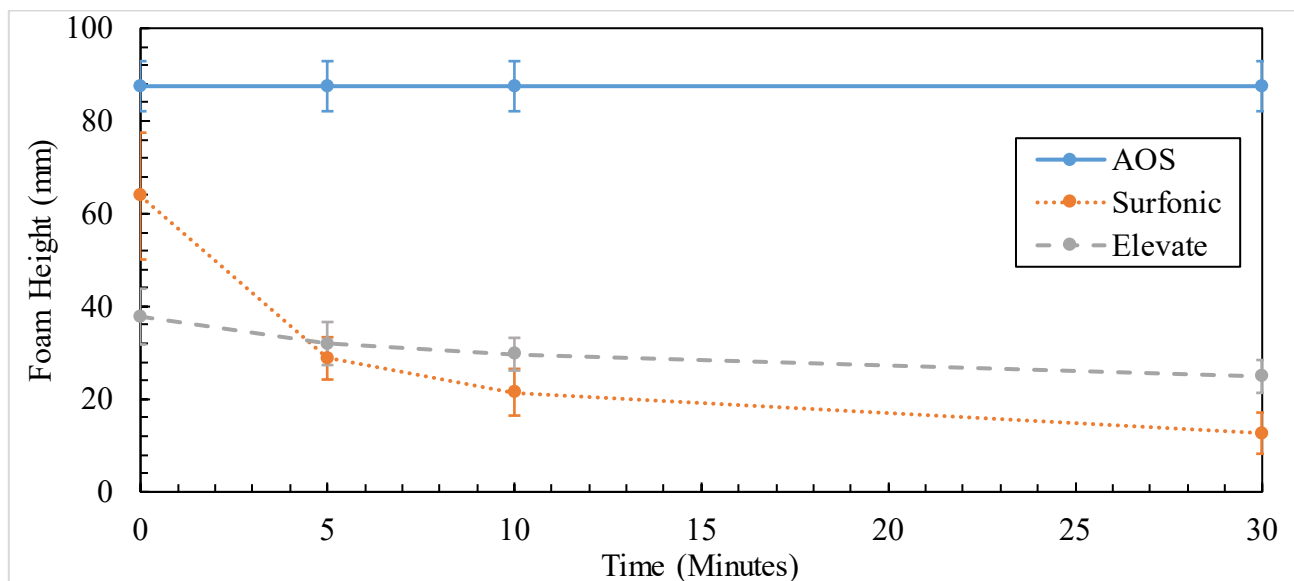


Figure 3.4 Foam height for fresh surfactants with time using test tubes

The texture of the foam was also noted in this experiment and an example is shown in Figure 3.5. In general, Elevate had the finest foam (smallest bubbles size) followed by Surfonic and then

AOS. It was noticed that Surfonic foam texture was inconsistent between runs while the other two had fairly consistent foam textures.

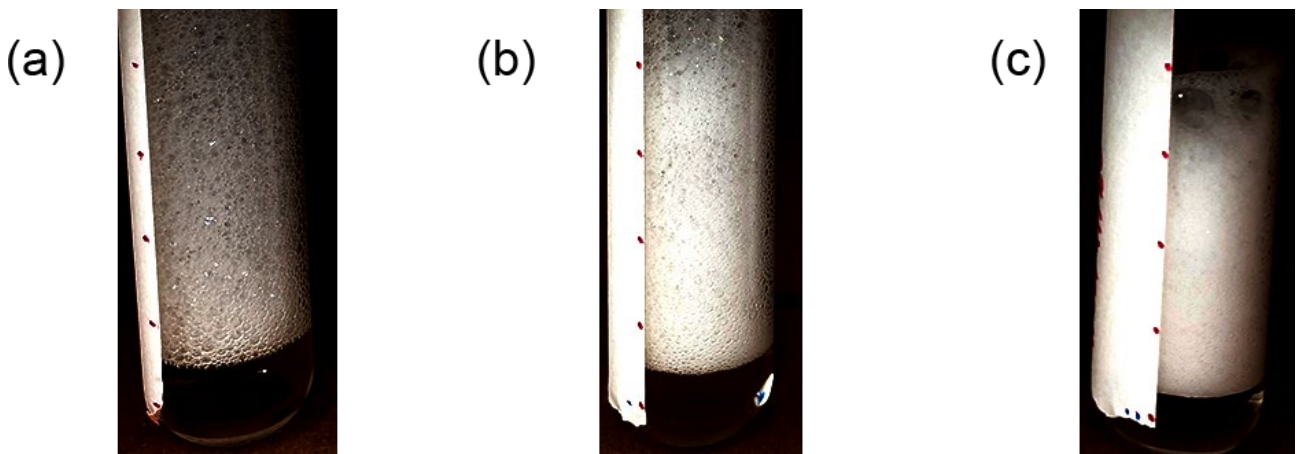


Figure 3.5 Foam texture from run 4 of the fresh experiment for (a) AOS, (b) Surfonic, (c) Elevate. Contrast is enhanced to highlight foam texture

### 3.4.2 Precipitation Test

The precipitation test serves the purpose of filtering surfactants that precipitate over the life of a steam-foam flood. Any surfactant that precipitates, demulsifies, or accumulates is unfit to be used in a steam-foam flood project since breaking out of the emulsion could plug pores which is undesirable. Fortunately, none of the three surfactants showed any signs of breaking out of emulsion as no precipitation or accumulation was visible, neither after two weeks nor after four months.

### 3.4.3 Aged Solution Foamability and Stability Tests

Aging surfactants and testing them can provide insight into their performance once they have resided in the reservoir for a long duration, perhaps into a second steam-foam flood. Aging can be done either by letting the surfactant solution stay at ambient conditions for an extended duration or by heating it up which accelerates the aging process through inducing higher activity on the surfactant. In our case, the solutions were just allowed to rest at ambient conditions for an extended period of time.

It was noticed that the height of the liquid in the test tube for all three surfactants was lower than the initial height at time of preparation. This is due to evaporation since the caps were not forming perfect seals. AOS was recorded at 12 mm, Surfonic at 15 mm, and Elevate at 13 mm indicating different rates of evaporation. To ensure that the tests were consistent with the fresh tests, the liquid height of each surfactant was increased to 18 mm by injecting DI water.

The results in Figure 3.6 show that after aging, AOS was the most foamable of the three, followed by Surfonic, and finally Elevate which is similar to the results from the fresh tests suggesting that aging does not affect the ranking. As for stability, the trend seen in the fresh samples is again repeated here with AOS being the most stable, maintaining 100% of its foam height after 30 minutes, Elevate coming second by maintaining 78% of its original height, and Surfonic coming last, maintaining only 49% of the original foam height. While AOS results did not change after aging, it was noticed that the foamability of both Surfonic and Elevate increased after aging by 22% and 39%, respectively and the stability of the two surfactants increased by 29% and 12%, respectively.

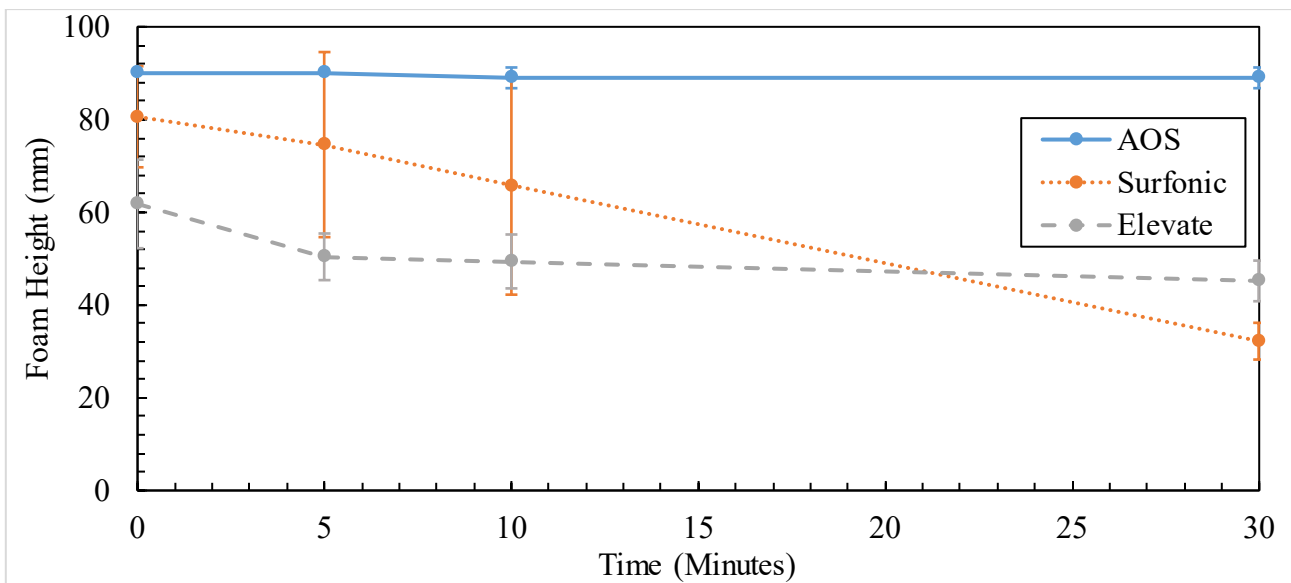


Figure 3.6 Foam height for aged surfactants with time using test tubes (error bars may be too small to be seen in AOS data)

Foam texture after 130 minutes, shown in Figure 3.7, highlights the dependence of foam texture on foam height. Even though all three foams were at different levels (90 mm, 10 mm, and 26 mm for AOS, Surfonic, and Elevate, respectively) the foams' gradual change from spherical to polyhedral seems to be uniform across all three surfactants.

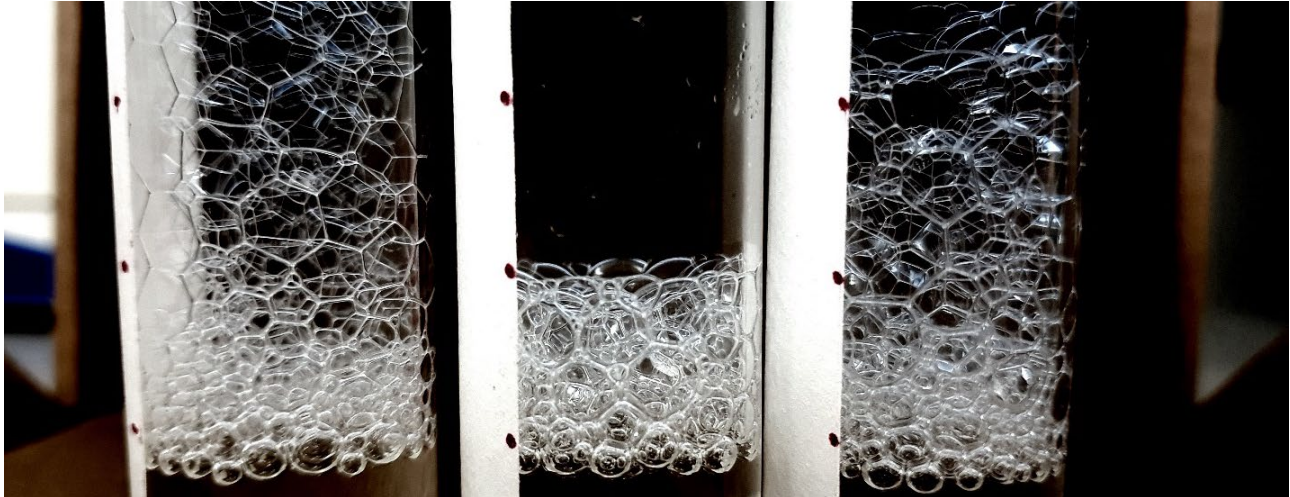


Figure 3.7 Foam texture for AOS, Surfonic, and Elevate (left to right) after 130 minutes from run 1 of the aged experiments

### 3.5 Discussion

It should be pointed out that when it comes to test tube experiments like the ones presented here, the gas used is often air as controlling for the gas in these experiments tends to be difficult. This presents a problem when evaluating foams that are meant to be used in different environments such as steam-foam floods where  $N_2$  or  $CO_2$  are the preferred injectants due to their non-condensable nature. Oxygen, which represents 21% of air, could have an impact of foam behavior that renders such experiments moot given its tendency to react with other substances. Additionally, in these experiments, the temperature was not controlled for and given that ambient temperatures in Colorado change drastically over the winter season (it is not uncommon to see an ambient temperature change of around 3 °C day-to-day in the lab) it is fairly possible that the behavior of the foam changes between experiments.

The foam texture from Figure 3.6 indicates that foam texture as a function of height, at least after much of the aging has taken place, primarily depends on the balance between gravity drainage and capillary forces as those two influence the lamellae thickness. As gravity drains the liquid from the top of the foam to the liquid surface, the lamellae become thinner, and these lamellae form capillaries which get smaller the higher they are in the foam.

This method does present a quick way to evaluate foams in bulk and can be used to quickly filter the different surfactants and qualify some for further analysis, but the question remains on whether or not it should be. We often see that the results from the test tube experiments tend to be used to compare surfactants and choose the better ones for further analysis even though, as mentioned previously, the test environments can differ wildly from the end use environment and even from the secondary test environment. To evaluate this methodology, we qualitatively compare the results shown here with the results presented in Chapters 4 and 5.

The test tube experiments for the fresh surfactants report AOS to be the most foamable with Surfonic coming second and Elevate last. Contrast this with the results to be presented in Chapter 4 using a modified Bikerman method at 70 °C where AOS was the most foamable and Elevate coming as a close second while Surfonic was far behind. If two surfactants were to be qualified for further testing based on foamability only, we may have chosen AOS and Surfonic, leaving behind Elevate which as it turns out is better at foaming than Surfonic using the Bikerman method. The same can be said about the stability. Using the test tube experiments, AOS was by far the most stable with Elevate coming second and Surfonic last, but from Chapter 5 we will see that for 70 °C Elevate was much more stable with Surfonic coming in second and AOS last. This shows that not only does the method employed matter, but the conditions for comparison and qualifications must match that of the target use case for the results to be meaningful. It is worth noting that Surfonic exhibited the greatest variation between runs (during the aged tests) where it could sometimes match AOS in

terms of foamability and short-term stability. We did also notice that aging improved the foamability and stability of Surfonic and Elevate which could indicate that either the change in ambient conditions while testing affected the results or that the surfactants did, indeed, become better at foaming and more stable with time. The increased performance from aging could be explained by the concentration used in this work. As we started with 1 wt% for our surfactant solutions, the aging would have reduced the active concentration of the surfactant to a more optimal value that promotes higher foamability and stability.

Our results highlight a critical flaw of this method, while it is quick at generating results, these results are not necessarily meaningful and caution should be taken when interpreting these results. Perhaps this method is suitable when the conditions of usage for the foams are similar to the test environment such as testing for household soaps.

## CHAPTER 4

### FOAMABILITY EVALUATION USING DYNAMIC FOAM EXPERIMENTS

This chapter presents laboratory experiments conducted to evaluate the effect of temperature on surfactant foams in terms of foamability and stability using a modified version of the Bikerman method and compare the results to those presented in Chapter 3 and those to be presented in Chapter 5. The purpose of the Bikerman method, the methodology, and the foamability results will be discussed.

#### **4.1 Introduction**

The Bikerman method is a dynamic foam experiment, that is, foam is continuously generated until an equilibrium between the generation rate and the destruction rate is achieved. It is a staple when it comes to evaluating foams due to its simplicity and its ability to be tailored to fit specific needs. The experiments in this chapter are based on the Bikerman method and were done to evaluate the foamability and stability of foams at ambient pressure for a variety of temperatures and compare them with test tube results and static foam results.

The concept behind the Bikerman method is to measure the change of foam volume with time. The foam is generated in a transparent cylindrical vessel that allows visual measurement of height change with time. As long as the area of the cylinder is known, we can convert height to volume, and if the area is constant, then there is no need for conversion as the height will serve as a perfect proxy for volume.

The foam can be generated by letting a liquid fall on top of another liquid in the cylinder (Ross-Miles method), or it can be generated at the bottom of the cylinder by bubbling gas through a surfactant solution. During the initial stage, where the bubbles rearrange themselves, foam

movement is dictated by phenomena and properties such as gravity (bubble displacement by size), resistance to displacement (liquid and foam viscosity), capillary action, and the cylinder's geometry. These phenomena and properties are not intrinsic to the foam and thus play no role when trying to measure the stability of the foam. This means that at this point, any measurement of foamability or stability is invalid since one would have to eliminate or minimize the effect of external forces (Iglesias et al. 1995; Turner et al. 1999; Tyrode et al. 2003).

For proper foamability and stability measurements, one would need to wait for the initial stage to reach its end so that a starting point, known as the zero-decay time, can be established. At the end of this stage, the foam should attain a dynamic equilibrium state, where the rate of foam generation is equal to the rate of decay, and the height of the column is at a constant level as per Bikerman's method. At this point, the bubbles have stopped moving and are no longer spherical. The foam column exhibits segregation by age, where the oldest bubbles settle at the top and the youngest at the bottom, and minimal rearrangement by size. The liquid drains downwards such that the foam quality is highest at the top and lowest at the bottom (foam quality is a measure of the amount of gas in the foam structure; higher gas content result in higher foam quality). The higher quality foam is more prone to breaking, so it breaks first. The top layer collapses, and the one below takes its place, dries out, and reaches the breaking point, and collapses. Since older bubbles break faster at the top of the column, at some point, the rate of collapse and the rate of foam generation become equal and dynamic equilibrium is attained. This dynamic equilibrium should generally last a few minutes and be stable. The foam height obtained from this equilibrium is the foamability of the surfactant solution and the foam can now be properly characterized (Iglesias et al. 1995; Morey et al. 1999; Turner et al. 1999; Tyrode et al. 2003).

## 4.2 Materials

The surfactants used in the Bikerman experiments are the same ones described in Chapter 3 and at the same concentration. A heat resistant glass tube was manufactured by Precision Glassblowing to serve as the foam column. The tube is 12 inches long with a diameter of 1 inch and is fused to a one-quarter inch steel tubing at each end which are used to connect to Swagelok tubing. The glass tube is wrapped in a HTSAmptek electric heating tape connected to a HTSAmptek BBA-300 SERIES Temperature Controller which is used to heat the system as needed. Two thermocouples are used to measure the system temperature; one connected to the temperature controller and is placed inside the tube approximately 2 inches from the top of the tube, while the other one is connected to a laptop through an Arduino setup and is freely moved around to check the temperature at different points in the system. The glass column is partially wrapped in one-half inch fiberglass insulation to reduce heat losses in the system (this covers approximately three-quarters of the glass tube while still allowing us to view the entire foam column unobstructed). The tube is connected to a plastic mixing chamber that serves as the foam source which is fitted with a one-quarter inch plastic tubing with a sparger assembly near its bottom. This chamber is connected to a Teledyne ISCO Model 500D pump. An industrial grade N<sub>2</sub> tank with a purity of 99.99% is used as the gas source and is connected to the ISCO pump. It is fitted with a Harris® Specialty Gas pressure regulator with a maximum pressure inlet of 4000 psi and outlet of 400 psi. The mixing chamber, foam column, and temperature controller are all placed inside a fume hood in case of any pressure buildup that results in the column exploding. The setup is shown in Figure 4.1.

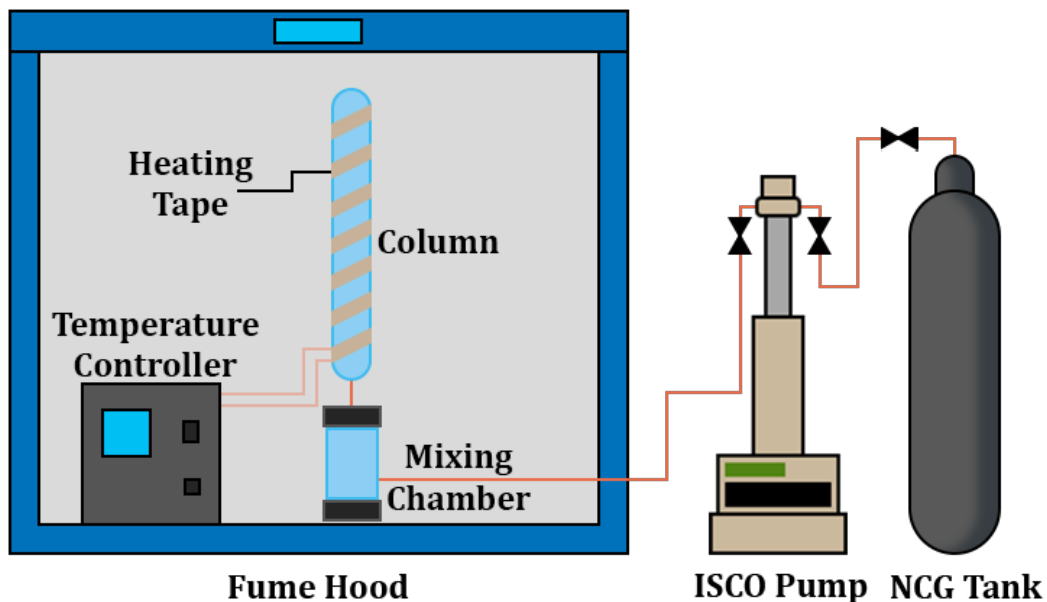


Figure 4.1 Experimental setup used for dynamic foam experiments

### 4.3 Setup and Procedure

For each surfactant, the mixing chamber needs to be prepared and the ISCO pump needs to be refilled with  $N_2$  before an experiment can be performed. The process is detailed below.

#### 4.3.1 Preparation of the Mixing Chamber

Before starting the experiment, the mixing chamber was disconnected from the system and cleaned thoroughly with DI water several times. Both water and air were circulated through the sparger in alternate order to remove any residual surfactant that may be stuck in the sparger. The sparger was considered clean once no more foam is generated when circulating either air or water through it. Once cleaned, the chamber was dried and approximately 200 ml of surfactant solution was poured into it. Immediately, the sparger tubing was connected to the ISCO pump to ensure that no liquid leaks out and the chamber was capped and connected to the glass column.

#### 4.3.2 Preparation of Nitrogen for the Experiment

With the mixing chamber connected to the system, setting up the  $N_2$  for the experiment can begin. First, the ISCO pump was filled with  $N_2$ . This was done by extending the piston to the zero

position, the pump was empty now. The outlet valve was closed and the inlet valve was opened. Then the N<sub>2</sub> tank valve was slowly opened and the pressure regulator was adjusted from the closed position to approximately 25 psi. The pump's piston was then fully retracted to withdraw approximately 500 ml of N<sub>2</sub>. After that the pump inlet valve was closed and the outlet valve was slowly opened to depressurize the pump. This generated foam in the system and allowed pre-filling of the mixing chamber with foam so that foam could immediately propagate into the column when the experiments were started.

### **4.3.3 Running the Experiment**

With both the mixing chamber and the N<sub>2</sub> ready, the experiments could start. The temperature controller was turned on and set to the desired temperature first. Once the temperature of the system stabilized at the target temperature, it was allowed to stay for a minimum of 10 minutes to ensure as much temperature uniformity in the system as possible. After this, N<sub>2</sub> was injected into the mixing chamber through the ISCO pump which controlled the flowrate. The N<sub>2</sub> flowing through the sparger creates small bubbles that propagate from the mixing chamber into the glass tube. As the bubbles move up the tube, they are heated to the system temperature.

The flowrate of N<sub>2</sub> was continuously adjusted so that the equilibrium foam height in each experiment was approximately 100 mm. Equilibrium height was determined when the flowrate did not need to be adjusted for approximately 10 minutes. This was done to ensure that the amount of foam generated never exceeds the glass tube height. The flowrate which results in the target equilibrium height was recorded. The process was initially meant to be repeated for temperatures of 20 °C, 50 °C, 70 °C, 90 °C, and 110 °C, however, due to the hydrostatic pressure from the liquid in the mixing chamber above the sparger, data for 20 °C and 50 °C could not be generated. The hydrostatic pressure of the water in the mixing chamber required a minimum flow rate of around 5 ml/min to generate consistent bubbles. This meant that the minimum flowrate of 5 ml/min resulted

in a foam height that overflowed the glass column. For that reason, data for only 70 °C, 90 °C, and 110 °C are presented.

This design choice to vary the injection rate rather than using a constant flowrate for the N<sub>2</sub> was due to the difficulty finding a suitable universal flowrate for N<sub>2</sub> which generated foam heights that are measurable within the confines of the 12-inch glass column; flowrates that were adequate for a surfactant would overflow for others, while flowrates that were adequate for another surfactant would barely generate any foam for other.

#### **4.4 Experimental Results**

The results show that for all three temperatures, AOS required the least flow rate to generate 100 mm high foam which translates to AOS being the most foamable of the three surfactants. On the other hand, Surfonic showed the least foamability at all three temperatures with Elevate being somewhere in between the two but closer to AOS at lower temperatures, as shown in Figure 4.2. It was observed that the flowrate and temperature exhibit a linear relationship along the temperature range tested. Additionally, the slopes in the figure indicate each surfactant's sensitivity to temperature. Elevate showed the highest sensitivity to temperature while AOS and Surfonic were less sensitive to temperature. Extrapolating the data shows that at 64 °C, AOS and Elevate intersect and flip such that, below that temperature, Elevate becomes the most foamable of the three. Table 4.1 shows the density of N<sub>2</sub> at the different temperatures (calculated using Soave-Redlich-Kwong equation of state) where 20 °C corresponds to the temperature in the ISCO pump. The multipliers are used to convert the reported flowrate by the ISCO pump to the actual flowrate in the foam column assuming that the N<sub>2</sub> is heated to the column temperature.

Table 4.1 N<sub>2</sub> density at different temperatures and the corresponding flowrate multiplier used to convert from injected flowrate to column flowrate

Temperature (°C)	N <sub>2</sub> Density (kg/m <sup>3</sup> )	Multiplier
20	1.1664	1.00
70	0.9956	1.17
90	0.9407	1.24
110	0.8915	1.31

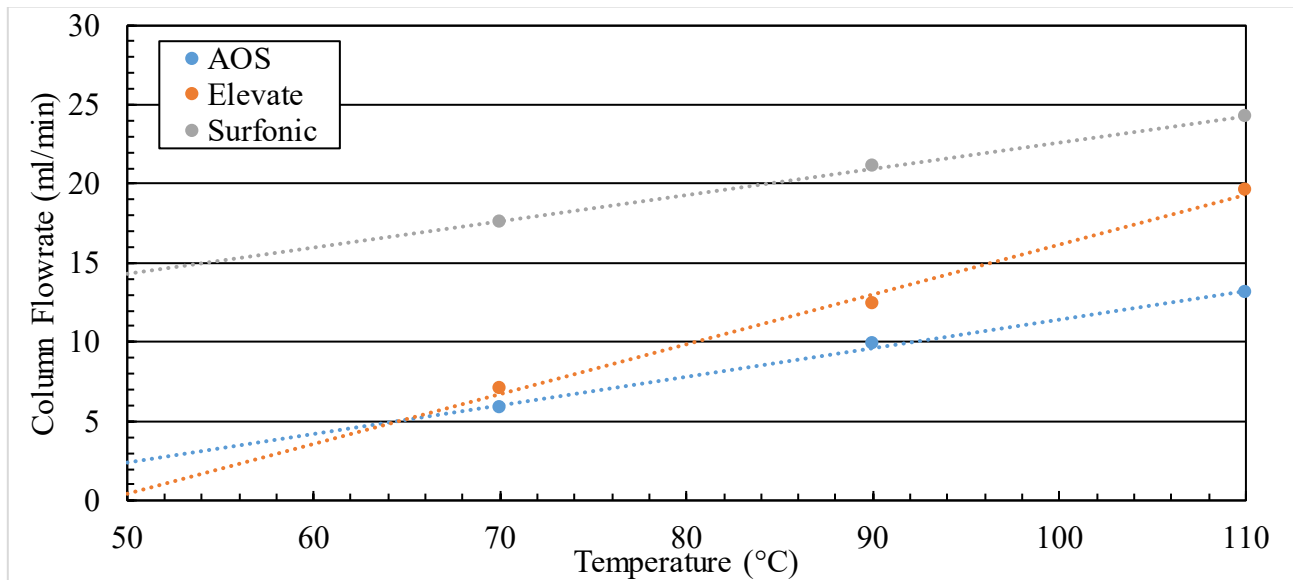


Figure 4.2 Foamability comparison between AOS, Surfonic, and Elevate using dynamic test

#### 4.5 Discussion

A few interesting behaviors can be interpreted from this experiment. The first is that different surfactants exhibit different degrees of sensitivity to temperature which is apparent from the slopes in Figure 4.2 and highlights the importance of testing surfactants at or close to their use case temperature. For example, just because Elevate outperforms Surfonic at the temperatures tested, does not guarantee that this relationship holds true for all temperatures. Often, it is seen that foams are evaluated at some conditions (e.g. standard conditions) and qualified for further testing based on those results, however, the secondary tests are done at different temperatures (e.g. reservoir

temperatures) which could result in some surfactants being dropped even though their performance could have very well matched or exceeded the qualified samples.

The second behavior of interest is the glaring linear behavior between the required flowrate of N<sub>2</sub> and temperature. Common sense dictates that at temperatures above the boiling point of water (94 °C at 12 psia) the required flow rate would be significantly higher than at temperatures below the boiling point due to the evaporation taking place, which is confirmed by the presence of steam coming out of the top of the glass column. Indeed, this suggests that another mechanism is taking place due to the elevated temperatures. We believe that the expansion of the N<sub>2</sub> as it rises through the column increases the volume of the foam and since we are at temperatures near the boiling point, the rate of evaporation is low enough that the destabilization caused by evaporation of water is not sufficient to counteract the N<sub>2</sub> expansion. At temperatures much above the boiling point, the evaporation rate is expected to be much higher to the point of overshadowing any foam volume increase from N<sub>2</sub> expansion.

The third observation was made at 110 °C for AOS only. It was observed that AOS would sometimes precipitate out of solution, most likely due to localized variations in concentration and temperature. As shown in Figure 4.3 AOS precipitation only occurred at the top of the column where evaporation was highest. When this happens, foam propagation is retarded significantly until enough of the precipitate is redissolved in solution allowing the foam to reach its equilibrium height. An implication of this for reservoir use is that the precipitate could plug pores and the subsequent loss of surfactant could permanently reduce the effectiveness of a steam-foam flood. It is of use to note that none of the tested surfactants showed any form of precipitation in the precipitation tests discussed in Chapter 2 and none of them precipitated at lower temperatures. While increasing the temperature should increase anionic surfactant solubility in water and thus lower the possibility of precipitation, the increased temperature does cause water to boil which

creates localized fluctuations in surfactant concentration. This further demonstrates the importance of testing at use case temperatures to catch possible problems that would otherwise go unnoticed at lower temperatures.

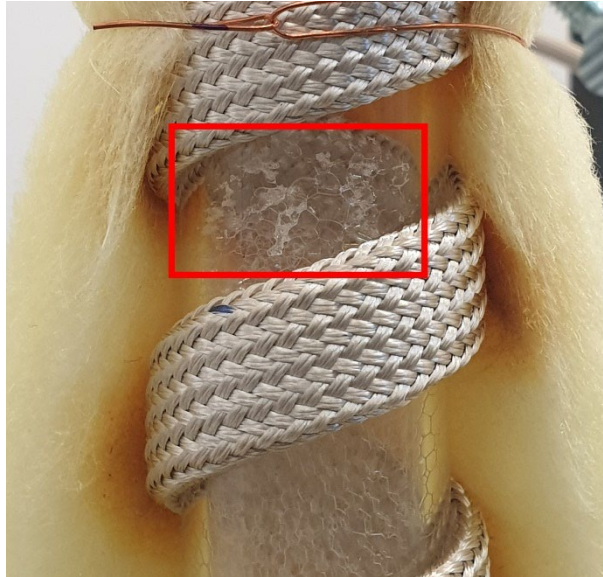


Figure 4.3 AOS precipitate at 110 °C due to evaporation of water (highlighted in the red box)

## CHAPTER 5

### STATIC FOAM EXPERIMENTS IN CLOSED ENVIRONMENTS

This chapter will present laboratory experiments conducted for a closed environment static foam to evaluate foam behavior with temperature, and will discuss the purpose, methodology, and experimental results in regards to the effect of temperature on interfacial tension, humidity, foamability, stability, morphology, and decay pattern.

#### **5.1 Introduction**

Unlike the dynamic foam experiments where pressure could not be controlled due to the fragility of the glass column, the static foam experiments presented in this chapter are performed in a HPHT cell that utilizes a sapphire window allowing us to visually analyze the foam while having precise control of the temperature and the ability to pressurize the system. These experiments will serve as the bulk of this project and are also based on the Bikerman method. However, since these experiments are static, instead of continuously flowing  $N_2$  through the liquid solution, a closed environment is established that consists exclusively of  $N_2$  and surfactant solution where the foam is generated through agitation and measurements are taken after the agitation stops. Mechanical stirring of the system is our way of imparting energy into the system to generate the foam.

#### **5.2 Materials**

The surfactants used in these experiments are the same ones presented in Chapter 2. Each surfactant solution was prepared two days prior to conducting experiments with it to ensure that a fair comparison is made between all surfactants. The apparatuses used for foamability and stability test and the apparatus used for IFT measurements are discussed below.

### 5.2.1 Foamability and Stability Apparatus

For foamability and stability tests, we used a Core Lab PVT SYSTEM 400/1000 – Full Visibility (Figure 5.1) apparatus that was originally designed for reservoir fluid analysis such as composition expansion, differential vaporization, viscosity measurements, Z factor determination, and other tests. The system is designed to work with temperatures up to 200 °C and pressures up to 14,500 psia. The HPHT cell is made of steel, with a cross-sectional area of 3,800 mm<sup>2</sup> and a working volume range of 6.27 ml to 400 ml. The cell volume is adjusted using a motorized piston that is indirectly connected to the cell through a hydraulic packing system that guarantees leak-free operation of the cell. A sapphire viewing window is fitted that looks top-down into the cell facilitating full view of the cell as shown in Figure 5.2, albeit one sided only. On the other end of the cell, a magnetic stirrer allows mixing of the cell's contents without employing any mechanical attachment into the cell. The cell has a built-in electrical temperature control system and comes with thermal jackets to minimize heat losses and reduce temperature fluctuations. A digital camera is equipped that captures the cell's contents to facilitate recording of experiments and is connected directly to a nearby computer. A N<sub>2</sub> tank is connected to the system and is used as the N<sub>2</sub> source and to pressurize the system.

The cell is connected to two pneumatic valves that serve as the main valves to isolate the cell from the outside. Each pneumatic valve is connected to four other manual valves. Of the four top valves, three are used: one is connected to the N<sub>2</sub> tank, another is connected to an atmospheric pressure sensor, and the last is used as an inlet for surfactant solution. Of the four bottom valves, none are used except one as an outlet for both cleaning and expelling surfactant solution and N<sub>2</sub> from the cell.

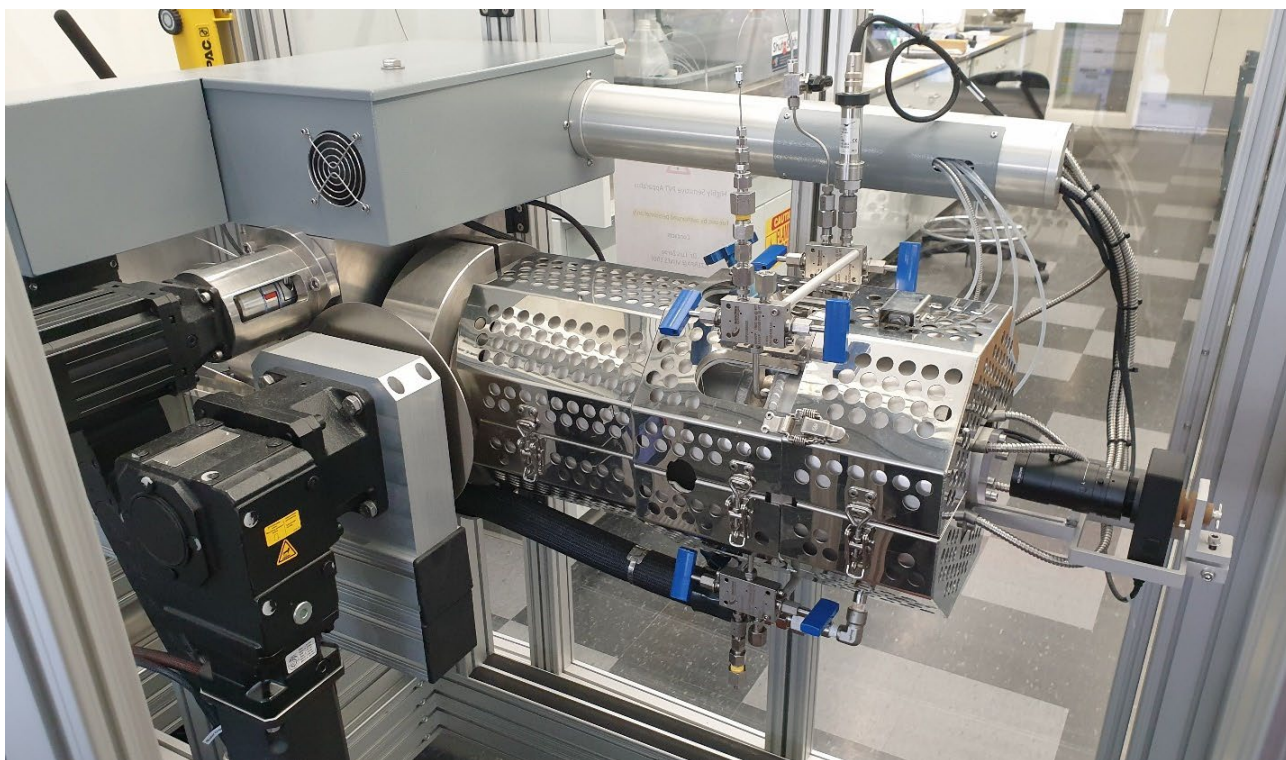


Figure 5.1 Apparatus used for foamability and stability during the static foam tests

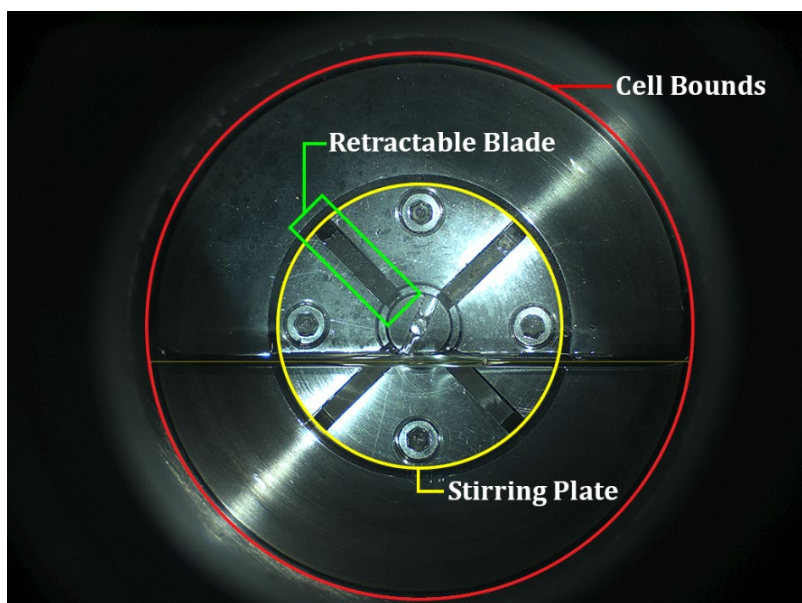


Figure 5.2 A view of the HPHT cell and its components

### 5.2.2 IFT Measurement Apparatus

The IFT measurement apparatus we used for this project was composed of two pieces of equipment, a HPHT system manufactured by Eurotechnica and a Drop Shape Analyzer (DSA) 100

by KRÜSS GmbH as shown in Figure 5.3. The HPHT system is made of a cylindrical vessel with viewing windows on either end. The vessel is connected to an electrical temperature control system and is equipped with a manual pressurizing mechanism. The vessel has four ports of which three are used. The top port is used to fill the cell with surfactant solution, the bottom port was used to inject the N<sub>2</sub> into the cell during experiments, and a side port was connected to a temperature sensor. The DSA 100 rests on top of the Eurotechnica HPHT system and contains three main parts, a diffused light source that serves to illuminate the vessel's contents, a camera to record the contents of the vessel and to analyze the images, and a dosing unit (a motorized syringe for automated liquid/gas injection) which is not used in this project as all injection was done manually.

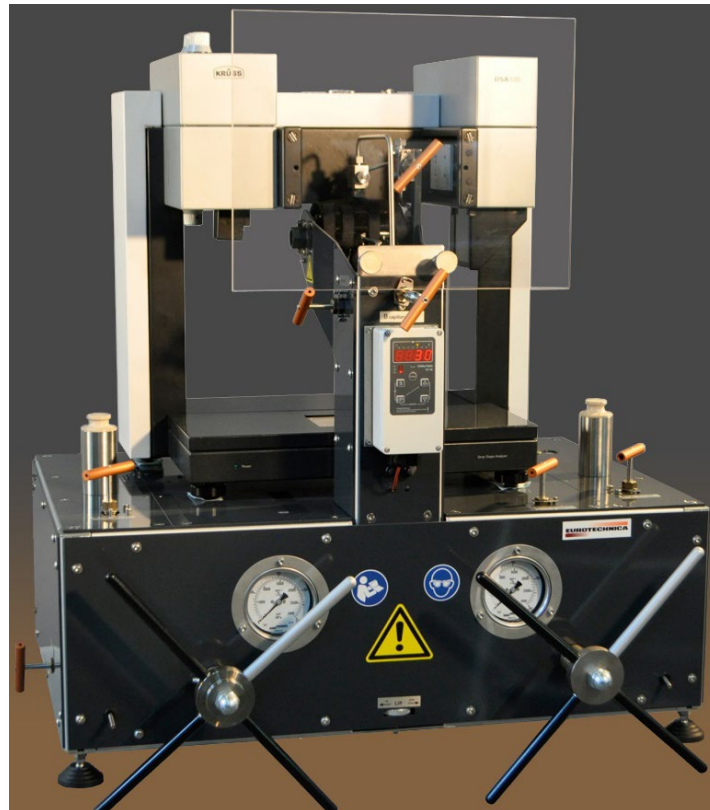


Figure 5.3 Apparatus used for IFT measurements. The bottom large part is the Eurotechnica HPHT system and the top small part is the DSA100

### 5.3 Setup and Procedure

The setup and procedure for performing the foamability and stability test and the IFT measurements will be discussed below.

#### 5.3.1 Foamability and Stability Procedure

Due to previous crude oil residuals in the PVT system, we needed to perform a one-time flushing procedure to remove all the oil in the system. This was done by initially circulating toluene through the system until no more crude oil was produced. After that, toluene was injected into the cell to soak for a day which was then flushed out using more toluene. This was repeated several times. After this, the cell was flushed with DI water and AOS surfactant solution several times until no more clouding of the cell was visible from injecting surfactant solution (clouding of the surfactant solution indicates the presence of crude oil or toluene in the system).

Before conducting an experiment, the cell was cleaned with DI water several times to ensure that any liquid in the cell and connection ports was not leftover from previous surfactant runs. This was followed by purging the cell with  $N_2$  to remove any liquid in the cell and to ensure that no air was left in the cell. To prepare the cell with the surfactant solution, the motorized piston was set to the smallest volume position (6.27 ml), a disposable 30 ml syringe was filled with the surfactant solution and connected to one of the top inlets of the cell. The cell volume was expanded to 30 ml by retracting the piston. The expansion of the cell withdraws the surfactant solution from the syringe into the cell. Once a volume of 30 ml was reached, the piston was moved back to a cell volume of 15 ml, this pushes any excess liquid and gas out of the cell, leaving only the surfactant solution in. Following that, the valve connecting the surfactant was closed and another valve connecting to the  $N_2$  tank was opened. The pressure regulator on the  $N_2$  tank was slowly opened to pressurize the system slightly and ensure flow of  $N_2$  into the cell. The piston was then set to the 35 ml position which fills the remaining unoccupied volume (20 ml) in the cell with  $N_2$ . This procedure

was designed to maximize efficiency and minimize contamination of the cell with undesired liquids or gases.

Due to the stirrer requiring a minimum cell volume of 35 ml to operate, we had to work with this volume. However, at this volume, the depth of cell is approximately 9 mm which was deemed small enough to satisfy our requirement to use the cell's cross-sectional area as a proxy for the volume and to treat the cell as a two-dimensional system. This allows us to simply use the foam as seen through the viewing window in our stability and foamability calculations without concerns for the depth.

For each surfactant, 12 experiments were carried at 6 different temperatures (21 °C, 30 °C, 40 °C, 50 °C, 70 °C, and 90 °C). The first 6 experiments were carried while increasing the temperature from 21 °C to 90 °C testing each temperature in between, while the second 6 runs were performed while the temperature was lowered from 90 °C to 21 °C, again testing each temperature in between. The second set of runs allows us to test for the effect of thermal degradation on the surfactants and also to test for repeatability. During each experiment, the cell was heated to the target temperature and allowed to soak for 60 minutes to ensure thermal equilibrium within the cell. After that, the image capture system was turned on and was set to capture 1 image per 30 seconds (determined to be reasonable from prior test runs). After exactly 10 seconds, the stirrer was turned on and ran for exactly 60 seconds to allow for thorough mixing of the surfactant solution and N<sub>2</sub> for foam generation. Once the stirring was done and the stirrer was turned off, the instrument was left to record the foam decay until almost no foam was left in the cell, which can range from several hours to days. Once the run was done and the foam has completely decayed, the images were taken and processed on a computer using ImageJ software. The images were analyzed in chronological order where images with no significant change in foam volume are discarded. For each analyzed image,

using ImageJ, a border was drawn around the foam perimeter (Figure 5.4) and the area inside was automatically calculated. This process was repeated for each of the three surfactants.

This method is a version of the Bikerman experiment wherein the area of the foam is used as a proxy for the volume instead of the foam height, as in Equation 5.1 below:

$$\text{Stability} = \frac{V}{V_0} = \frac{A}{A_0} \quad (5.1)$$

where  $V$  is the volume,  $V_0$  is the initial volume,  $A$  is the area, and  $A_0$  is the initial area. This also affords us more surface area to observe the foam and its morphology as opposed to using a tube and having the middle parts of the foam obscured by the foam facing the walls of the tube.

We would like to point out that a limitation of our adopted approach is that since we operate at constant volume and since we do not have a safe pressure venting system in place, the cell pressure increases with increasing temperature. Changing the cell volume would compromise the integrity of the experiments, specifically, increasing the cell volume to reduce the pressure would not allow us to use the cell areas as a proxy for volume anymore and the constant piston movement throughout the runs to equilibrate pressure would disturb the system mechanically.

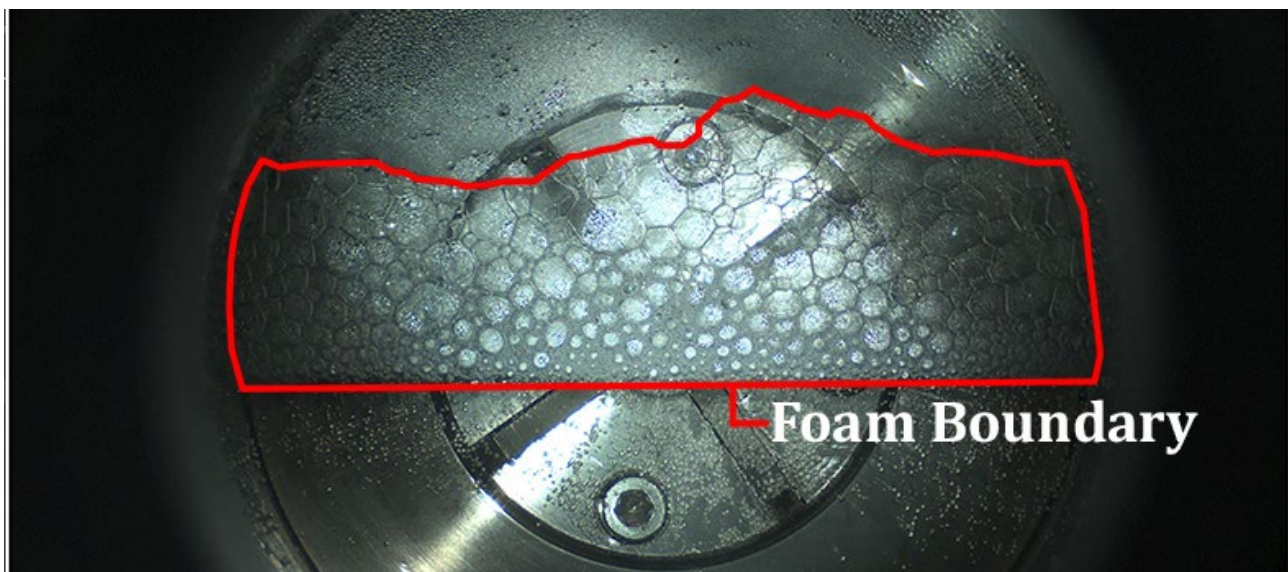


Figure 5.4 Example foam boundary using ImageJ software.

### 5.3.2 High Pressure Stability and Foamability Procedure

AOS was subjected to another set of experiments at higher pressures to evaluate the effect of pressure on the observed foam decay behavior with temperature. However, these experiments were only conducted while increasing the temperature for a total of 27 experiments. A set was conducted at a starting pressure of 30 psia, another at 100 psia, and the last one at a starting pressure of 200 psia, all of which had a drastic pressure increase as temperature was increased. The experimental matrix for this is shown in Table 5.1 to illustrate the increase in pressure with temperature. The procedure followed in these experiments is the same one described in the previous section.

Table 5.1 Experimental matrix for the high pressure foamability and stability experiments for AOS

Temperature (°C)	Set 1 Pressure (psia)	Set 2 Pressure (psia)	Set 3 Pressure (psia)
21	32	100	198
30	36	107	199
40	35	107	205
50	32	109	212
70	36	117	229
90	45	127	250
120	53	154	291
150	88	201	351
180	155	271	441

### 5.3.3 IFT Measurement Procedure

For each surfactant, the HPHT vessel is filled with that surfactant solution using a 100 ml glass syringe. Then, the temperature regulator is turned on and set to the target temperature. Once the temperature of the system reaches the target, it is allowed to soak for approximately 60 minutes to ensure the cell is at equilibrium. A one-sixteenth inch needle that is connected to the bottom of the cell is used to inject N<sub>2</sub> into the surfactant solution. This needle protrudes into the middle of the cell

such that a bubble formed at the tip of the needle is completely surrounded by the surfactant solution. For each temperature, a single bubble of N<sub>2</sub> is introduced, as shown in Figure 5.5, and its shape is analyzed using the pendant drop method. The shape of a bubble is related to the IFT and gravity. As a bubble is formed, the pressure difference between the two phases is related through the Young-Laplace equation:

$$\Delta P = \sigma \left( \frac{1}{r_1} + \frac{1}{r_2} \right) \quad (5.2)$$

where  $\Delta P$  is the pressure difference,  $\sigma$  is the IFT, and  $r$  are the radii of curvature of the bubble's surface. Ideally the bubble should be spherical but due to the difference in density between the two phases the bubble deforms and its shape resembles that of a pear. The degree of deformation is related to the IFT and the weight of the bubble and as long as the densities of the two phases are known, the IFT can be calculated. This calculation is done automatically by the DSA100 through the use of numerical curve fitting. The measurements were repeated for temperatures of 21 °C, 30 °C, 40 °C, 50 °C, 70 °C, and 90 °C.

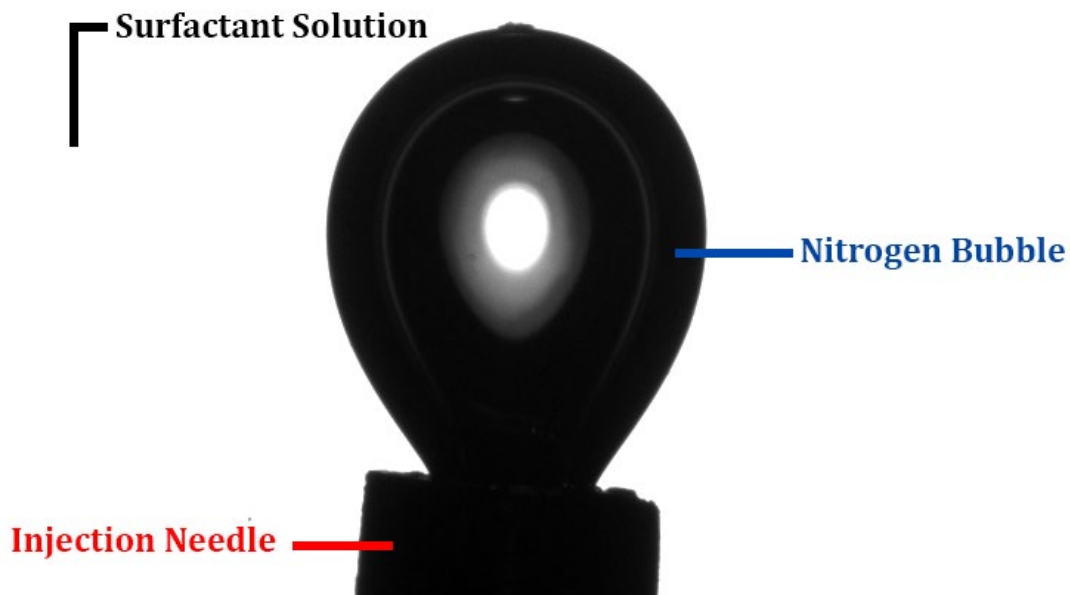


Figure 5.5 A N<sub>2</sub> bubble protruding from the injection needle in AOS surfactant solution

## 5.4 Experimental Results

Figures 5.6 through 5.11 show the kinematics of the foam decay for each experiment. Each figure has six data sets, one for each temperature, and corresponds to either a run with increasing temperature or a run with decreasing temperature. The x-axis represents time in seconds while the y-axis is the foam area divided by the original foam area. The x-axis is in log scale to better show the decline profile. The figures highlight the difference in time scale of the decay as temperature increases.

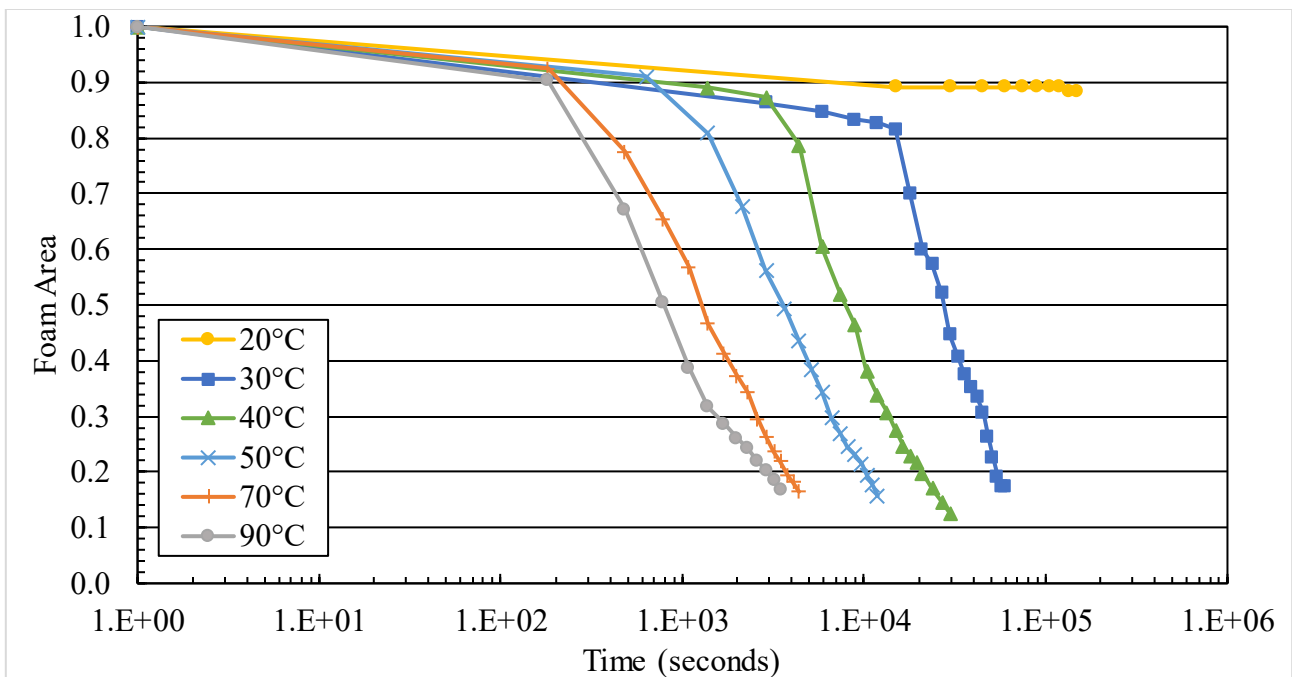


Figure 5.6 Kinematics of the decay for AOS while increasing the temperature

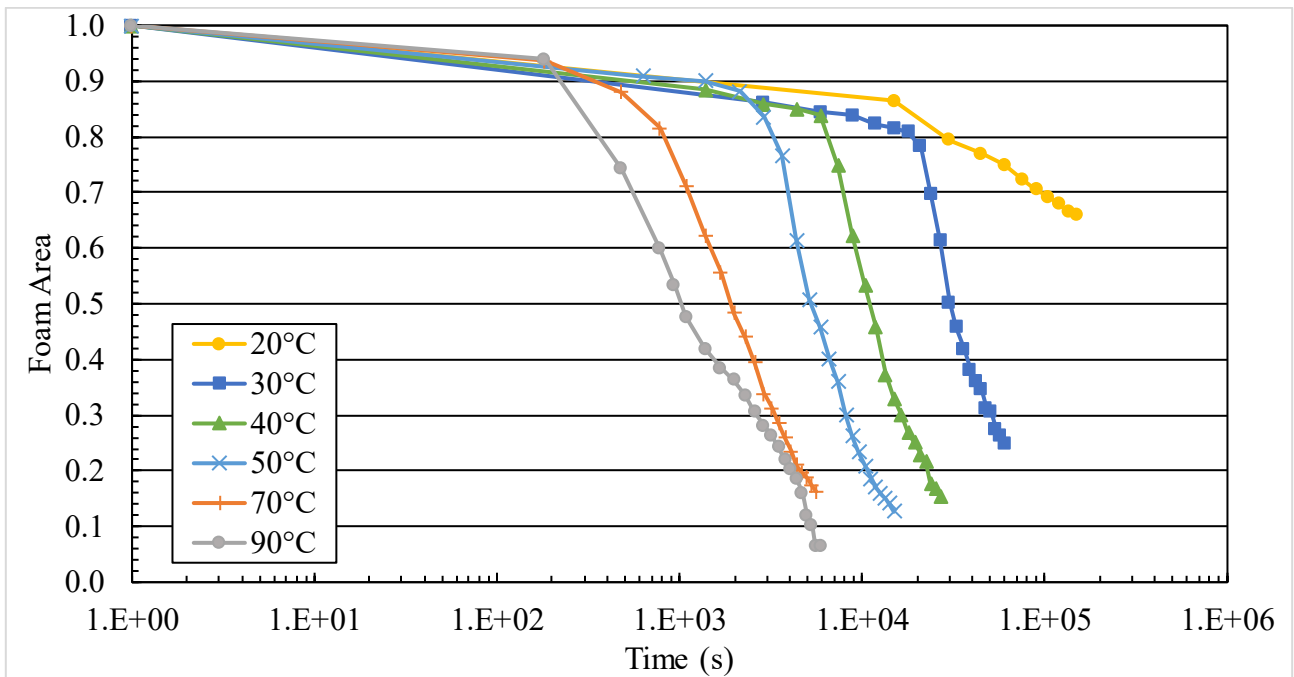


Figure 5.7 Kinematics of the decay for AOS while decreasing the temperature

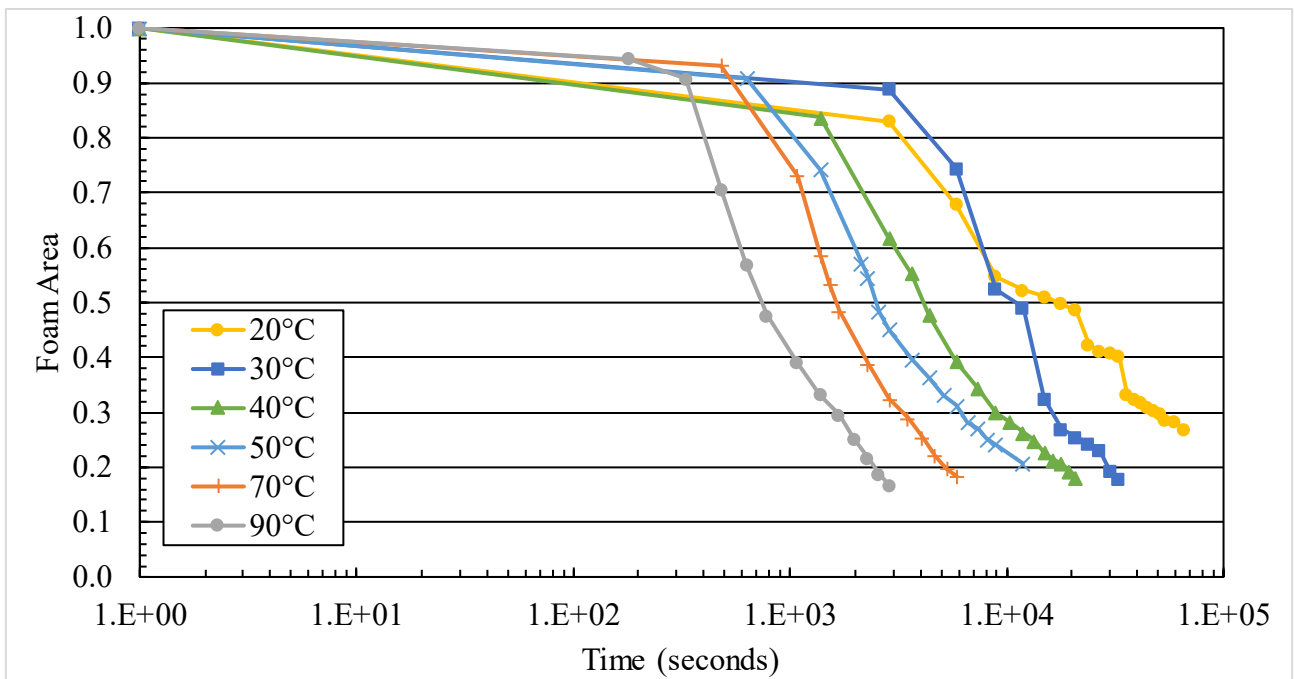


Figure 5.8 Kinematics of the decay for Surfonic while increasing the temperature

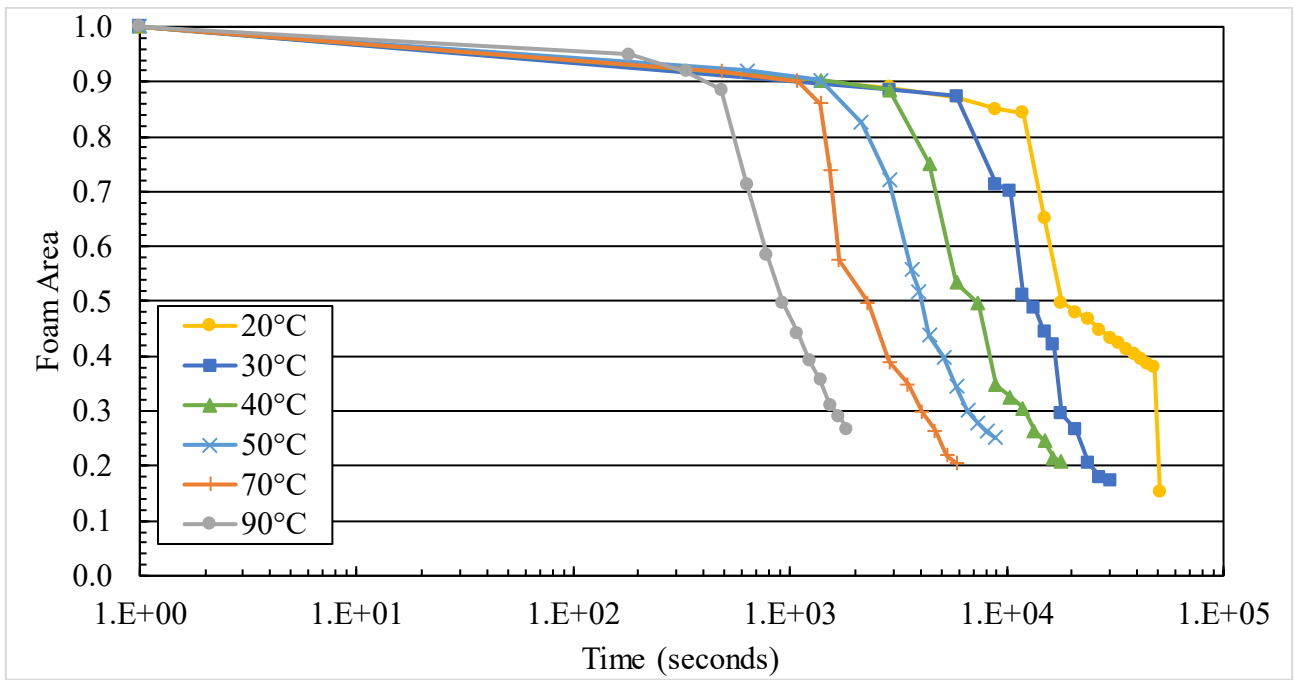


Figure 5.9 Kinematics of the decay for Surfonic while decreasing the temperature

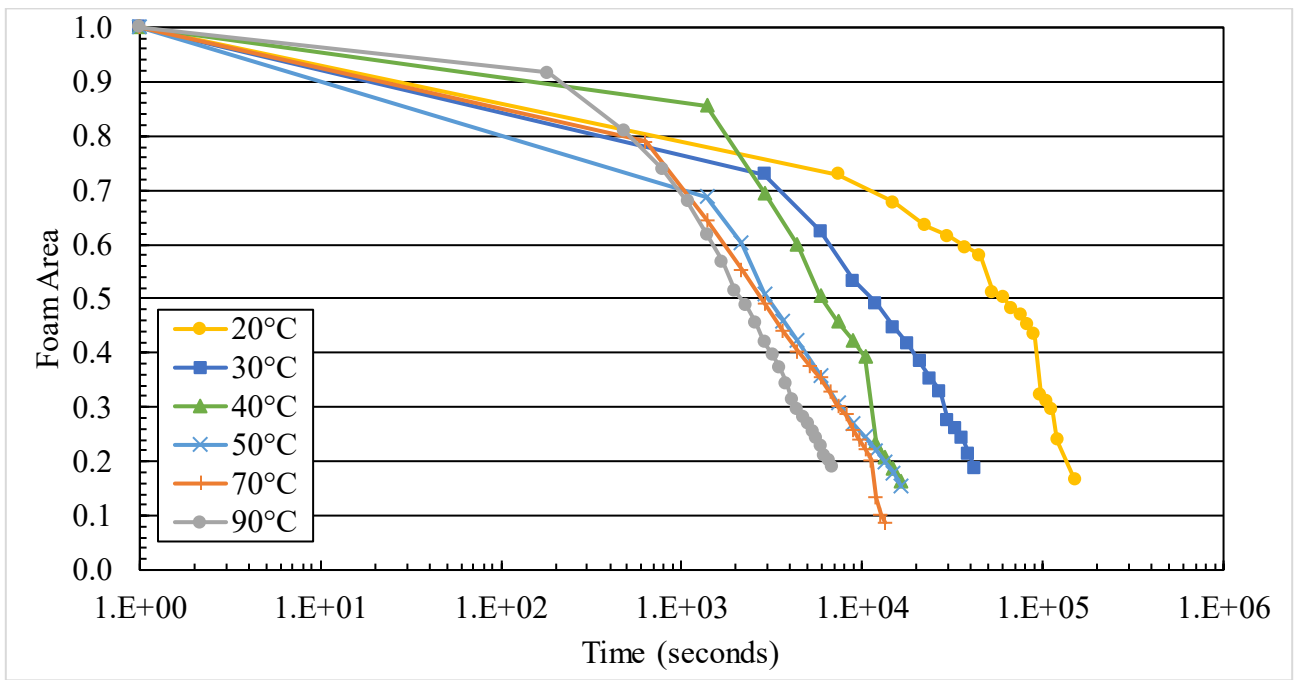


Figure 5.10 Kinematics of the decay for Elevate while increasing the temperature

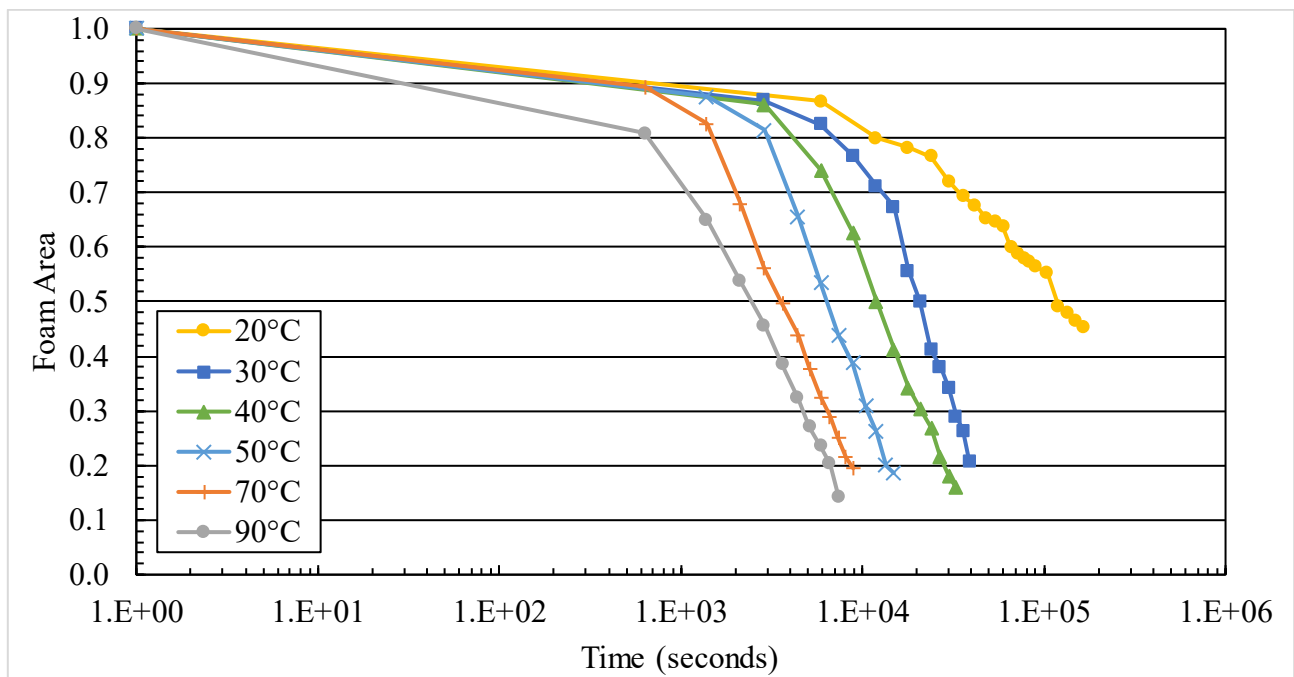


Figure 5.11 Kinematics of the decay for Elevate while decreasing the temperature

#### 5.4.1 Effect of Temperature on Interfacial Tension

In Figure 5.12, we show the effect of temperature on the IFT between each surfactant solution and  $N_2$ , in addition a reference IFT of DI water and  $N_2$  is included to illustrate the impact each surfactant has on IFT. As can be seen, the IFT of DI water and  $N_2$  starts at approximately 75 mN/m at 21 °C and steadily decreases to around 61 mN/m at 90 °C. This is to be expected since increasing the temperature decreases the intermolecular cohesive forces. For anionic surfactants, we expect the increase in temperature to decrease the IFT less than for pure DI water. Since the solubility of the surfactant molecules tends to increase with increasing temperature, the CMC is expected to increase via the increased monomer solubility (increasing the likelihood of micelle formation) which in turn increases the IFT (Schramm 1994; Myers 2020). As for nonionic surfactants, the increase in temperature leads to a decrease in solubility instead (due to dehydration of the hydrophilic parts) (Tadros 2003; Myers 2020) which should theoretically further decrease the IFT. This dynamic between decreased intermolecular forces, increased solubility, and decreased hydration means we

have multiple competing mechanisms that affect the IFT in our surfactant solutions. AOS displayed insensitivity to temperature as the IFT hovered around  $33 \pm 2$  mN/m for all temperatures tested which is an indication of the counterbalance between the two mechanisms. Surfonic exhibited a steady decrease of IFT from 40 mN/m at 22 °C to 30 mN/m at 90 °C which is unexpected for this nonionic surfactant. Elevate showed a steady decrease in IFT as temperature increased which ranged from 44 mN/m at 21 °C to 33 mN/m at 90 °C which is a smaller decrease compared to DI water as expected. We also note that in terms of IFT reduction capabilities, AOS was generally the best at lower temperatures, but all three surfactants showed similar IFT reduction capabilities at higher temperatures (50 °C and above).

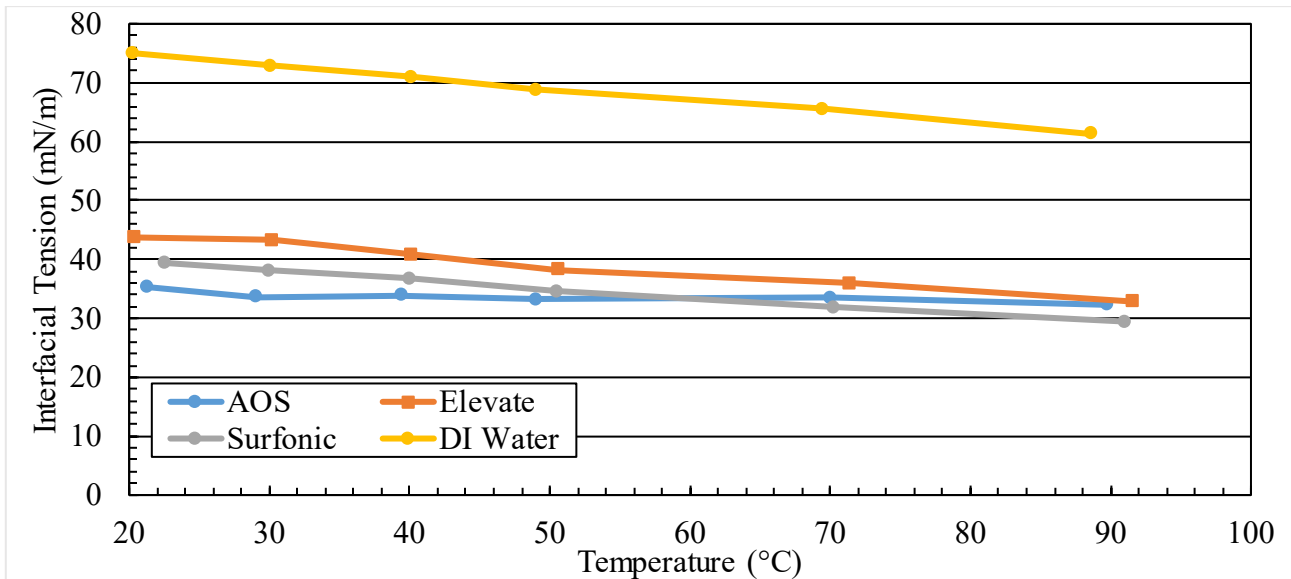


Figure 5.12 IFT measurements for AOS, Surfonic, Elevate, and DI water

#### 5.4.2 Effect of Temperature on Cell Humidity

With the cell forming a closed system and with no N<sub>2</sub> circulation, mechanical disturbances from gas flow do not apply, however, this means we need to be cognizant of secondary effects of changing the temperature in a closed system. As the temperature of the cell increases, we noticed that more condensation was taking place as can be seen in Figure 5.13 which shows the cell at each temperature after temperature stabilization but before running an experiment. At 21 °C we noticed

minimal to no condensation since this temperature is close to ambient conditions surrounding the cell, however at 30 °C we start seeing an increase in condensation inside the cell (we confirm that the condensation is inside the cell due to no visible condensation below the liquid level). This condensation increases drastically with temperature and larger drops of water start to form on the viewing window. We noticed this condensation behavior for all three surfactants.

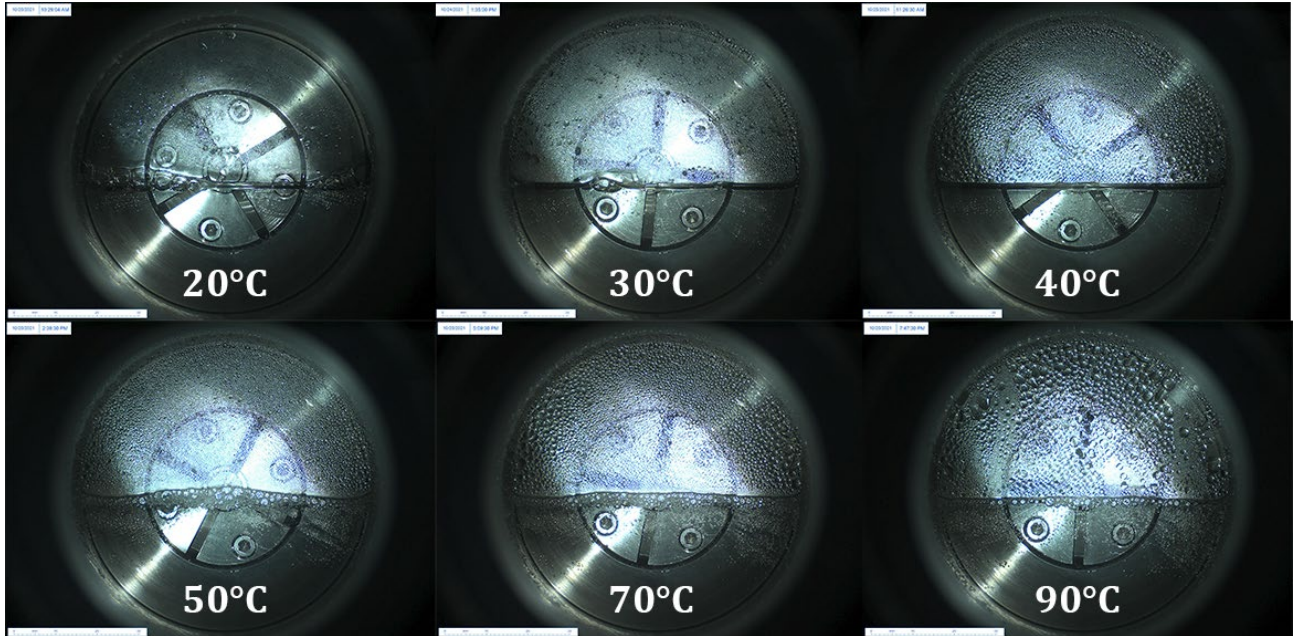


Figure 5.13 Condensation comparison at different temperatures for an AOS run

Since our system did not have a built-in hygrometer to directly measure the humidity, we opted to use Calsep PVTsim Nova 5 software to perform vapor-liquid equilibrium (VLE) and determine the molar fraction of water in the gas phase at different temperatures. A modified version of the (Buck 1981; Buck Research Instruments 2012) is used to calculate the saturation pressure of water at each temperature as in Equation 5.3 below and the molar fraction is used to calculate the partial pressure of water as shown in Equation 5.4. Both pressures can then be used to calculate the relative humidity through Equation 5.5.

$$P_s(T) = 611.21e^{\left(\left(18.678 - \frac{T}{234.5}\right)\left(\frac{T}{257.14 + T}\right)\right)} \quad (5.3)$$

$$P_{water} = P_{total} * mol\%_{water} \quad (5.4)$$

$$RH = \frac{P_{water}}{P_s(T)} \quad (5.5)$$

where  $P_s(T)$  is the saturation pressure as a function of temperature,  $T$  is the temperature,  $P_{water}$  is the water partial pressure,  $P_{total}$  is the pressure of the system as measured during the experiment,  $mol\%_{water}$  is the molar fraction obtained from Calsep PVTsim, and  $RH$  is the relative humidity. Our model showed that the molar fraction of water increases drastically as temperature increases, resulting in an increase in the relative humidity of the vapor phase from 73% at 21 °C to 89% at 90 °C as shown in Figure 5.14. The calculated relative humidity values suggests that no condensation should occur in the cell, however, we believe the visible condensation was due to one of two possibilities:

- The calculated relative humidity values are lower than the actual values which are at or above 100% such that any particle of dust or impurities in the system can provide nucleation sites for the water to condensate.
- The viewing window is cooler than the cell causing condensation even though in theory the sapphire window should be at the cell's temperature and given its thickness, cooling from ambient air should not be significant enough to drop the temperature of the cell facing side.

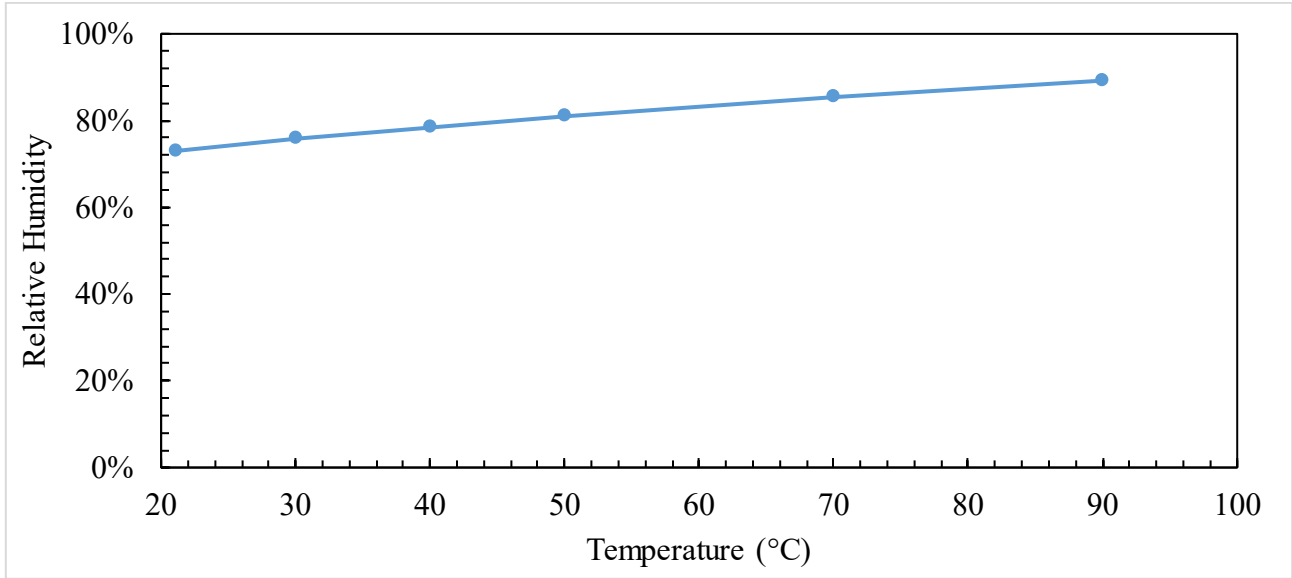


Figure 5.14 Equilibrium relative humidity vs. temperature

We were also able to estimate the equilibrium moisture content of the gas phase and the absolute humidity using VLE. Moisture content is the mass of water per mass of dry N<sub>2</sub> as shown in Equation 5.6 and absolute humidity is the mass of water per cubic meter net volume as in Equation 5.7.

$$\zeta = \frac{m_{\text{water}}}{m_{\text{nitrogen}}} = \frac{n_{\text{water}} * MW_{\text{nitrogen}}}{n_{\text{nitrogen}} * MW_{\text{water}}} \quad (5.6)$$

$$AH = \frac{m_{\text{water}}}{V_{\text{net}}} = \frac{P_{\text{water}} * MW_{\text{water}}}{RT} \quad (5.7)$$

where  $\zeta$  is the moisture content,  $m$  is the mass,  $n$  is the moles,  $MW$  is the molecular weight,  $AH$  is the absolute humidity,  $V$  is the volume of the gas phase, and  $R$  is the gas constant. The compressibility factor in equation 5.7 for water vapor is omitted as it is assumed to be equal to one for the temperature range in this study as shown by Nezbeda (2016). The results show that both the moisture content and the absolute humidity increase drastically with temperature. As shown in Figure 5.15, which includes both variables on the y-axis on a log scale, at each successive temperature, there is approximately a doubling of each variable and moisture content increases from 13 g/kg at 21 °C to 402 g/kg at 90 °C which is an increase of around 3,000% whereas absolute

humidity increases from 21 g/m<sup>3</sup> at 21 °C to 581 g/m<sup>3</sup> at 90 °C which is an increase of 2,800%. This drastic increase in the water content of the vapor phase along with the increase in relative humidity could help explain why foams remain wet during their lifetime at higher temperatures since the bubble films would replenish some of their liquid inventory from the moisture in the vapor phase.

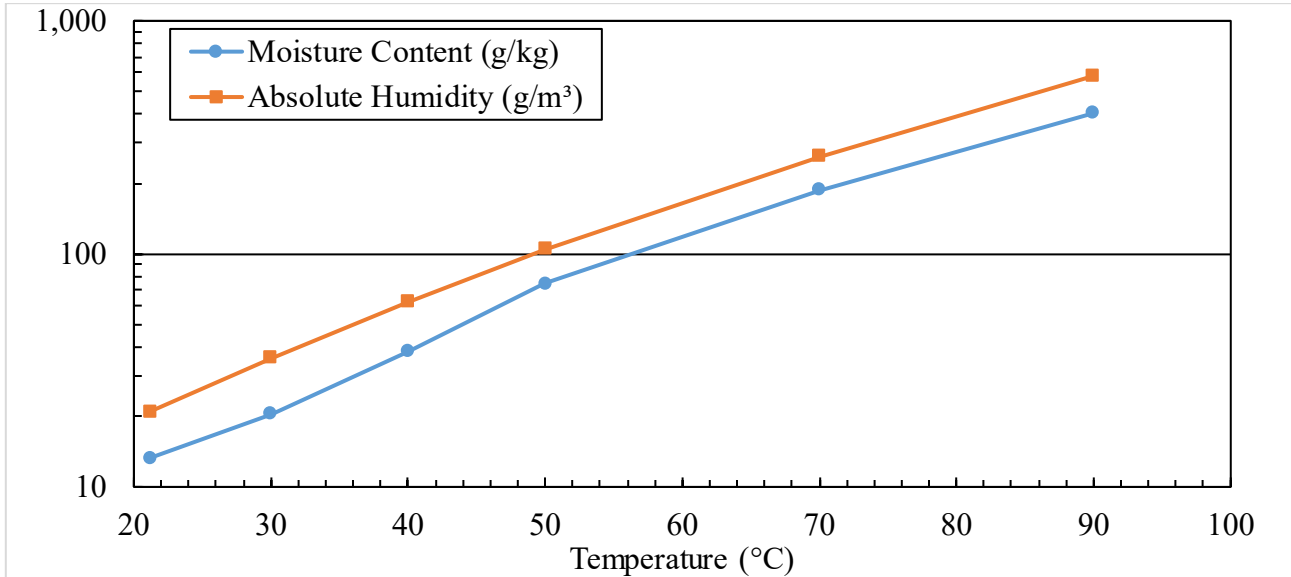


Figure 5.15 Moisture content and absolute humidity vs. temperature

### 5.4.3 Effect of Temperature on Foamability

The initial area occupied by the foam will generally vary between runs due to inaccuracies in the stirrer shut-off timing and the image capturing timing but it is expected to occupy at least 2,300 mm<sup>2</sup>, assuming complete foaming of the cell, as this represents the area occupied by the N<sub>2</sub> in the cell and since some of the water will be in the foam phase, the bulk water area will be less while foam exists. We take our foamability value at approximately 20 seconds after stirring stops to minimize the impact gravity drainage has on foamability values. It is imperative to note here that for every temperature, the foam occupied the entire cell volume minus that of the bulk liquid. This means we could not assess the impact temperature had on foamability, and this represents a limitation of our approach. Since the cell volume is small, if our surfactant solutions are too foamable, as in our case, the real initial foam value will be greater than our cell volume and all we

would see is liquid and foam. Once a high enough temperature is reached, the foam will occupy only a portion of the gas phase and that would represent true foamability. However, this does not render our results useless, as we noticed that there is a trend in the foamability measured with temperature. As shown in Figure 5.16, all three surfactants exhibited a steady decline in foamability as temperature increased even though there was no visible coalescence. While Surfonic and Elevate had similar foamability values across the temperature range, AOS was noticeably higher indicating a more favorable drainage behavior. We expected our foamability values to slightly decrease with temperature even if the cell was completely occupied with foam and liquid. As per equations 5.8 to 5.10 from Neethling et al. (2005) the velocity of water primarily depends on the density, viscosity, and interfacial tension of the aqueous phase:

$$v_1 = -k_1 A - \frac{k_2}{\sqrt{A}} \frac{\partial A}{\partial y} + v_g \quad (5.8)$$

$$k_1 = \frac{\rho g}{3C_{PB}\mu} \quad (5.9)$$

$$k_2 = \frac{\sigma \sqrt{\sqrt{3}-\pi/2}}{6C_{BP}\mu} \quad (5.10)$$

where  $v$  is the liquid velocity (negative is downward direction),  $A$  is the plateau border area,  $v_g$  is the gas velocity which is zero in our case,  $k_1$  and  $k_2$  are combinations of physical parameters,  $\rho$  is the liquid density,  $g$  is the gravity constant,  $C_{PB}$  is the plateau border drag coefficient,  $\mu$  is the viscosity, and  $\sigma$  is the IFT. Table 5.2 shows the calculated viscosity, density, and IFT of a pure water-N<sub>2</sub> system using Calsep PVTsim. It can be seen that as the temperature increases, the viscosity decreases much more rapidly than density or IFT which results in an increase in the  $k_1$  and  $k_2$  parameters leading to an overall increase in drainage velocity.

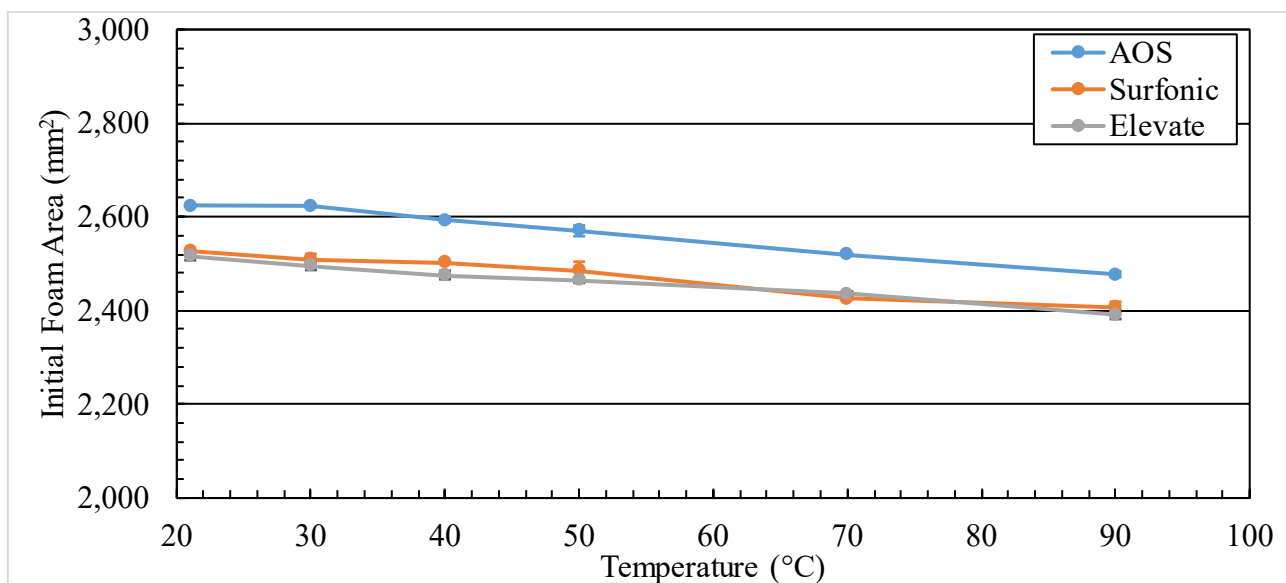


Figure 5.16 Averaged initial foam area from the ascending and descending runs vs. temperature (error bars may be too small to be seen for some data points)

Table 5.2 Physical properties of the aqueous phase for a pure water-N<sub>2</sub> system

Temperature (°C)	Viscosity (cp)	Density (kg/m <sup>3</sup> )	Interfacial Tension (mN/m)
21	0.973	993.641	67.88
30	0.797	985.627	65.14
40	0.654	976.287	62.26
50	0.548	966.657	59.58
70	0.406	946.512	54.69
90	0.317	925.098	50.36

#### 5.4.4 Effect of Temperature on Stability

The results show that stability of the foams is greatly impacted by temperature and it can be noticed that the stability of the foam for each surfactant decreases with temperature as shown in Figure 5.17. This is expected and has been shown in previous studies such as Kapetas et al. (2015) and Wang et al. (2017). For AOS, the half-life at 21°C exceeded 2 days and was deemed too high to measure but above this temperature, the stability of AOS decreases significantly starting at a half-life above 2 days at 21 °C to 15 minutes at 90 °C. Surfonic exhibited the lowest stability at 21 °C at

just 293 minutes, however, the decrease with temperature was much lower than AOS and at 90 °C its half-life was 14 minutes. Elevate showed a lower stability than AOS at low temperatures (below 40 °C) but at higher temperatures (50 °C and above) it consistently had the highest stability. In terms of sensitivity to temperature, AOS showed the highest sensitivity to temperature with significant stability loss at each temperature while Surfonic had the lowest overall sensitivity to temperature. At high temperatures, Elevate showed the least sensitivity to temperature while the other 2 surfactants had comparable depreciation in stability.

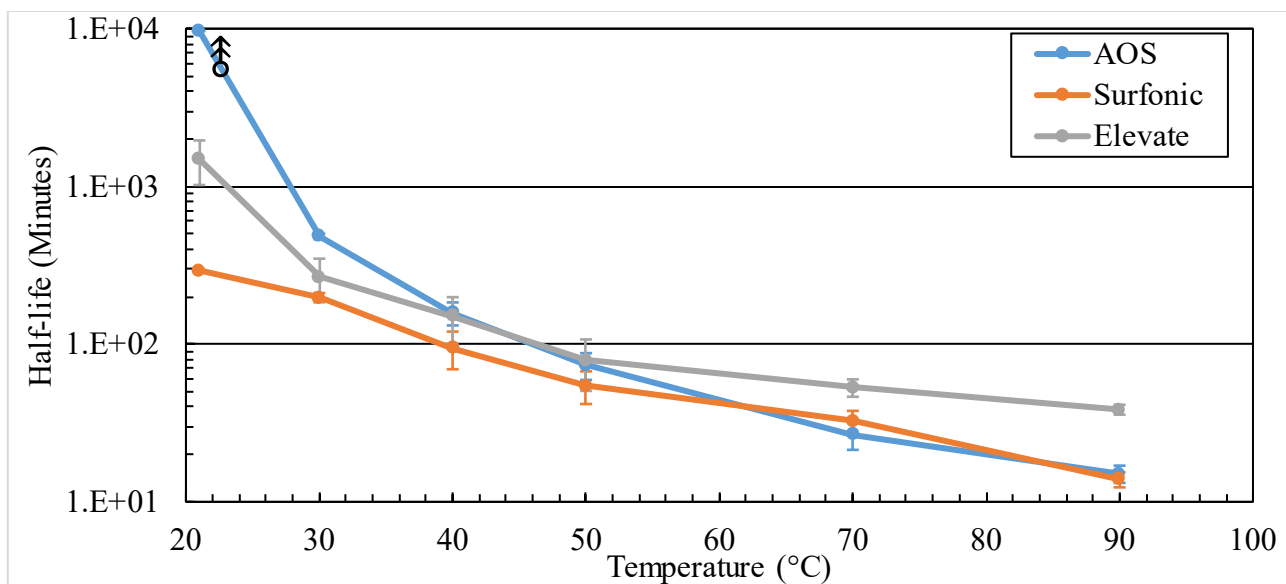


Figure 5.17 Averaged half-life from the ascending and descending runs vs. temperature (⌘ symbol indicates the value is higher than reported, error bars may be too small to be seen for some data points)

#### 5.4.5 Effect of Temperature on Morphology

We compare the morphology of the foams at the half-life as it provides us with a consistent measurement point across the different temperatures. The experimental results show that, in general, foam morphology can be described in one of two ways depending on the size and shape of the bubbles:

- Large, nonuniformly sized polyhedral bubbles observed at lower temperatures. In this case, the classical vertical profile for the bubble shape can be observed where spherical bubbles exist near the liquid surface and polyhedral bubbles above those.
- Small, consistently sized spherical bubbles observed at higher temperatures. Here, a vertical slice of the foam shows a gradient in bubble size but no geometric transition with height.

For AOS, as shown in Figure 5.18, at low temperatures (21 °C and 30 °C), we observed that the foam was able to dry and as such, smaller bubbles coalesce into larger ones and the shape of the bubbles turned from spherical to polyhedral. In fact, before much of the decay occurs, the foam is already primarily large polyhedral bubbles. We also noticed that due to gravity drainage, lamellae thickness increases the closer the bubbles are to the liquid surface. At higher temperatures (50 °C, 70 °C, and 90 °C), the foam remained spherical during its lifetime, the bubbles remain small, and the lamellae thickness show no noticeable variation with distance to the liquid surface. At 40 °C we noticed that foam was transitioning between the two morphologies.

Surfonic exhibited similar behavior to AOS except at low temperatures the polyhedral bubbles were smaller as shown in Figure 5.19. At low temperatures the foam was mainly polyhedral bubbles with thick films while at high temperatures the foam was almost completely made of small spherical bubbles which were denser (smaller size and higher in number) than AOS or Elevate. Overall, Surfonic had consistently smaller bubbles throughout the temperature range tested as compared to the other two surfactants.

As for Elevate (Figure 5.20), at 21 °C the foam consisted of large polyhedral bubbles with thinner films at the top and thicker near the liquid surface just like AOS. At 30 °C and 40 °C we noticed that the foam was composed of both large polyhedral bubbles and small spherical bubbles indicating that this is the temperature range of transition for this surfactant which is more gradual

than AOS. At 50 °C, 70 °C, and 90 °C the foam was in the second regime being entirely made of small spherical bubbles.

In general, we noticed that a transition between the two morphologies generally occurred around 40 °C regardless of the surfactant. The sphericity of the foam at higher temperatures indicates that the foam does not have enough time to drain, and this is likely partially due to the increased moisture content in the vapor phase. When the temperature increases, more of the water evaporates into the gas phase, this leads to an increase in water saturation of the gas phase as shown by the increase in absolute humidity and moisture content (corroborated by the observed increase in condensation with temperature). When foam is generated, the higher moisture content slows down the drying of the bubbles since partial replenishment of the liquid in the films can occur through condensation of the water molecules from the surrounding gas phase into the liquid films, hence the observe thicker lamellae at higher temperatures.

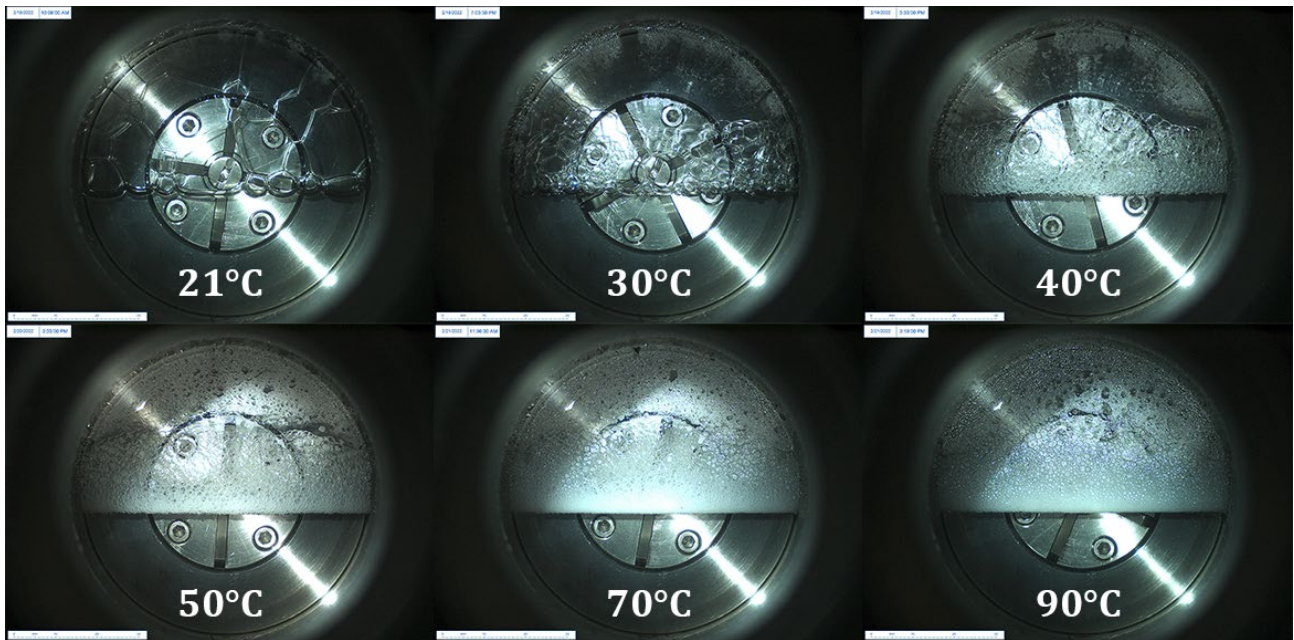


Figure 5.18 AOS foam morphology at the half-life at different temperatures (21 °C is not at the half-life as explained above)

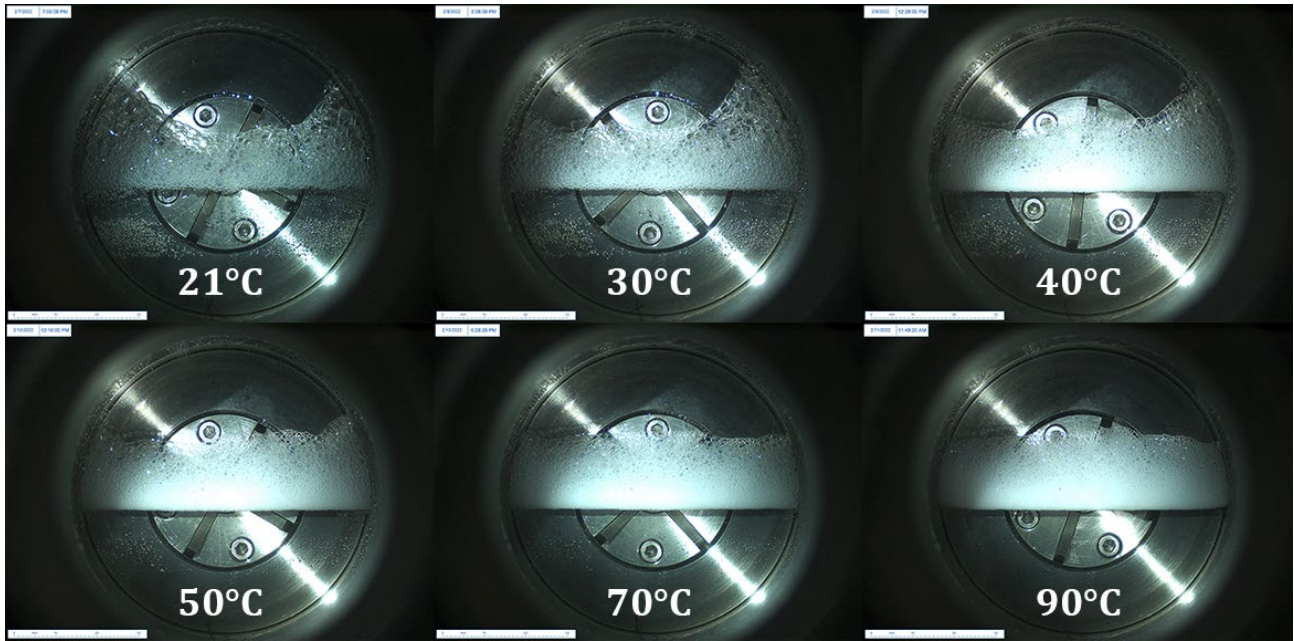


Figure 5.19 Surfonic foam morphology at the half-life at different temperatures

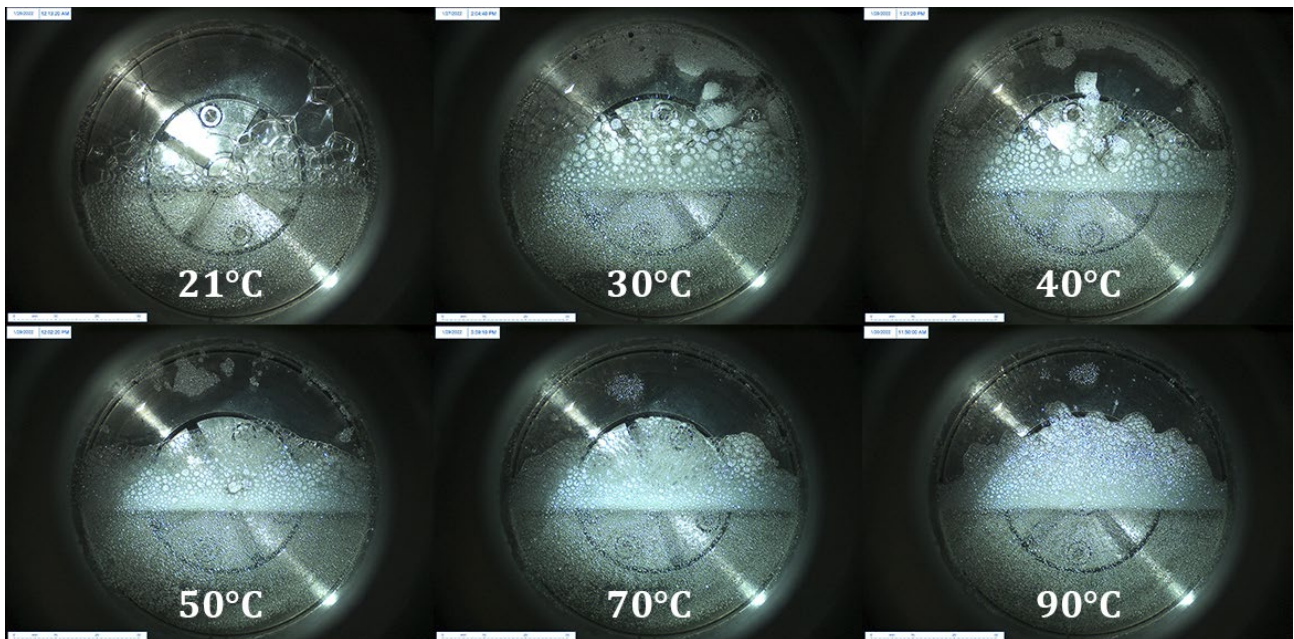


Figure 5.20 Elevate foam morphology at the half-life at different temperatures

#### 5.4.6 Effect of Temperature on Decay Pattern

We use the term decay pattern to refer to the overall behavior of the foam as it decays. This includes the foamability, stability, and morphology. Our experiments show that the conventional understanding of foam decay from evaporation does not necessarily provide a thorough picture.

While we observed similar decay behavior for the three surfactants at low temperatures, AOS and Elevate exhibited a different decay behavior than Surfonic at high temperatures.

#### **5.4.6.1 Anionic Surfactants**

Stability loss from evaporation is typically expressed in terms of liquid content loss of the lamellae but for anionic surfactants our observations indicate that this stability loss is actually primarily driven by the stochastic nature of evaporation which we refer to as nonuniform evaporation. As water evaporates more rapidly due to higher temperatures, micro fluctuations in water concentration along the bubble films are exacerbated and lead to local variations in surfactant concentration along those bubble films. These fluctuations in surfactant concentration cause the bubbles to burst. As described by Li et al. (2012), nonuniform evaporation causes the evaporated part of a bubble to lose water thus increasing the local surfactant concentration in that area. This in turn results in a surface tension gradient around the bubble with low surface tension in the evaporated zone and high surface tension away from the evaporated zone. Due to this gradient, a Marangoni flow is induced which further pulls water away from the evaporated region, thinning the lamella even more, ultimately resulting in the bubble bursting (Figure 5.21). Even though evaporation causes a local decrease in temperature leading to a higher IFT (Mills et al. 2005), the IFT decrease due to evaporative cooling is far smaller than the IFT increase due to the increased concentration (Yaminsky et al. 2010).

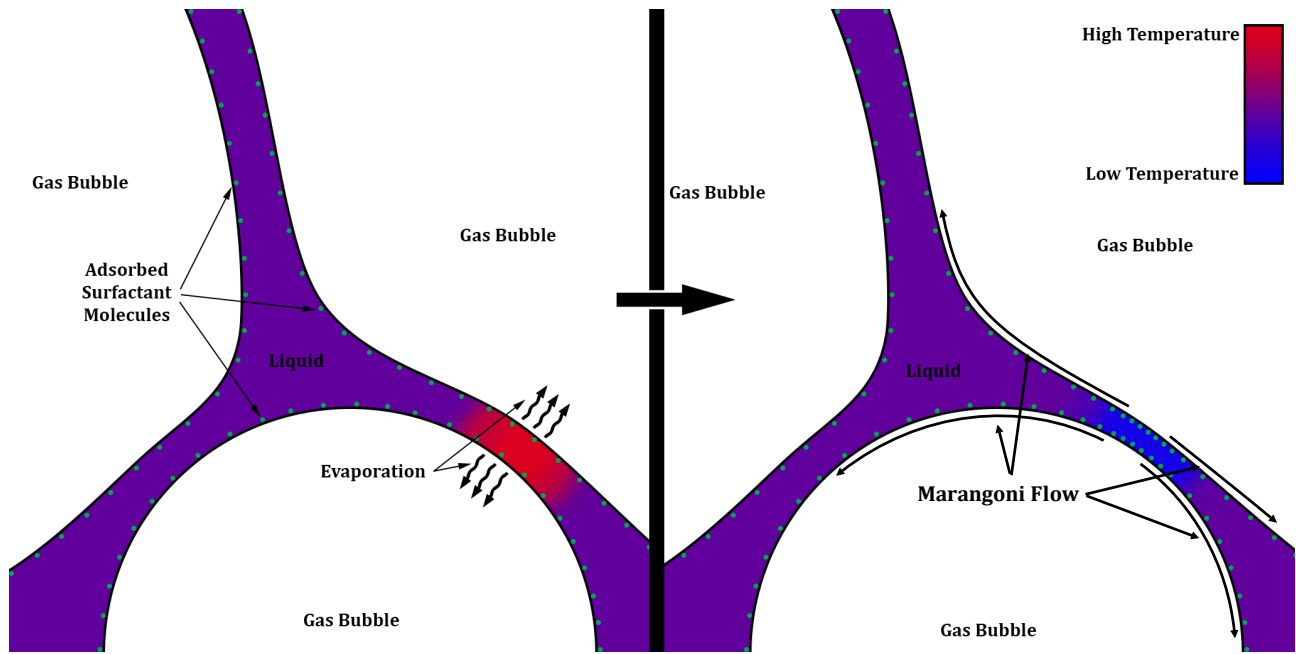


Figure 5.21 Marangoni flow induced by nonuniform evaporation

According to the Maxwell-Boltzmann distribution of molecular velocity, which can be obtained from Equation 5.11 below

$$f(T) = \frac{4}{\sqrt{\pi}} \left( \frac{MW}{2R_gT} \right)^{\frac{3}{2}} v^2(T) \exp\left(-\frac{MWv^2(T)}{2R_gT}\right) \quad (5.11)$$

where  $f(T)$  is the probability density function,  $MW$  is the molecular weight,  $R_g$  is the gas constant,  $T$  is temperature, and  $v(T)$  is the velocity as a function of temperature, the distribution of molecular velocity within a system spreads apart more as temperature increases. The molecular velocity can be represented in terms of the kinetic energy of molecules using Equation 5.12 below

$$E = \frac{1}{2} MW v^2 \quad (5.12)$$

where  $E$  is the energy,  $MW$  is the molecular weight, and  $v$  is the velocity. Figure 5.22 shows the Maxwell-Boltzmann distribution in terms of kinetic energy and highlights the increasing stochasticity of the system with temperature which we believe could explain why nonuniform evaporation becomes more apparent the higher the temperature. In Figure 5.23, we show the likelihood that a water molecule would be in an energy level at a certain temperature compared to

one at 20 °C. The 20 °C line in Figure 5.23 is at 100% for all energy levels since it is the baseline. It can be seen that for each temperature, the higher the energy level, the more likely it is to occur compared to 20 °C. Additionally, the higher the temperature, the more likely that a molecule will be at a higher energy level.

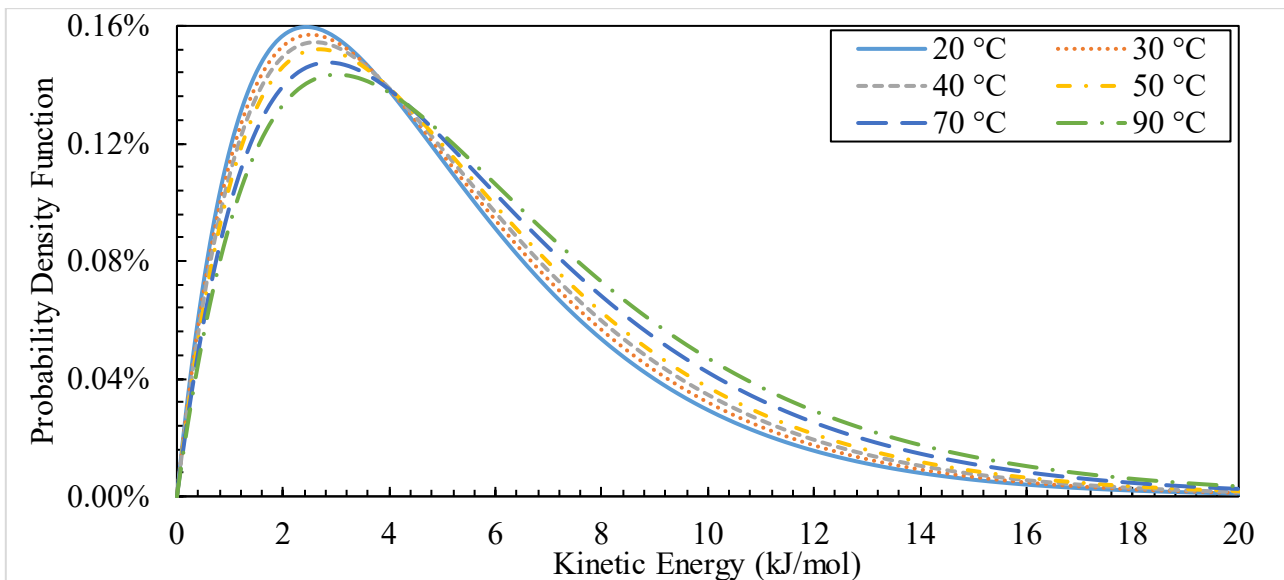


Figure 5.22 Maxwell-Boltzmann energy distribution

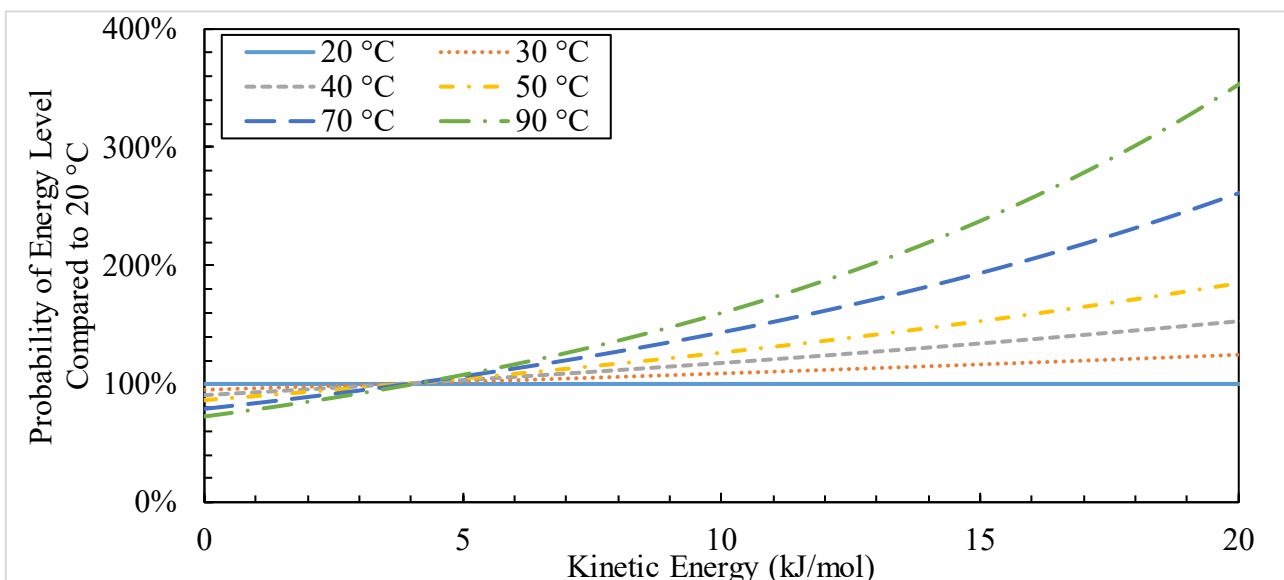


Figure 5.23 Probability of a molecule being in an energy state for a given temperature compared to a molecule at 20 °C.

The observed dichotomous foam behavior with temperature indicates that there are multiple mechanisms governing foam decay and those mechanisms are not always meaningfully present. For example, for AOS at lower temperatures (below 40 °C), one or several mechanisms dictate the decay behavior of the foam, while at higher temperatures, (50 °C and above), other mechanisms take over resulting in a completely different decay behavior. At 40 °C, a mix of the low and high temperature behaviors is observed indicating a transition in these mechanisms. This is supported by the observed foam morphology and stability. Often, it is stipulated that coalescence occurs primarily due to gravity drainage and evaporation of the liquid film. We found this to be true at low temperatures but not necessarily so at higher temperatures. Gravity drainage does not appear to be a dominating mechanism in this study at higher temperatures, otherwise it would be observed that foam film thickness would vary from high near the bulk liquid surface to low away from the liquid surface. Evaporation on the other hand, does seem to be the likely culprit. Evaporation, if uniform, would cause the foam film to be evenly depleted of water and once the liquid volume is below the threshold for stability, the bubble would burst (Exerowa et al. 1997). However, as Li et al. (2012) noted, bubbles do burst even if their liquid inventory is not fully depleted. To corroborate their statement, in our experiments, it was observed that even bubbles with thick films would burst lending credence to the hypothesis presented by Li et al. (2012). This is why nonuniform evaporation becomes a favorable mechanism for us to consider.

At low temperatures, foam decay can be characterized as a slow process where the foam initially undergoes a period of drainage and aging (bubbles at the top start losing liquid so their walls are thinner than bubbles at the bottom), drainage continues until the gravitational forces are cancelled by the capillary forces. As the lamellae get thinner, the shape of the bubbles starts changing to polyhedral where at the plateau borders, the curvature is higher thus resulting in low-pressure region compared to the lamellae region. This pressure difference drives more liquid into

the plateau border causing the film to thin further (Schramm 1994). This process is supplemented by evaporation, which, at low temperatures, is more likely to be uniform across a bubble's surface since the energy distribution is narrower as shown by the Maxwell-Boltzmann distribution. These two mechanisms govern the decay of foam and are in-line with the experimental observation of this study.

As for high temperatures, foam decay is characterized as a rapid process where the foam decays before much of the draining takes place. Here, the foam throughout its life remains spherical with relatively thick films partially due to the high moisture content within the vapor phase, and its decay primarily occurs through gas diffusion and splitting (larger bubbles bursting into smaller bubbles with some degree of gas loss). Splitting is observed when bubbles with thick lamellae at any location within the foam burst. Due to the abundance of liquid inventory in these lamellae and the condensed water inside the bubbles, some of the gas mixes with the liquid forming smaller bubbles, while the remaining gas escapes the foam phase. This is shown in Figure 5.24 where on the left, a large bubble can be seen in the middle of the foam, after 30 seconds, the image in the middle was taken which shows a blurry silhouette of smaller bubbles in place of the large bubble, and after 30 seconds, the image on the right was taken showing a new set of small bubbles in place of the original large bubble. It can also be noticed in the figure that the peak highlighted decreased in height after the splitting event illustrating the height decay caused by the splitting. We believe that the forming of smaller bubbles confirms the existence of sufficiently high liquid inventory in the original bubble and refutes any claim of loss of liquid through evaporation as the only primary cause for the decay since the forming of smaller bubbles requires the creation of more surface area compared to one large bubble which in turn requires more liquid. If the large bubble lost enough liquid inventory that it could not maintain the integrity of its film, then in no way would the same liquid inventory be able to maintain a larger surface area. In this case, due to the higher

temperatures, the evaporation rate is higher, resulting in more nonuniform depletion of the liquid in the lamellae, which, in turn, triggers the Marangoni flow as mentioned previously.

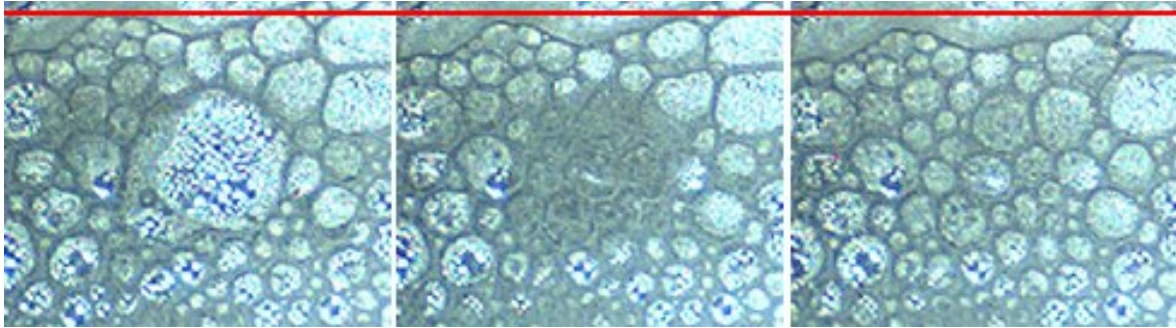


Figure 5.24 Splitting of an AOS bubble (left to right) into smaller ones reducing the overall foam height at 70 °C (the reference line at the top of the left peak is to illustrate height decay)

#### 5.4.6.2 Nonionic Surfactants

Unlike anionic surfactants, Surfonic, the nonionic surfactant, exhibited a different decay behavior at higher temperatures. Throughout the decay, no condensation was visible for all temperatures which we believe to be primarily due to the surfactant's high affinity for water.

At low temperatures (21 °C and 30 °C), the foam decay was similar to that described for anionic surfactants where an initial period of drainage and ripening is present. As this process continues, the shape of the bubbles changes from spherical to polyhedral. With evaporation taking place and the thin lamellae rupturing, the foam collapses from the top.

At high temperatures (40 °C, 50 °C, and 70 °C) a transition was observed with the foam becoming more densely packed and the decay was driven by drainage and evaporation similar to lower temperatures. However, it was also noticed that some collapse occurred near the foam-liquid interface indicating a difference mechanism in play.

At 90 °C the decay of the foam exhibited two distinct behaviors. At early time the decay was primarily driven by diffusion and coalescence from drainage and evaporation, however, most of the decay after the short drainage period was observed at the foam-liquid interface where the foam would simply shift downwards as the bubbles in contact with the bulk liquid collapsed.

We believe that the behavior observed for the foam collapse at the different temperatures was primarily driven by the behavior of the nonionic surfactant with temperature. In Figure 5.25 a phase diagram for a generic nonionic surfactant is presented. The blue dots represent the temperature and concentration combinations that were tested in this work. It can be seen that for a nonionic surfactant, as temperature increases the surfactant solution undergoes different phases where the preferential structure of the surfactant monomers change. This is attributed to the decrease in strength of the hydrogen bonds (Tadros 2003; Myers 2020). As the temperature increases, more hydrogen bonds promoting the surfactant molecules to assume more favorable structures in the solution such as micelles, lamellar, and isotropic structures. We believe that as the degree of dehydration increases, the concentration of monomers in the bulk liquid decreases and that causes bubbles that come in contact with the bulk liquid to destabilize since the likelihood of the surface monomers migrating into the bulk to form more complex structures with lower energy states increases. While no phase separation was visible at the temperature range tested, we believe that at 90 °C, the surfactant was near its phase separation temperature due to the strong decay observed at the liquid-foam interface.

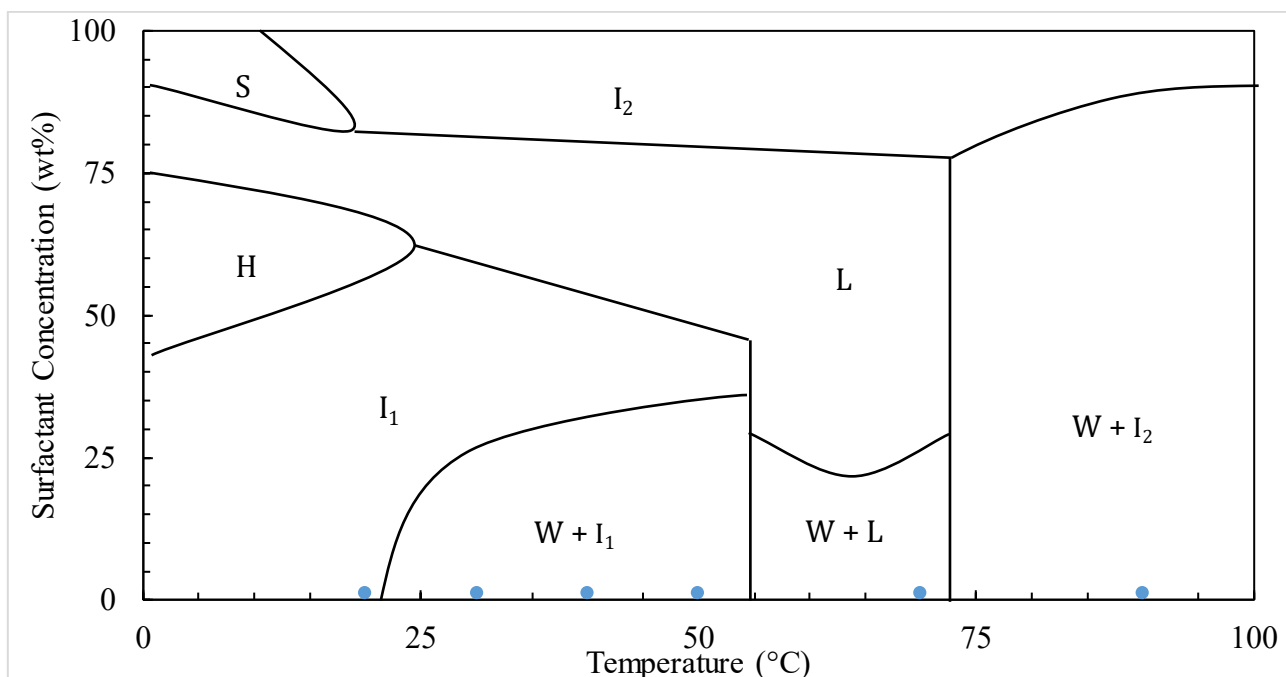


Figure 5.25 Complex phase diagram for a typical nonionic surfactant (W: water, H: hexagonal, L: lamellar,  $I_1$  and  $I_2$ : isotropic phases, S: solid).  $I_1$  is normally a micellar solution. Blue dots represent the temperatures and concentration tested in this work (Adapted with permission from Myers 2020)

#### 5.4.7 Thermal Degradation of Surfactants

Allawzi and Patton (1994) and Cuenca et al. (2014) showed that thermal degradation of surfactants can occur for a wide range of temperatures albeit at different rates. While we do not believe that significant degradation should occur at the temperatures tested, it is possible that surfactant performance could degrade enough to cause an observable loss of foamability and stability. In this work, the surfactants were subjected to two rounds of testing, the first was with temperature increasing, and the second was with temperature decreasing. The difference in performance between the two rounds indicates the effect of thermal degradation. Our results show that for all surfactants, the foamability did not change, however, the stability increased across the board.

### 5.4.7.1 Thermal Degradation Effect on Foamability

The foamability of our surfactants was shown to be significant enough that no foamability loss was observed due to temperature so it is expected that even after aging the surfactants, no foamability change should be observed as that would require significant degradation to occur. This is indeed what our results demonstrate. Shown in Figures 5.26 through 5.28 are the results for each surfactant. It can be seen that the values are nearly identical between the two rounds and that drainage is equally present in the form of lower foamability at higher temperatures.

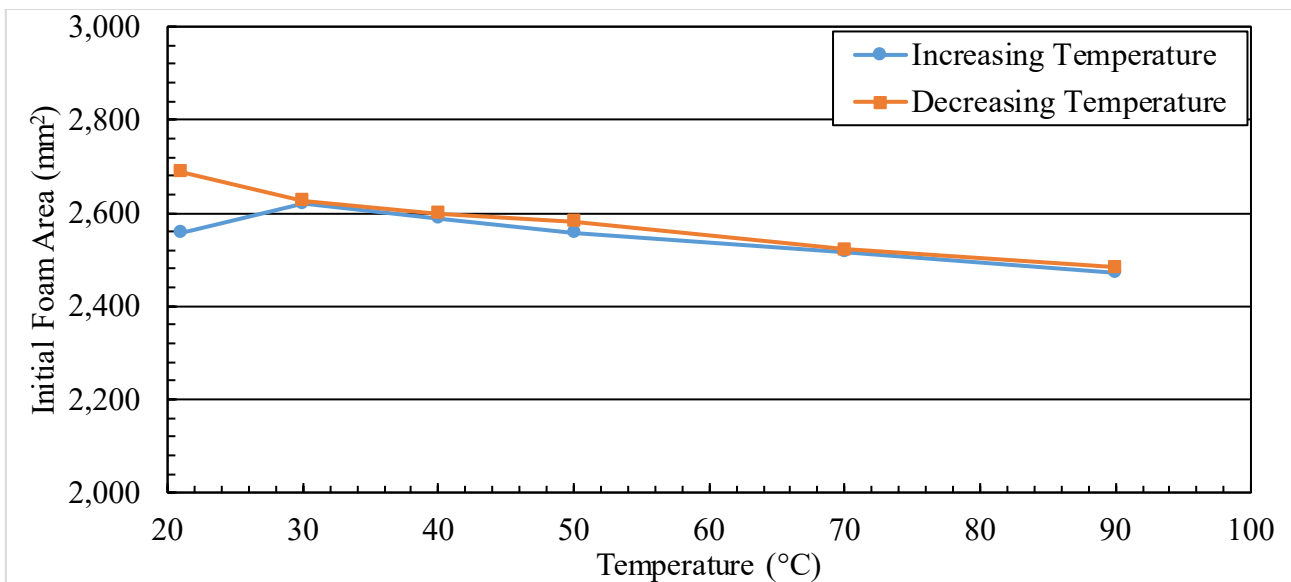


Figure 5.26 Thermal degradation effect on AOS foamability

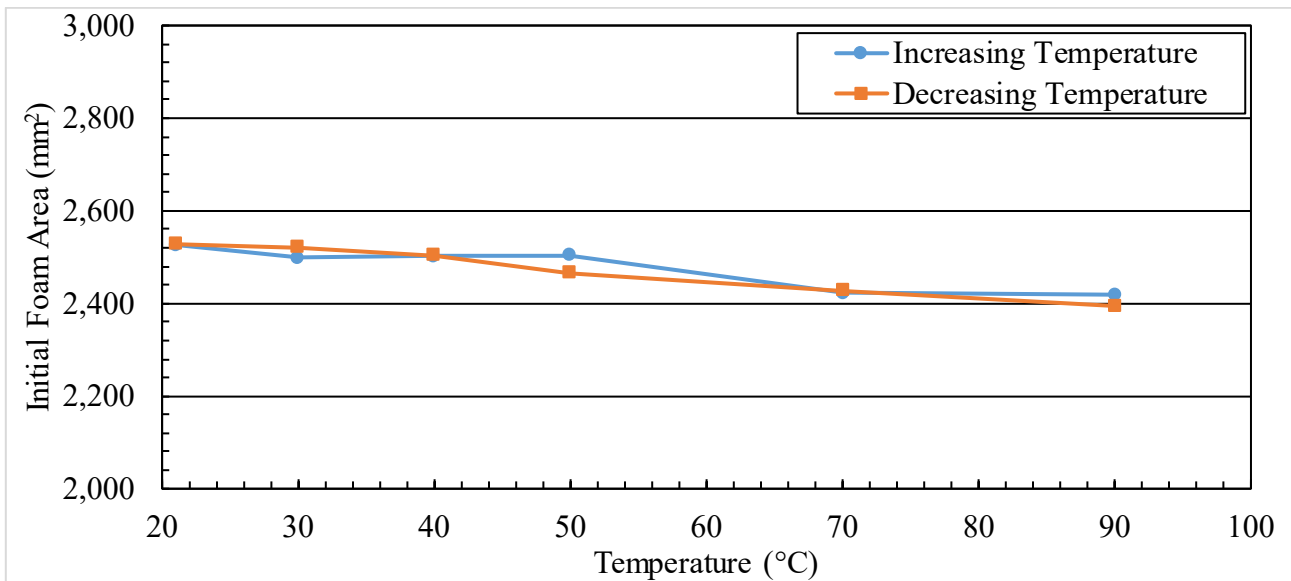


Figure 5.27 Thermal degradation effect on Surfonic foamability

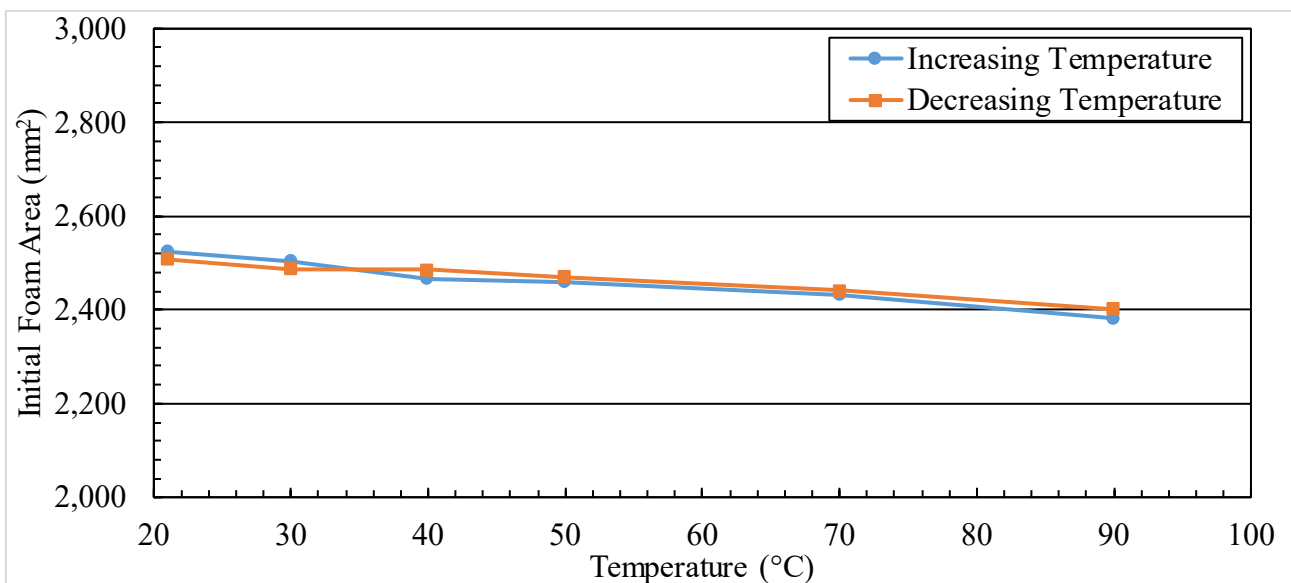


Figure 5.28 Thermal degradation effect on Elevate foamability

#### 5.4.7.2 Thermal Degradation Effect on Stability

We expect the stability to either show no change or to suffer slightly after the soaking process since some thermal degradation is bound to occur for the surfactants however miniscule. Overall, the results show that, unexpectedly, every surfactant became more stable during the second round of testing with decreasing temperature (after thermal degradation) as shown in Figures 5.29 through 5.31. The half-life at every temperature increased and in some cases a doubling of the half-life was

observed as is the case with Elevate. As explained in Chapter 3, it is likely that the thermal degradation process lowered the surfactant concentration activity level to a more optimal point that improved the stability of the surfactants.

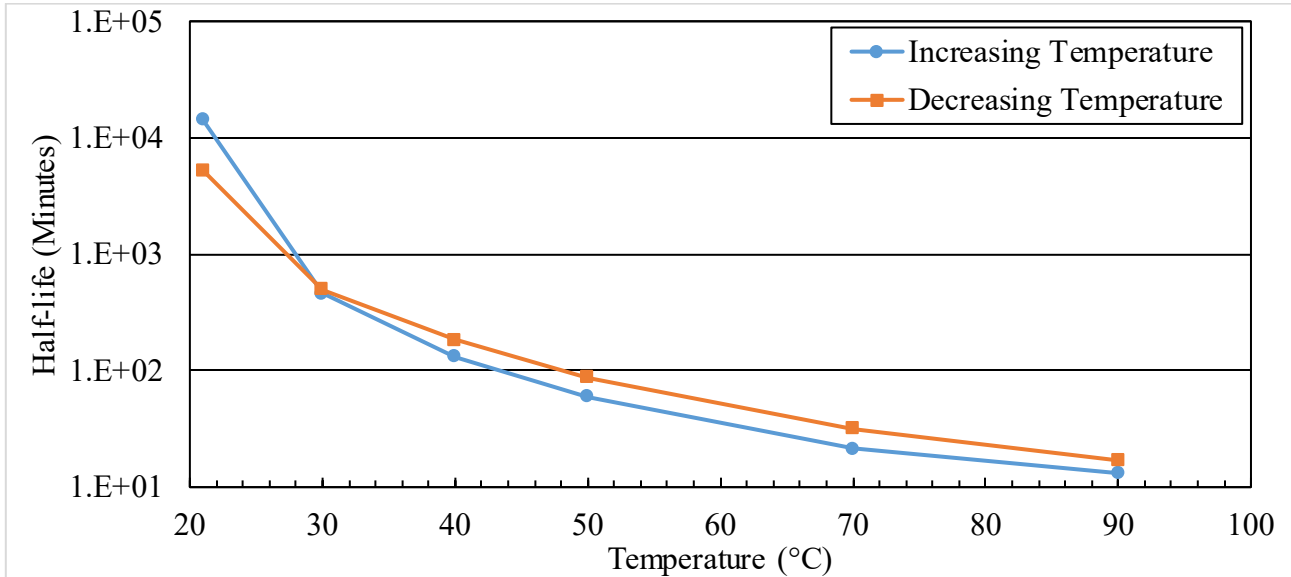


Figure 5.29 Thermal degradation effect on AOS stability

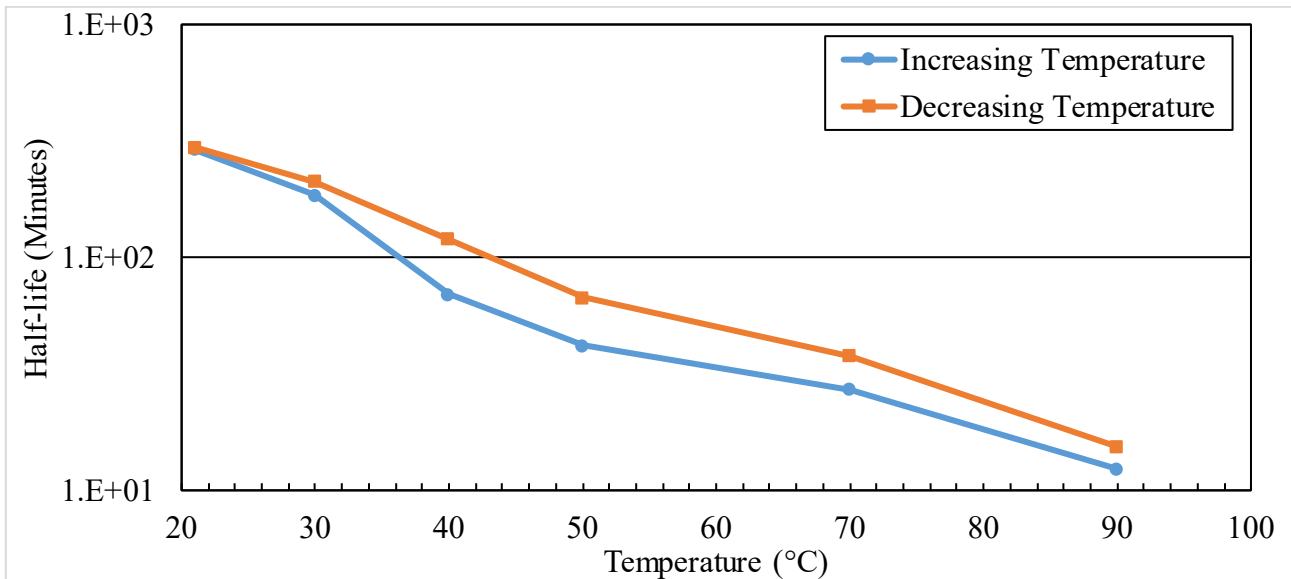


Figure 5.30 Thermal degradation effect on Surfonic stability

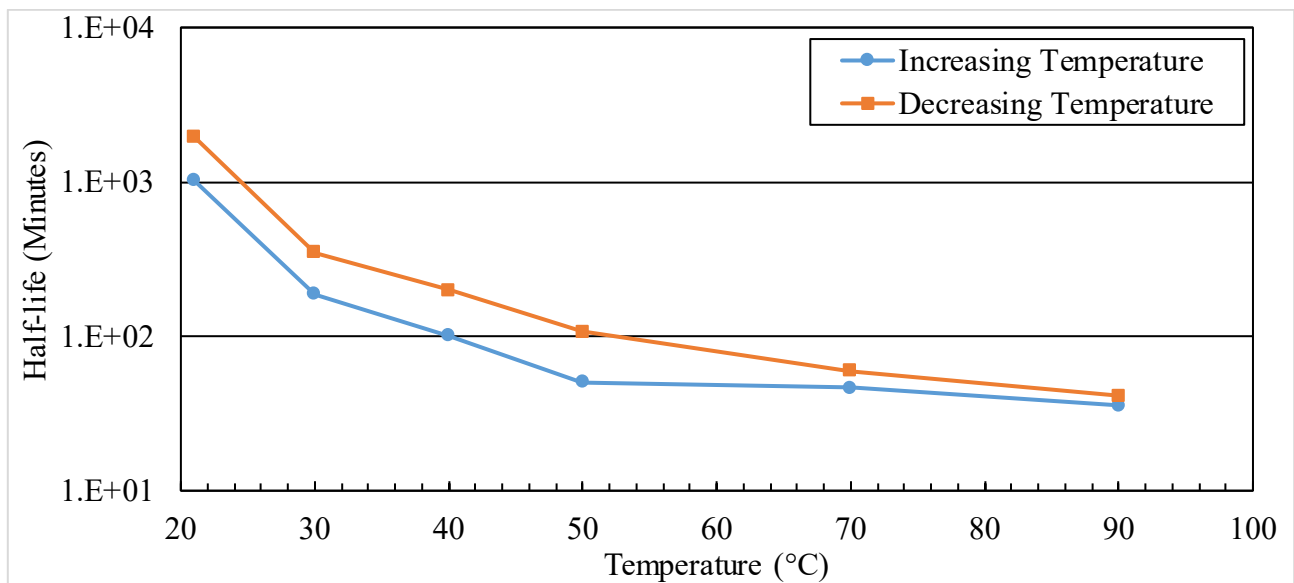


Figure 5.31 Thermal degradation effect on Elevate stability

#### 5.4.8 High Pressure Foamability and Stability Results

Since all of the previous runs were performed at a low pressure, it was of interest to investigate the effect temperature on foamability and stability at higher pressures and whether the observations at low pressures would apply to higher pressures. The pressure was increased by a factor of three and six across the temperature range, and while the pressures used in this study were not in the range encountered in reservoirs, the pressure increase factors should be enough to detect if pressure affects the way temperature changes foamability and stability. The results are inconclusive regarding the effect of pressure on foamability while stability was shown to be affected by pressure. By generating isotherms, we can provide insight into pressure trends at different temperatures.

##### 5.4.8.1 Temperature Effect on Foamability at High Pressures

Figure 5.32 shows the data for 30, 100, and 200 psia runs which includes three more temperature points (120 °C, 150 °C, and 180 °C) to highlight the decrease in foamability due to temperature and the effect of pressure on that decrease. The results show that foamability was highest for the 100 psia run up to 80 °C after which the 30 psia run shows more foamability. This could be attributed to run-to-run variance but it could also be due to the gravity drainage rate being

dependent on density, viscosity, and interfacial tension, all of which are affected by pressure at different rates resulting in nonlinear drainage behavior with temperature. For example, at low temperatures (20 °C to 40 °C), both 100 psia and 200 psia runs show the same foamability which is higher than the run at 30 psia. At high temperatures (50 °C to 120 °C), the highest foamability observed, corresponding to the lowest drainage rate, was consistently for the 100 psia run. At very high temperatures (150 °C to 180 °C) we noticed the foamability of the 30 psia run to be higher than the 100 psia and 200 psia runs.

We noticed that above 120 °C, the foamability of AOS suffers greatly especially at higher pressures and the effect of temperature can be observed in this range as foam never fully occupies the cell after stirring is stopped. For the 100 psia run, the foamability of AOS at 150 °C is 74% that of 20 °C and is 72% at 180 °C, while for the 200 psia run, the foamability of AOS at 150 °C was 83% compared to 20 °C and 75% at 180 °C.

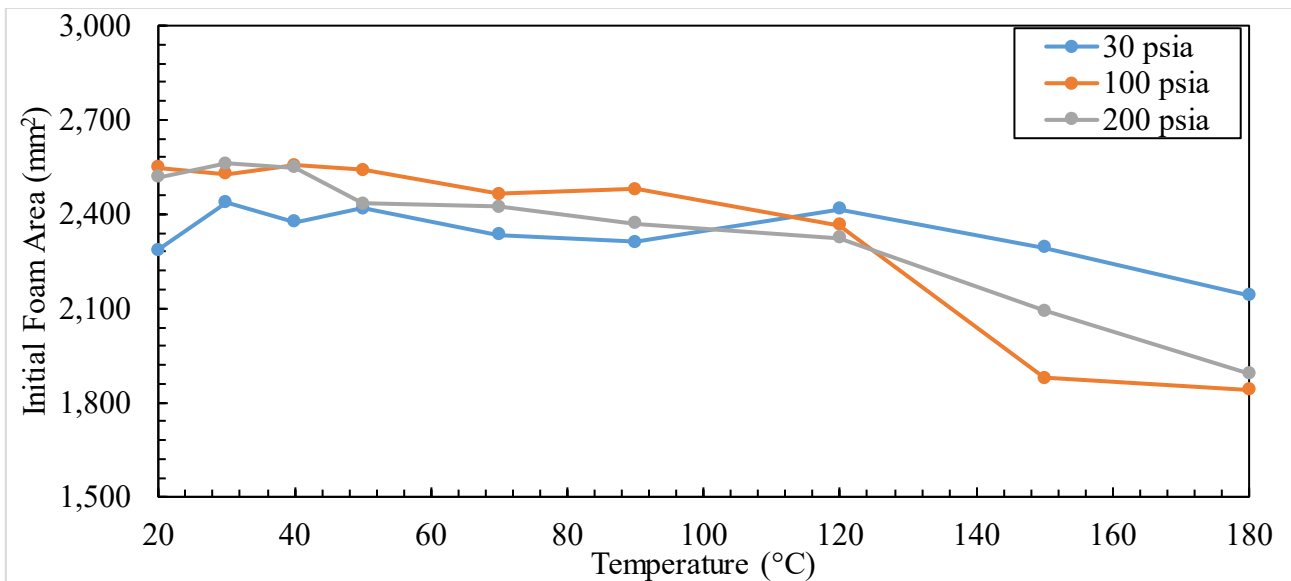


Figure 5.32 AOS foamability results for 30, 100, and 200 psia runs

#### 5.4.8.2 Temperature Effect on Stability at High Pressures

Figure 5.33 shows that, in general, as pressure increases, the stability of AOS increases. This is to be expected as the rate of condensation depends on the pressure while the evaporation rate is

dependent almost exclusively on temperature, meaning that for every temperature, the evaporation rate is constant at the different pressures and the stability will be affected by the increased condensation which tends to stabilize foams by retaining the films' liquid inventory. The 100 psia and 200 psia runs exhibit similar trends where stability steadily decreases as temperature increases while the 30 psia run shows a large dip in stability around the 50 °C mark then picks up at 120 °C at which point the trends behaves similar to the other runs. In Figure 5.34, which shows the isotherms in log-log scale for AOS stability, it can be noticed that the effect of pressure depends on the temperature: at 20 °C and 30 °C stability exponentially grows with pressure, between 40 °C and 120 °C, inclusive, stability logarithmically grows with pressure, and at temperatures above 120 °C, stability increases then decreases with pressure showing a peak at around 200 psia for 150 °C and at around 270 psia for 180 °C.

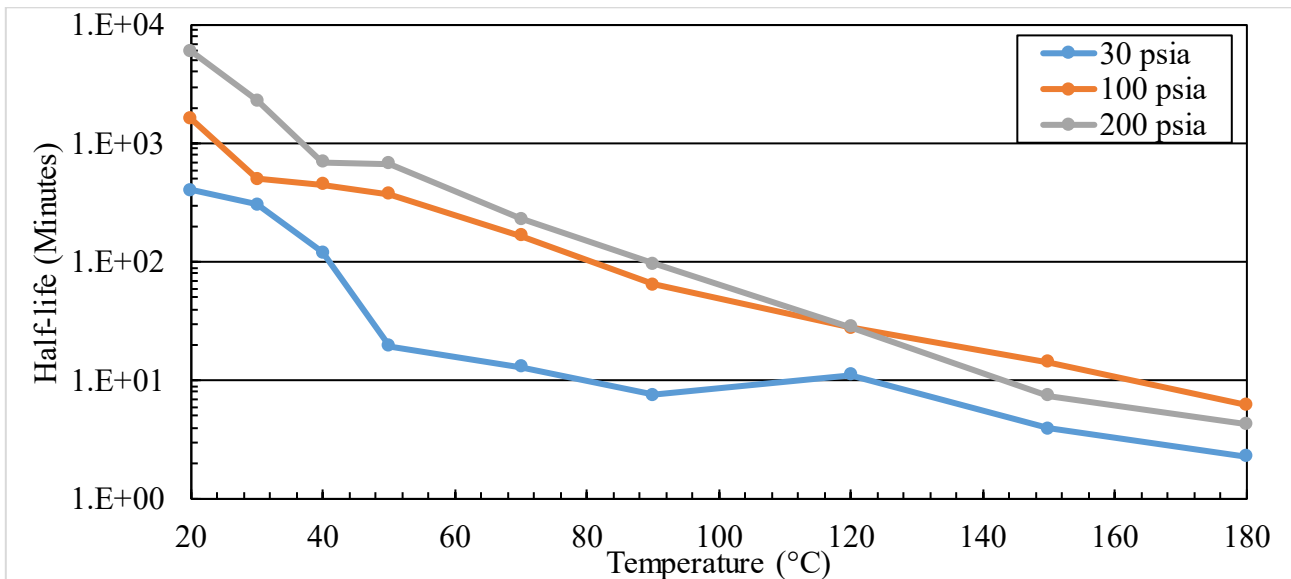


Figure 5.33 AOS stability results for 30, 100, and 200 psia runs

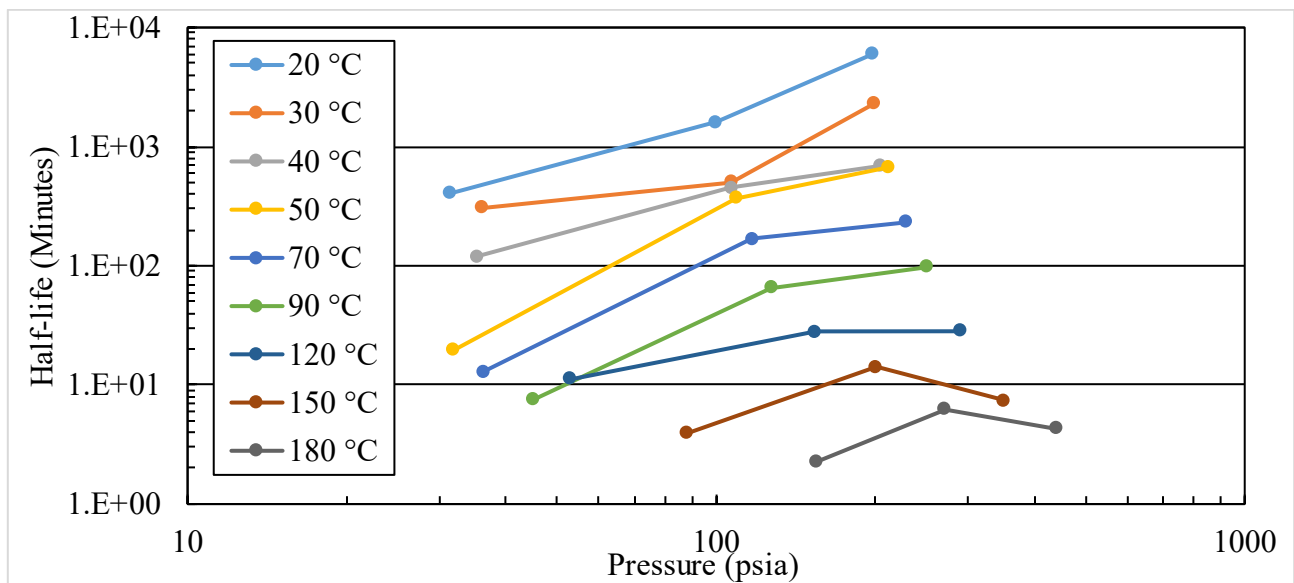


Figure 5.34 AOS half-life isotherms in log-log scale

### 5.4.8.3 Temperature Effect on Morphology at High Pressures

We have discussed earlier that the morphology of AOS at the half-life seemed to split around the 40 °C mark where below, the foam was mainly large polyhedral bubbles but at higher temperatures it was mainly composed of small spherical bubbles. We have also attempted to explain the morphology in terms of decay behavior and the mechanisms governing the two temperature ranges. In the high-pressure experiments, the goal was to explore if this behavior persists with pressure and whether temperature was indeed the primary contributor to this dichotomous behavior. In Figures 5.35 through 5.37, the morphology for AOS at the half-life is shown for each pressure tested over the whole temperature range (20 °C to 180 °C). It can be seen that pressure does change the morphology slightly by spreading the transition region (the morphology at 40 °C for the 30 psia run starts to appear around the 30 °C and 50 °C for the 100 psia and 200 psia runs) while every other temperature appears to look the same across the different pressures indicating insensitivity to pressure. One would be tempted to think that the morphology would depend on time which would be correct if absolute time was considered since drainage slows down with pressure and increases

with temperature. In terms of the life of the foam, however, it seems that the foam morphology is mostly independent of pressure, while being primarily a function of temperature.

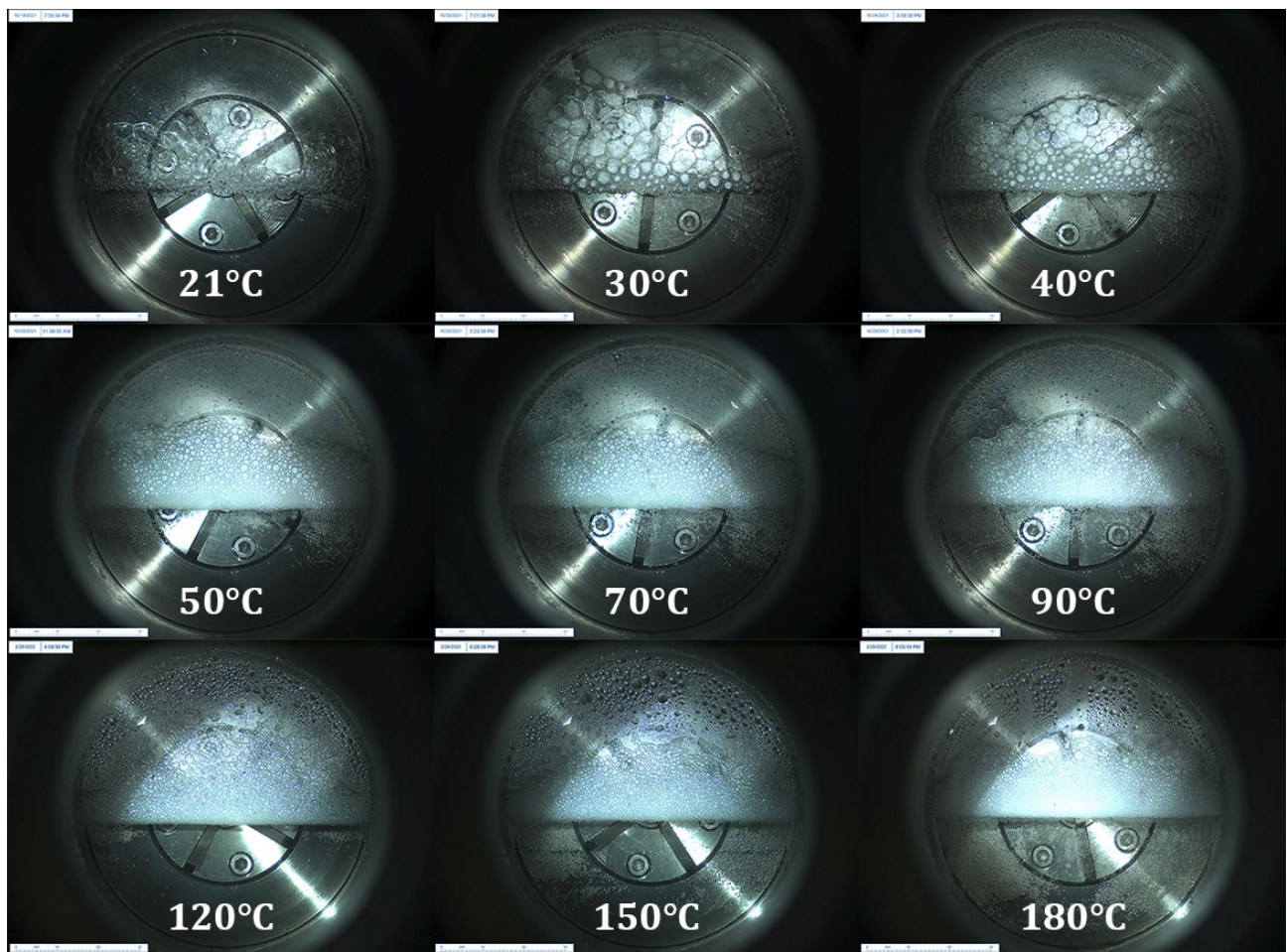


Figure 5.35 AOS morphology at the half-life for the 30 psia run

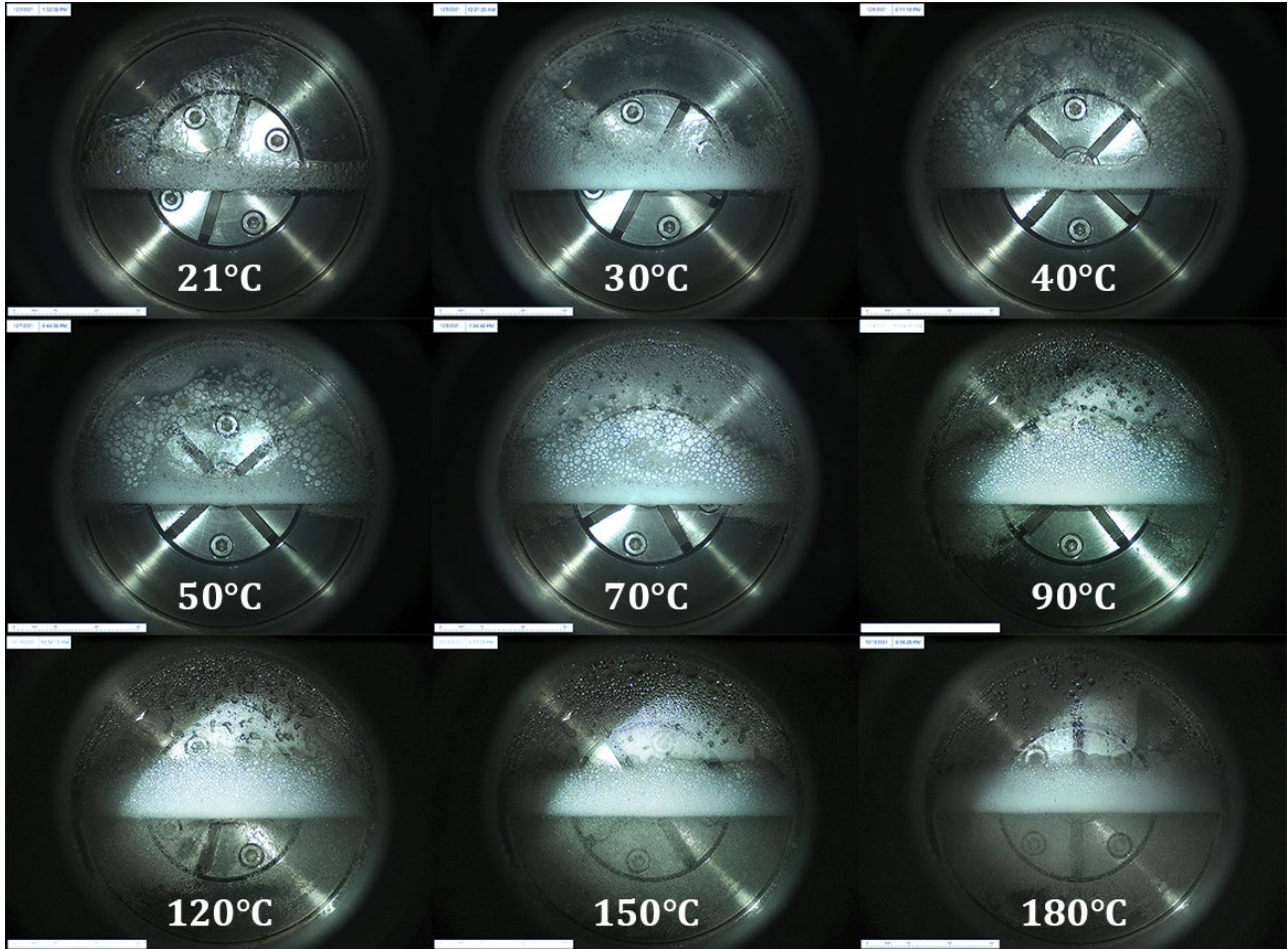


Figure 5.36 AOS morphology at the half-life for the 100 psia run

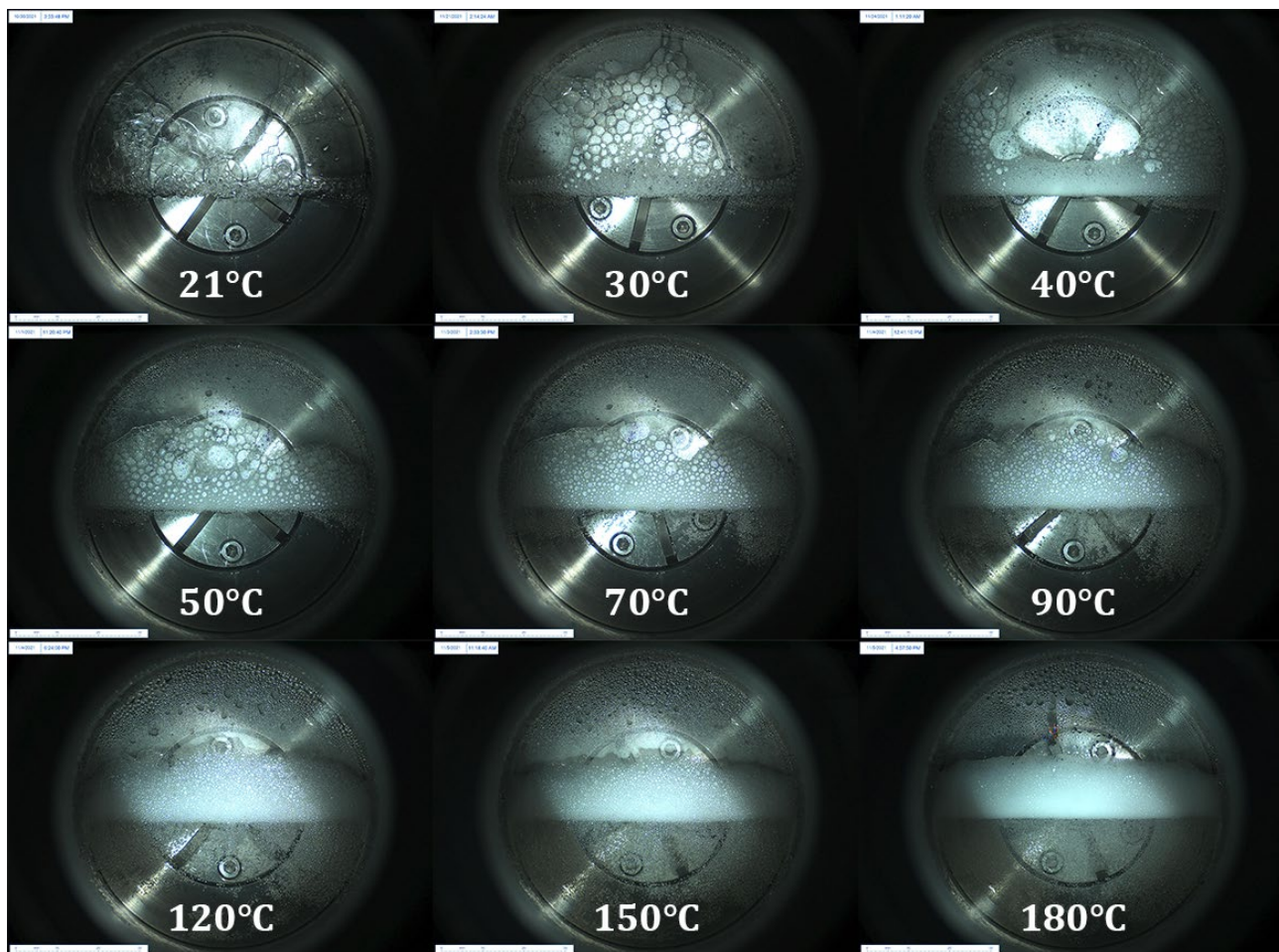


Figure 5.37 AOS morphology at the half-life for the 200 psia run

#### 5.4.8.4 Temperature Effect on Decay Pattern at High Pressures

We noticed that at high temperatures (120 °C and above) and pressures the foam can be split into three different regions that exhibit different decay behaviors. These regions are shown in Figure 5.38 and are designated as top, middle, and lower layers/regions. The top layer is characterized by fine bubbles with thin lamellae and this layer exhibits decay in the form of liquid inventory loss, the middle layer is composed of coarse bubbles with thick lamellae that decay through the Marangoni flow, and the bottom layer is fairly similar to the middle layer with the exception that minimal decay is observed in this layer. It was noticed that the top layer will often decay independently from the middle layer and in many cases, the top layer will decay slower than the middle layer. We noticed that the middle layer decays much faster than the top layer such that the foam height

decreases while bubbles in the top layer remained intact, maintaining both their shape and size, but shifting downwards. This behavior can deceptively make it seem as if the top layer is the one decaying when in reality larger bubbles in the middle layer will split resulting in a collapse of the middle layer which shifts the top layer along the entire foam stretch. Again, similar to our explanation at lower pressures, we believe that this decay is primarily driven by the Marangoni flow since bubbles in this layer are characterized by thicker films and are in general of larger size making them prime targets for larger temperature fluctuations along their surfaces.

In Figure 5.39, this decay behavior is shown in three consecutive images that display the entire foam “column” over a period of one minute (30 seconds between each image) and it can be observed that bubbles in the top layer maintain their shape and size while shifting downwards causing the foam height to change. It is often thought in literature that the top layer is the primary decay region which collapses and the layer below it becomes the new top layer which then collapses but this contradicts the observations made in these experiments. This demonstrates that even at higher temperatures, we still observe a Marangoni flow decay behavior and even though the overall size of the bubbles within the foam becomes smaller as temperature increases, bubble splitting is observable, albeit more difficult.

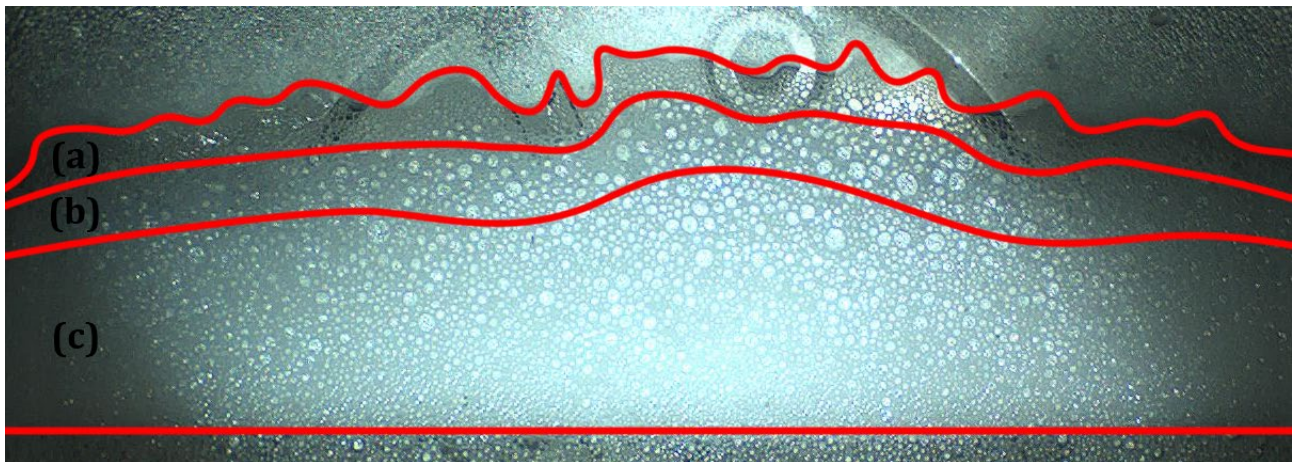


Figure 5.38 AOS foam regions at 150 °C and 200 psia: (a) top layer, fine foam that decays through liquid inventory loss; (b) middle layer, coarse foam that decays through Marangoni flow; (c) bottom layer, coarse foam that does not exhibit decay

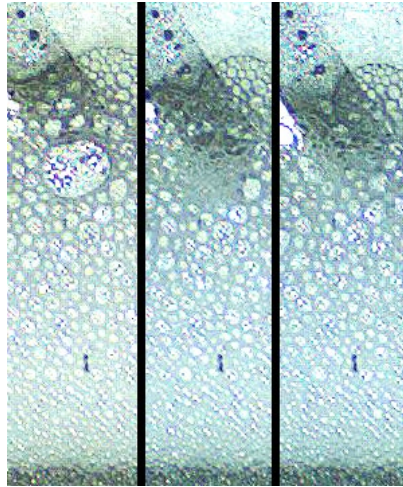


Figure 5.39 AOS bubbles in the middle layer exhibiting splitting decay behavior (left to right) while bubbles in the top layer remain unaffected (taken from 100 psia run at 150 °C)

## 5.5 Discussion

Our experiments have shown that  $N_2$  foams exhibit two distinct decay behaviors with temperature in closed environments; one at low temperatures and another at high temperatures and that high temperature decay behavior was dependent on the type of surfactant. The experiments also showed that for anionic surfactants, decay behaviors are independent from pressure. Different foam morphologies were observed for each decay pattern and each pattern exhibits different modes of bubble bursting.

At lower temperatures, the foams decayed in a manner that allowed them to coalesce and drain so that the morphology became characterized by large polyhedral bubbles which we believe means that the dominating mechanisms for decay at these temperatures are gravity drainage and uniform evaporation since these two mechanisms result in foam lamellae thinning and that in turn changes the shape of the bubbles from spherical to polyhedral.

For anionic surfactants, at high temperatures the cell humidity increased which provided more water replenishment capabilities in the gas phase delaying gravity drainage. However, higher temperatures result in a higher rate of evaporation and increased stochasticity which exacerbates nonuniform evaporation. This results in foam bubbles bursting due to the Marangoni flow which

manifested itself in the form of larger bubbles splitting into smaller ones. This is because larger bubbles have higher surface area making them prone to differential evaporation and given our observation of how these larger bubbles end up forming smaller bubbles, this meant that the original bubbles had sufficient liquid in their films thus it was not possible for these bubbles to burst due to mechanisms that cause loss of liquid inventory. The forming of smaller bubbles is likely to be caused by the difference in pressure of the two bubbles adjacent to the ruptured film. The influx of gas from the smaller bubble due to its higher pressure to the larger bubble causes liquid and gas to mix with enough shearing power to generate new smaller bubbles.

For nonionic surfactants, the decay at elevated temperatures is more complex and depends on the phase diagram for the specific surfactant used. In the case of Surfonic, at 90 °C, the decay at the interface between the bulk liquid and the foam is likely due to the forming of larger isotropic structures from the surfactant molecules in an effort to reduce the energy of the system. This is caused by the dehydration of the hydrophilic parts of the surfactant. The loss of surfactant molecules from the bubble surfaces in contact with the bulk liquid to the isotropic structures causes an IFT gradient inducing a Marangoni flow which ruptures the lamellae.

## CHAPTER 6

### SUMMARY AND CONCLUSIONS

#### 6.1 Summary

Beginning with our hypothesis that foam decay is dependent on temperature and that different mechanisms dictate the decay at different temperatures, we designed a series of experiments to visually investigate the validity of our hypothesis while at the same time test methodologies adopted in the literature to validate their effectiveness in qualifying surfactants for high temperature use. We investigated a common method in which test tubes are filled with surfactant solutions and mechanically agitated to generate foam which is then measured with time. We ended up using this method to generate preliminary results for ranking the surfactants in terms of foamability and stability. Another method we investigated uses dynamic foams generated in a glass column at different temperatures by bubbling gas from the bottom of the column so that the foam height could be measured with time. Our design took advantage of a HPHT cell that could be visually inspected to generate foams at different temperatures and pressures in an environment that was void of mechanical disturbances such that only temperature (and humidity) was paramount to the decay of the foam. We selected three surfactants to experiment on: an alpha olefin sulfonate, an ethoxylated alcohol, and a mixture surfactant.

The test tube experiments showed us that AOS was by far the most foamable and stable at ambient conditions and that the other two surfactants could not compete with it. Even after aging the surfactants for four months, the results were similar, AOS was the most foamable, followed by Surfonic, then Elevate, while in terms of stability, AOS was the most stable, followed by Elevate, then Surfonic. We also observed no precipitation on any of the surfactants over the course of four months. Due to the speed of this method in generating results it was often used as a rapid filtering

method to qualify surfactants for more thorough investigations. We noted that using this method for such purpose can be detrimental since measuring surfactant performance at ambient conditions is in no way a proxy for surfactant performance at high temperatures as shown by our results using the HPHT cell, at least in terms of stability.

Dynamic foam experiments provided us with a better understanding of foam behavior with temperature as we were able to observe the different sensitivities of each surfactant's foamability to temperature. The results indicated that AOS was the most foamable, just as the test tube experiments had shown, with Elevate being more foamable than Surfonic, in contrast to the test tube experiments. As for the sensitivity of foamability with temperature (the change in foamability with temperature), Surfonic was the least sensitive followed very closely by AOS while Elevate was shown to be highly sensitive to temperature. We were also able to observe precipitation of AOS due to local variations in temperature and surfactant concentration caused by evaporation. The foamability results obtained from these experiments were not in agreement with the results from the test tube experiments, highlighting the importance of testing at the target temperature. We also noted that the observed linear behavior in foamability with temperature indicated a secondary effect in play at temperatures slightly above the boiling point of water which is the expansion of the  $N_2$  inside the bubbles which in turn increases the apparent height of the foam.

Our static foam experiments using the HPHT cell which formed the bulk of this work provided us with significant insight into the decay behavior of  $N_2$  foams and facilitated novel observations of foam decay patterns with temperature. Primarily, our results showed that for all three of our surfactants, there was a clear distinction between the decay behavior of foams at low temperatures and at high temperatures. We noted that at low temperatures, the decay of foam was slow and resulted in the drying of foam through gravity drainage and uniform evaporation which led the foams to become mainly large polyhedral bubbles with thin lamellae, while at high temperatures,

the foam decay was fast and primarily dictated by the Marangoni flow induced by nonuniform evaporation for anionic surfactants and by the thermodynamic behavior of the surfactant monomers for nonionic surfactants and that during the life of the foams they were entirely composed of small spherical bubbles that we attributed to be facilitated by the increased humidity in our system at those temperatures.

The visual cell experiments with its ability to capture high resolution images of the foam allowed us to observe the unique foam collapse behavior at higher temperatures for anionic surfactants where three layers can be identified for the foam and contrary to the conventional understanding of foam collapse behavior which stipulates that foam decay occurs at the top layer due to the lamellae thinning from evaporation and drainage, our observations indicated that the decay was in fact occurring at the middle layer instead and it was primarily driven by the Marangoni flow which causes bubbles to split into smaller ones effectively reducing the foam volume.

Our belief that foam decay at higher temperatures is caused by nonuniform evaporation leading to a Marangoni flow that destabilizes the lamellae stems from our observations and statistical mechanics. The splitting phenomenon we observed at higher temperatures that occurred primarily between bubbles of significant size difference in the middle layer of the foam which had thicker lamellae compared to bubbles in the top layer caused said bubbles to collapse and form smaller bubbles due to the influx of gas from the smaller bubble to the larger one. The forming of smaller bubbles indicates that the original bubbles had enough liquid inventory to create smaller bubbles meaning the lamellae is thicker than to burst due to drainage or uniform evaporation. Additionally, from the Maxwell-Boltzmann distribution, we know as temperature of the system increases, the stochasticity of the energy of molecules, and therefore the speed, increases too. We believe this leads to a more nonuniform heat distribution in the system, even at equilibrium, and as such, along

the surface of bubbles, water molecules evaporate at different rates causing local variations in surfactant concentration inducing a Marangoni flow. One can understand how larger bubbles with their larger surface are more susceptible to this phenomenon as our observations indicated.

We were also able to observe a unique decay behavior for nonionic surfactants where the decay occurs at the liquid-foam interface due to the complex behavior of nonionic surfactants. We stipulated that this decay is driven by the decrease in solubility of the surfactant as temperature increases. The solubility decrease is due to the breakage of hydrogen bonds which forces the monomers to aggregate into large isotropic structures in order to reduce the energy of the system.

In a steam-foam flood, the temperature of the steam injected is typically around 250 °C, and the foam is expected to be active around temperatures higher than those tested in this work. It is again imperative to note that foam tests should be conducted at temperatures at or close to those of the target use case and in steam-foam floods, the temperatures would be between the reservoir temperature and the temperature of the injected steam. A reservoir simulation should be able to generate the temperature range where the foam is expected to be most active.

## **6.2 Conclusions**

The finding of this study can be summarized as the following:

1. Temperature effect on foam behavior is significant enough to warrant testing at the target temperature, rendering test methodologies such as test tube unsuitable for high temperature foam studies.
2. Sensitivity of surfactants to temperature varies from one to the other and comparative analysis done at a low temperature to rank foamability and stability may not hold true at higher temperatures.

3. In general, surfactant N<sub>2</sub> foams display two distinct foam decay behaviors; one at low temperatures and one at high temperatures. In our tests, the temperature cutoff hovered around 40 °C regardless of the pressure.
4. Gravity drainage and uniform evaporation were the leading mechanisms of foam decay at low temperatures and resulted in foam bubbles becoming large and polyhedral.
5. For anionic surfactants, nonuniform evaporation induced Marangoni flow dictated foam decay at higher temperature which manifested as bubbles splitting into smaller ones.
6. For nonionic surfactants, the decay behavior at higher temperatures is influenced by the solubility of the surfactant and can manifest as a Marangoni flow induced by monomer concentration difference at the liquid-foam interface.
7. In closed systems at higher temperatures, foam collapse does not necessarily occur at the top layer as conventionally observed in foam decay experiments.
8. The use of closed system such as a HPHT cell provides a more accurate method to analyze foam decay at higher temperatures and pressures as compared to a foam column as used in Chapter 4 due to the improved control over temperature and pressure and the ability to properly visualize the foam as it decays.

### **6.3 Future Work**

This study laid the groundwork for a number of investigative paths that can be explored to better understand foam decay with temperature. We would like to suggest a few directions that are worth pursuing in the following:

1. While our conclusions draw on statistical mechanics and our observation of bubbles collapse in the form of splitting to state that nonuniform evaporation induces a Marangoni flow, it would be beneficial to attempt to directly observe this behavior by using a thermal imaging camera. A bubble can be generated between two thin sheets,

one made of glass, and another of a nonreflective material. This bubble would be generated at different temperatures and using the thermal imaging camera, one could attempt to capture the temperature along the bubble's film. Temperature variations along the bubble's film and their increase with temperature would support our conclusions.

2. Supplementing the above suggestion is another approach to capture the collapse of a bubble using both a thermal imaging camera and a high-speed camera in a similar design to the one mentioned in the first suggestion to verify whether the collapse starts at the high temperature regions or not. Since in our study we postulated that the collapse is due to the Marangoni flow, we expect a bubble to start bursting at regions of high temperature which should be possible to observe using this method.
3. One of the issues faced in this study was the unavoidable pressure increase alongside temperature since the volume was held constant. To eliminate this pressure increase and generate isobaric data for foamability and stability, an ISCO pump could be connected to one of the PVT system's ports and used to both supply  $N_2$  and to regulate the system's pressure while increasing the temperature. However, care should be taken as the humidity of the system will likely be affected given the increased volume of the system which could result in a different system altogether.
4. Further investigation into nonionic surfactants seems warranted and by performing a similar static test without the presence of bulk liquid could provide more insight on whether higher-order isotropic structures in the bulk liquid affect foam stability.
5. Since none of the surfactants studied in this work were cationic or amphoteric, it would be of interest to generate similar data for these surfactant types and contrast them to anionic and nonionic surfactants.

6. Given that the study presented results in bulk foams, we believe it would be useful to perform core floods at similar temperatures and compare the improvement in apparent viscosity at each temperature step for each surfactant studied in this work with the results obtained here. While our findings pertain to bulk foams, they could potentially translate to foam behavior in porous media, specifically the stability results at higher temperatures since evaporation becomes a dictating mechanism for the destruction of foams in porous media at higher temperatures.

## REFERENCES

- Ahmed, S., Elraies, K.A., Tan, I.M., and Hashmet, M.R. 2017. Experimental investigation of associative polymer performance for CO<sub>2</sub> foam enhanced oil recovery. *Journal of Petroleum Science and Engineering* **157**: 971–979. <https://doi.org/10.1016/j.petrol.2017.08.018>.
- Al Yousef, Z.A., Almobarky, M.A., and Schechter, D.S. 2020. Surfactant and a mixture of surfactant and nanoparticles to stabilize CO<sub>2</sub>/brine foam, control gas mobility, and enhance oil recovery. *Journal of Petroleum Exploration and Production Technology* **10** (2): 439–445. <https://doi.org/10.1007/s13202-019-0695-9>.
- Al-Khafaji, A.A., Castanier, L.M., and Brigham, W.E. 1985. Effect of Temperature on Degradation, Adsorption and Phase Partitioning of Surfactants Used in Steam Injection for Oil Recovery. Report, Contract No. DE-AC03-81SF-11564, US DOE, Washington, DC (January 1985).
- Allawzi, M.A. and Patton, J.T. 1994. Thermal Stability of Foam Additive in Steamflood Core Tests. Paper presented at the SPE/DOE Improved Oil Recovery Symposium, Tulsa, Oklahoma, USA, 17–20 April. SPE-27790-MS. <https://doi.org/10.2118/27790-MS>.
- Alvares-Jurgenson, G., Oetter, G., Kurkal-Siebert, V., Garcia, M.R., Stein, S., and Szabo, G. 2012. Compositions comprising alkylalkoxysulfonates for the production of high temperature stable foams. International (PCT) Patent No. WO2012113861A1
- Bashir, A., Haddad, A.S., and Rafati, R. 2019. Nanoparticle/polymer-enhanced alpha olefin sulfonate solution for foam generation in the presence of oil phase at high temperature conditions. *Colloids and Surfaces A: Physicochemical and Engineering Aspects* **582**: 123875. <https://doi.org/10.1016/j.colsurfa.2019.123875>.
- Bayat, A.E., Rajaei, K., and Junin, R. 2016. Assessing the effects of nanoparticle type and concentration on the stability of CO<sub>2</sub> foams and the performance in enhanced oil recovery. *Colloids and Surfaces A: Physicochemical and Engineering Aspects* **511**: 222–231. <https://doi.org/10.1016/j.colsurfa.2016.09.083>.
- Boeijs, C.S., Vad Bennetzen, M., and Rossen, W.R. 2017. A Methodology for Screening Surfactants for Foam Enhanced Oil Recovery in an Oil-Wet Reservoir. *SPE Reservoir Evaluation & Engineering* **20** (04): 0795–0808. <https://doi.org/10.2118/185182-PA>.
- Buck, A.L. 1981. New Equations for Computing Vapor Pressure and Enhancement Factor. *Journal of Applied Meteorology (1962-1982)* **20** (02): 1527–1532.
- Buck Research Instruments. 2012. Model CR-1A Hygrometer with Autofill Operating Manual. Boulder, Colorado: Buck Research Instruments.
- Chen, Y., Elhag, A. S., Worthen, A. J., Reddy, P. P., Ou, A. M., Hirasaki, G. J., Nguyen, Q. P., Biswal, S. L., and Johnston, K. P. 2016. High Temperature CO<sub>2</sub>-in-Water Foams Stabilized

- with Cationic Quaternary Ammonium Surfactants. *Journal of Chemical & Engineering Data* **61** (08): 2761–2770. <https://doi.org/10.1021/acs.jced.6b00135>.
- Cuenca, A., Lacombe, E., Morvan, M., Le Drogo, V., Giordanengo, R., Chabert, M., and Delamaide, E. 2014. Design of Thermally Stable Surfactants Formulations for Steam Foam Injection. Paper presented at the SPE Heavy Oil Conference-Canada, Calgary, Alberta, Canada, 10–12 June. SPE-170129-MS. <https://doi.org/10.2118/170129-MS>.
- Delamaide, E., Cuenca, A., and Chabert, M. 2016. State of the Art Review of the Steam Foam Process. Paper presented at the SPE Latin America and Caribbean Heavy and Extra Heavy Oil Conference, Lima, Peru, 19–20 October. SPE-181160-MS. <https://doi.org/10.2118/181160-MS>.
- Dilgren, R.E., Deemer, A.R., and Owens, K.B. 1982. The Laboratory Development and Field Testing of Steam/Noncondensable Gas Foams for Mobility Control in Heavy Oil Recovery. Paper presented at the SPE California Regional Meeting, San Francisco, California, USA, 24–26 March. SPE-10774-MS. <https://doi.org/10.2118/10774-MS>.
- EIA. 2022. Proved Reserves of Crude Oil and Natural Gas in the United States, Year-End 2020, <https://www.eia.gov/naturalgas/crudeoilreserves/> (accessed 14 February 2022).
- Emrani, A.S. and Nasr-El-Din, H.A. 2017. An experimental study of nanoparticle-polymer-stabilized CO<sub>2</sub> foam. *Colloids and Surfaces A: Physicochemical and Engineering Aspects* **524**: 17–27. <https://doi.org/10.1016/j.colsurfa.2017.04.023>.
- Etminan, S.R., Goldman, J., and Wassmuth, F. 2016. Determination of Optimal Conditions for Addition of Foam to Steam for Conformance Control. Paper presented at the SPE EOR Conference at Oil and Gas West Asia, Muscat, Oman, 21–23 March, SPE-179841-MS. <https://doi.org/10.2118/179841-MS>.
- Exerowa, D. and Kruglyakov, P.M. 1997. *Foam and Foam Films: Theory, Experiment, Application*. Amsterdam, The Netherlands: Elsevier Science B.V.
- Farajzadeh, R., Krastev, R., and Zitha, P.L.J. 2008. Foam films stabilized with alpha olefin sulfonate (AOS). *Colloids and Surfaces A: Physicochemical and Engineering Aspects* **324** (01–03): 35–40. <https://doi.org/10.1016/j.colsurfa.2008.03.024>.
- Farajzadeh, R., Andrianov, A., Krastev, R., Hirasaki, G.J., and Rossen, W.R. 2012. Foam–oil interaction in porous media: Implications for foam assisted enhanced oil recovery. *Advances in Colloid and Interface Science* **183–184**: 01–13. <https://doi.org/10.1016/j.cis.2012.07.002>.
- Hama, M.Q., Wei, M., Saleh, L.D., and Bai, B. 2014. Updated Screening Criteria for Steam Flooding Based on Oil Field Projects Data. Paper presented at the SPE Heavy Oil Conference-Canada, Calgary, Alberta, Canada, 10–12 June. SPE-170031-MS. <https://doi.org/10.2118/170031-MS>.
- Hirasaki, G.J. 1989. The Steam-Foam Process. *Journal of Petroleum Technology* **41** (05): 449–456. <https://doi.org/10.2118/19505-PA>.

- IEA. 2021. Global Energy Review 2021, <https://www.iea.org/reports/global-energy-review-2021> (accessed 14 February 2022).
- Iglesias, E., Anderez, J., Forgiarini, A., and Salager, J-L. 1995. A new method to estimate the stability of short-life foams. *Colloids and Surfaces A: Physicochemical and Engineering Aspects* **98** (01–02): 167–174. [https://doi.org/10.1016/0927-7757\(95\)03101-I](https://doi.org/10.1016/0927-7757(95)03101-I).
- Jones, S.A., van der Bent, V., Farajzadeh, R., Rossen, W.R., and Vincent-Bonnieu, S. 2016. Surfactant screening for foam EOR: Correlation between bulk and core-flood experiments. *Colloids and Surfaces A: Physicochemical and Engineering Aspects* **500**: 166–176. <https://doi.org/10.1016/j.colsurfa.2016.03.072>.
- Kamal, M.S. 2019. A Novel Approach to Stabilize Foam Using Fluorinated Surfactants. *Energies* **12** (06): 1163. <https://doi.org/10.3390/en12061163>.
- Kapetas, L., Bonnieu, S. Vincent, Danelis, S., Rossen, W. R. R., Farajzadeh, R., Eftekhari, A. A. A., Shafian, S. R., and R. Z. Bahrim. 2015. Effect of Temperature on Foam Flow in Porous Media. Paper presented at the SPE Middle East Oil & Gas Show and Conference, Manama, Bahrain, 08–11 March. SPE-172781-MS. <https://doi.org/SPE-172781-MS>.
- Lau, H.C. 1986. Alkali-enhanced steam foam oil recovery process. US Patent No. 4,609,044.
- Lau, H.C. 1988. Trona-enhanced steam foam oil recovery process. US Patent No. 4,727,938.
- Lau, H.C. 2011. Alkaline Steam Foam: Concepts and Experimental Results. Paper presented at the SPE Enhanced Oil Recovery Conference, Kuala Lumpur, Malaysia, 19–21 July. SPE-144968-MS. <https://doi.org/10.2118/144968-MS>.
- Lau, H.C. and Borchardt, J.K. 1991. Improved Steam-Foam Formulations: Concepts and Laboratory Results. *SPE Reservoir Engineering* **6** (04): 470–476. <https://doi.org/10.2118/18783-PA>.
- Lau, H.C. and O'Brien, S.M. 1988a. Effects of Spreading and Nonspreading Oils on Foam Propagation Through Porous Media. *SPE Reservoir Engineering* **3** (03): 893–896. <https://doi.org/10.2118/15668-PA>.
- Lau, H.C. and O'Brien, S.M. 1988b. Surfactant Transport Through Porous Media in Steam-Foam Processes. *SPE Reservoir Engineering* **3** (04): 1177–1185. <https://doi.org/10.2118/14391-PA>.
- Li, X., Shaw, R., and Stevenson, P. 2010. Effect of humidity on dynamic foam stability. *International Journal of Mineral Processing* **94** (01): 14–19. <https://doi.org/10.1016/j.minpro.2009.10.002>.
- Li, X., Karakashev, S.I., Evans, G.M., and Stevenson, P. 2012. Effect of Environmental Humidity on Static Foam Stability. *Langmuir* **28** (09): 4060–4068. <https://doi.org/10.1021/la205101d>.
- Liu, Y., Grigg, R.B., and Svec, R.K. 2005. CO<sub>2</sub> Foam Behavior: Influence of Temperature, Pressure, and Concentration of Surfactant. Paper presented at the SPE Production

- Operations Symposium, Oklahoma City, Oklahoma, USA, 17–19 April. SPE-94307-MS. <https://doi.org/10.2118/94307-MS>.
- Majeed, T., Kamal, M.S., Zhou, X., and Solling, T. 2021. A Review on Foam Stabilizers for Enhanced Oil Recovery. *Energy & Fuels* **35** (07): 5594–5612. <https://doi.org/10.1021/acs.energyfuels.1c00035>.
- Meyer, R.F., Attanasi, E.D., and Freeman, P.A. 2007. Heavy Oil and Natural Bitumen Resources in Geological Basins of the World. Open-File Report 2007-1084, U.S. Geological Survey, Reston, Virginia (2007).
- Mills, K., Hondros, E., and Li, Z. 2005. Interfacial phenomena in high temperature processes. *Journal of Materials Science* **40** (09–10): 2403–2409. <https://doi.org/10.1007/s10853-005-1966-z>.
- Morey, M.D., Deshpande, N.S., and Barigou, M. 1999. Foam Destabilization by Mechanical and Ultrasonic Vibrations. *Journal of Colloid and Interface Science* **219** (01): 90–98. <https://doi.org/10.1006/jcis.1999.6451>.
- Muijs, H.M., Keijzer, P.P.M. and Wiersma, R.J. 1988. Surfactants for Mobility Control in High-Temperature Steam-Foam Applications. Paper presented at the SPE Enhanced Oil Recovery Symposium, Tulsa, Oklahoma, USA, 17–20 April. SPE-17361-MS. <https://doi.org/10.2118/17361-MS>.
- Myers, D. 2020. *Surfactant Science and Technology*, Fourth edition. Hoboken, New Jersey: Wiley.
- Neethling, S.J., Lee, H.T., and Grassia, P. 2005. The growth, drainage and breakdown of foams. *Colloids and Surfaces A: Physicochemical and Engineering Aspects* **263** (01): 184–196. <https://doi.org/10.1016/j.colsurfa.2004.12.014>.
- Negin, C., Ali, S. and Xie, Q. 2017. Most common surfactants employed in chemical enhanced oil recovery. *Petroleum* **3** (02): 197–211, <https://doi.org/10.1016/j.petlm.2016.11.007>.
- Nezbeda, I. 2016. Simulations of Vapor-Liquid Equilibria: Routine versus Thoroughness. *Journal of Chemical & Engineering Data*, **61**: 3964–3969. <https://doi.org/10.1021/acs.jced.6b00539>.
- Pandey, A., Sinha, A.S.K., Chaturvedi, K.R., and Sharma, T. 2021. Experimental investigation on effect of reservoir conditions on stability and rheology of carbon dioxide foams of nonionic surfactant and polymer: Implications of carbon geo-storage. *Energy*, **235**: 121445. <https://doi.org/10.1016/j.energy.2021.121445>.
- Patzek, T.W. and Koinis, M.T. 1990. Kern River Steam-Foam Pilots. *Journal of Petroleum Technology* **42** (04): 496–503. <https://doi.org/10.2118/17380-PA>.
- Patzek, T.W. and Myhill, N.A. 1989. Simulation of the Bishop Steam Foam Pilot. Paper presented at the SPE California Regional Meeting, Bakersfield, California, USA, 5–7 April. SPE-18786-MS. <https://doi.org/10.2118/18786-MS>.
- Radke, C.J. and Gillis, J.V. 1990. A Dual Gas Tracer Technique for Determining Trapped Gas Saturation During Steady Foam Flow in Porous Media. Paper presented at the SPE Annual

- Technical Conference and Exhibition, New Orleans, Louisiana, USA, 23–26 September. SPE-20519-MS. <https://doi.org/10.2118/20519-MS>.
- Raghav Chaturvedi, K., Kumar, R., Trivedi, J., Sheng, J.J., and Sharma, T. 2018. Stable Silica Nanofluids of an Oilfield Polymer for Enhanced CO<sub>2</sub> Absorption for Oilfield Applications. *Energy & Fuels* **32** (12): 12730–12741. <https://doi.org/10.1021/acs.energyfuels.8b02969>.
- Raney, K.H., Shpakoff, P.G., and Passwater, D.K. 1998. Use of high-active alpha olefin sulfonates in laundry powders. *Journal of Surfactants and Detergents* **1** (03): 361–369. <https://doi.org/10.1007/s11743-998-0037-z>.
- Romero-Zeron, L. and Kantzas, A. 2005. Pore-Scale Visualization of Foamed Gel Propagation and Trapping in a Pore Network Micromodel. *Journal of Canadian Petroleum Technology* **44** (05): 44–50. <https://doi.org/10.2118/05-05-03>.
- Saint-Jalmes, A. and Langevin, D. 2002. Time evolution of aqueous foams: drainage and coarsening. *Journal of Physics: Condensed Matter* **14** (40): 9397–9412. <https://doi.org/10.1088/0953-8984/14/40/325>.
- Sanders, A., Nguyen, M.N., Ren, G., Westmoreland, D., Nguyen, Q., Dong, S., and Rojas, C. 2017. Development of Novel Foaming Agents for High Temperature Steam Applications. Paper presented at the Abu Dhabi International Petroleum Exhibition & Conference, Abu Dhabi, UAE, 13–16 November. SPE-188682-MS. <https://doi.org/10.2118/188682-MS>.
- Schramm, L.L. 1994. *Foams: Fundamentals and Applications in the Petroleum Industry*. Washington, DC: Advances in chemistry series, 242, American Chemical Society.
- Speight, J.G. 2013. Thermal Methods of Recovery. In *Heavy Oil Production Processes*, ed. J. G. Speight, Chap. 5, 93–130. Massachusetts: Gulf Professional Publishing/Elsevier.
- Stoll, R.D., Gudenau, H.W., Lupik, M.W., and Smith, J.L. 1993. Mobility Control for Steamflooding with High-Temperature-Resistant Additives. *SPE Reservoir Engineering* **8** (04): 281–284. <https://doi.org/10.2118/21019-PA>.
- Sun, L., Bai, B., Wei, B., Pu, W., Wei, P., Li, D., and Zhang, C. 2019. Recent advances of surfactant-stabilized N<sub>2</sub>/CO<sub>2</sub> foams in enhanced oil recovery. *Fuel*, **241**: 83–93. <https://doi.org/10.1016/j.fuel.2018.12.016>.
- Tadros, T.F. 2003. Surfactants, Industrial Applications. In *Encyclopedia of Physical Science and Technology*, Third Edition, ed. R. A. Meyers, 423–438. New York: Academic Press/Elsevier
- Turner, D., Dlugogorski, B., and Palmer, T. 1999. Factors affecting the stability of foamed concentrated emulsions. *Colloids and Surfaces A: Physicochemical and Engineering Aspects* **150** (01–03): 171–184. [https://doi.org/10.1016/S0927-7757\(98\)00814-0](https://doi.org/10.1016/S0927-7757(98)00814-0).
- Tyrode, E., Pizzino, A., and Rojas, O.J. 2003. Foamability and foam stability at high pressures and temperatures. I. Instrument validation. *Review of Scientific Instruments* **74** (05): 2925–2932. <https://doi.org/10.1063/1.1569403>.

- Wang, H., Guo, W., Zheng, C., Wang, D., and Zhan, H. 2017. Effect of Temperature on Foaming Ability and Foam Stability of Typical Surfactants Used for Foaming Agent. *Journal of Surfactants and Detergents* **20** (03): 615–622. <http://dx.doi.org/10.1007/s11743-017-1953-9>.
- Wang, J., Nguyen, A.V., and Farrokhpay, S. 2016. A critical review of the growth, drainage and collapse of foams. *Advances in Colloid and Interface Science* **228**: 55–70. <https://doi.org/10.1016/j.cis.2015.11.009>.
- Wu, Z., Liu, H., Pang, Z., Wu, Y., Wang, X., Liu, D., and Gao, M. 2016. A visual investigation of enhanced heavy oil recovery by foam flooding after hot water injection. *Journal of Petroleum Science and Engineering* **147**: 361–370. <https://doi.org/10.1016/j.petrol.2016.08.023>.
- Xu, L., Rad, M.D., Telmadarreie, A., Qian, C., Liu, C., Bryant, S.L., and Dong, M. 2018. Synergy of surface-treated nanoparticle and anionic-nonionic surfactant on stabilization of natural gas foams. *Colloids and Surfaces A: Physicochemical and Engineering Aspects* **550**: 176–185. <https://doi.org/10.1016/j.colsurfa.2018.04.046>.
- Yaminsky, V.V., Ohnishi, S., Vogler, E.A., and Horn, R.G. 2010. Stability of Aqueous Films between Bubbles. Part 2. Effects of Trace Impurities and Evaporation. *Langmuir* **26** (11): 8075–8080. <https://doi.org/10.1021/la904482n>.
- Zhang, L., Jian, G., Puerto, M., Wang, X., Chen, Z., Da, C., Johnston, K., Hirasaki, G., and Biswal, S. L. 2020. Crude Oil Recovery with Duomeen CTM-Stabilized Supercritical CO<sub>2</sub> Foams for HPHT and Ultrahigh-Salinity Carbonate Reservoirs. *Energy & Fuels* **34** (12): 15727–15735. <https://doi.org/10.1021/acs.energyfuels.0c02048>.
- Zhou, W., Xin, C., Chen, S., Yu, Q., and Wang, K. 2020. Polymer-Enhanced Foam Flooding for Improving Heavy Oil Recovery in Thin Reservoirs. *Energy & Fuels* **34** (04): 4116–4128. <https://doi.org/10.1021/acs.energyfuels.9b04298>.

## APPENDIX A

### SUPPLEMENTAL COPYRIGHT PERMISSIONS

This appendix includes the copyright permissions for the figures (2.3, 2.5, 3.3, and 5.25) used from books and journal articles.



**Book:** Foams: Fundamentals and Applications in the Petroleum Industry

**Chapter:** Foams: Basic Principles

**Author:** Laurier L. Schramm, Fred Wassmuth

**Publisher:** American Chemical Society

**Date:** Oct 1, 1994

*Copyright © 1994, American Chemical Society*

#### PERMISSION/LICENSE IS GRANTED FOR YOUR ORDER AT NO CHARGE

This type of permission/license, instead of the standard Terms and Conditions, is sent to you because no fee is being charged for your order. Please note the following:

- Permission is granted for your request in both print and electronic formats, and translations.
- If figures and/or tables were requested, they may be adapted or used in part.
- Please print this page for your records and send a copy of it to your publisher/graduate school.
- Appropriate credit for the requested material should be given as follows: "Reprinted (adapted) with permission from {COMPLETE REFERENCE CITATION}. Copyright {YEAR} American Chemical Society." Insert appropriate information in place of the capitalized words.
- One-time permission is granted only for the use specified in your RightsLink request. No additional uses are granted (such as derivative works or other editions). For any uses, please submit a new request.

If credit is given to another source for the material you requested from RightsLink, permission must be obtained from that source.

BACK

CLOSE WINDOW

This is a License Agreement between Hamed Al-Riyami ("User") and Copyright Clearance Center, Inc. ("CCC") on behalf of the Rightsholder identified in the order details below. The license consists of the order details, the CCC Terms and Conditions below, and any Rightsholder Terms and Conditions which are included below.  
All payments must be made in full to CCC in accordance with the CCC Terms and Conditions below.

Order Date	01-Apr-2022	Type of Use	Republish in a thesis/dissertation
Order License ID	1206218-2	Publisher	Society of Petroleum Engineers
ISBN-13	978-1-55563-545-9	Portion	Chart/graph/table/figure

#### LICENSED CONTENT

Publication Title	SPE Annual Technical Conference and Exhibition	Country	United States of America
Author/Editor	Society of Petroleum Engineers	Rightsholder	Society of Petroleum Engineers (SPE)
Date	12/31/1989	Publication Type	e-Book
Language	English		

#### REQUEST DETAILS

Portion Type	Chart/graph/table/figure	Distribution	United States
Number of charts / graphs / tables / figures requested	1	Translation	Original language of publication
Format (select all that apply)	Print, Electronic	Copies for the disabled?	No
Who will republish the content?	Academic institution	Minor editing privileges?	Yes
Duration of Use	Life of current edition	Incidental promotional use?	No
Lifetime Unit Quantity	Up to 499	Currency	USD
Rights Requested	Main product		

#### NEW WORK DETAILS

Title	INVESTIGATION INTO THE EFFECT OF TEMPERATURE ON NITROGEN FOAM BEHAVIOR	Institution name	Colorado School of Mines
Instructor name	Luis Zerpa	Expected presentation date	2022-03-14

#### ADDITIONAL DETAILS

Order reference number	N/A	The requesting person / organization to appear on the license	Hamed Al-Riyami
------------------------	-----	---	-----------------

#### REUSE CONTENT DETAILS

Title, description or numeric reference of the portion(s)	Fig 2	Title of the article/chapter the portion is from	A Dual Gas Tracer Technique for Determining Trapped Gas Saturation During Steady Foam Flow in Porous Media
Editor of portion(s)	N/A	Author of portion(s)	Society of Petroleum Engineers
Volume of serial or monograph	N/A	Issue, if republishing an article from a serial	N/A
Page or page range of portion	482	Publication date of portion	1989-12-31



This is a License Agreement between Hamed Al-Riyami ("User") and Copyright Clearance Center, Inc. ("CCC") on behalf of the Rightsholder identified in the order details below. The license consists of the order details, the CCC Terms and Conditions below, and any Rightsholder Terms and Conditions which are included below.  
 All payments must be made in full to CCC in accordance with the CCC Terms and Conditions below.

<b>Order Date</b>	01-Apr-2022	<b>Type of Use</b>	Republish in a thesis/dissertation
<b>Order License ID</b>	1206218-1	<b>Publisher</b>	SOCIETY OF PETROLEUM ENGINEERS
<b>ISSN</b>	1094-6470	<b>Portion</b>	Chart/graph/table/figure

#### LICENSED CONTENT

<b>Publication Title</b>	SPE reservoir evaluation & engineering	<b>Country</b>	United States of America
<b>Author/Editor</b>	Society of Petroleum Engineers (U.S.)	<b>Rightsholder</b>	Society of Petroleum Engineers (SPE)
<b>Date</b>	12/31/1997	<b>Publication Type</b>	Journal
<b>Language</b>	English		

#### REQUEST DETAILS

<b>Portion Type</b>	Chart/graph/table/figure	<b>Distribution</b>	United States
<b>Number of charts / graphs / tables / figures requested</b>	1	<b>Translation</b>	Original language of publication
<b>Format (select all that apply)</b>	Print, Electronic	<b>Copies for the disabled?</b>	No
<b>Who will republish the content?</b>	Academic institution	<b>Minor editing privileges?</b>	Yes
<b>Duration of Use</b>	Life of current edition	<b>Incidental promotional use?</b>	No
<b>Lifetime Unit Quantity</b>	Up to 499	<b>Currency</b>	USD
<b>Rights Requested</b>	Main product		

#### NEW WORK DETAILS

<b>Title</b>	INVESTIGATION INTO THE EFFECT OF TEMPERATURE ON NITROGEN FOAM BEHAVIOR	<b>Institution name</b>	Colorado School of Mines
<b>Instructor name</b>	Luis Zerpa	<b>Expected presentation date</b>	2022-03-14

#### ADDITIONAL DETAILS

<b>Order reference number</b>	N/A	<b>The requesting person / organization to appear on the license</b>	Hamed Al-Riyami
-------------------------------	-----	--	-----------------

#### REUSE CONTENT DETAILS

<b>Title, description or numeric reference of the portion(s)</b>	Fig 2	<b>Title of the article/chapter the portion is from</b>	A Methodology for Screening Surfactants for Foam Enhanced Oil Recovery in an Oil-Wet Reservoir
<b>Editor of portion(s)</b>	N/A	<b>Author of portion(s)</b>	Society of Petroleum Engineers (U.S.)
<b>Volume of serial or monograph</b>	N/A	<b>Issue, if republishing an article from a serial</b>	N/A
<b>Page or page range of portion</b>	798	<b>Publication date of portion</b>	1997-12-31

## Order Completed

Thank you for your order.

This Agreement between Mr. Hamed Al-Riyami ("You") and John Wiley and Sons ("John Wiley and Sons") consists of your license details and the terms and conditions provided by John Wiley and Sons and Copyright Clearance Center.

Your confirmation email will contain your order number for future reference.

License Number 5260470799449

[Printable Details](#)

License date Mar 01, 2022

### Licensed Content

Licensed Content Publisher	John Wiley and Sons
Licensed Content Publication	Wiley Books
Licensed Content Title	An Overview of Surfactant Science and Technology
Licensed Content Date	Jun 19, 2020
Licensed Content Pages	16

### Order Details

Type of use	Dissertation/Thesis
Requestor type	University/Academic
Format	Print and electronic
Portion	Figure/table
Number of figures/tables	1
Will you be translating?	No

### About Your Work

Title	INVESTIGATION INTO THE EFFECT OF TEMPERATURE ON NITROGEN FOAM BEHAVIOR
Institution name	Colorado School of Mines
Expected presentation date	Mar 2022

### Additional Data

Portions	Figure 7.4 on page 169
----------	------------------------

### Requestor Location

Mr. Hamed Al-Riyami

### Tax Details

Publisher Tax ID	EU826007151
------------------	-------------